Remote Characterization of Underground Ventilation Systems using Tracer Gas and CFD

Guang Xu

Dissertation submitted to the faculty of Virginia Polytechnic Institute & State University in partial fulfillment of the requirements for the degree of

Doctor of Philosophy
in
Mining Engineering

Kramer D. Luxbacher, Chair
Greg T. Adel
Saad A. Ragab
Gerrit V.R. Goodman
Michael E. Karmis

February 15, 2013
Blacksburg, Virginia

Keywords: underground mine ventilation, mine incident, CFD modeling, tracer gas, gas chromatography

Remote Characterization of Underground Ventilation Systems using Tracer Gas and CFD

Guang Xu

ABSTRACT

Following an unexpected event in an underground mine, it is important to know the state of the mine immediately to manage the situation effectively. Particularly when part or the whole mine is inaccessible, remotely and quickly ascertaining the ventilation status is one of the pieces of essential information that can help mine personnel and rescue teams make decisions. This study developed a methodology that uses tracer gas techniques and CFD modeling to analyze underground mine ventilation system status remotely. After an unanticipated event that has damaged ventilation controls, the first step of the methodology is to assess and estimate the level of the damage and the possible ventilation changes based on the available information. Then CFD models will be built to model the normal ventilation status before the event, as well as possible ventilation damage scenarios. At the same time, tracer gas tests will be designed and performed on-site. Tracer gas will be released at a designated location with constant or transient release techniques. Gas samples will be collected at other locations and analyzed using Gas Chromatography (GC). Finally, through comparing the CFD simulated results and the tracer on-site test results, the general characterization of the ventilation system can be determined.

A review of CFD applications in mining engineering is provided in the beginning of this dissertation. The basic principles of CFD are reviewed and six turbulence models commonly used are discussed with some examples of their application and guidelines on choosing an appropriate turbulence model. General modeling procedures are also provided with particular emphasis on conducting a mesh independence study and different validation methods, further improving the accuracy of a model. CFD applications in mining engineering research and design areas are reviewed, which illustrate the success of CFD and highlight challenging issues.

Experiments were conducted both in the laboratory and on-site. These experiments showed that the developed methodology is feasible for characterizing underground ventilation systems remotely. Limitations of the study are also addressed. For example, the CFD model requires detailed ventilation survey data for an accurate CFD modeling and takes much longer time compared to network modeling.

Some common problems encountered when using tracer gases in underground mines are discussed based on previously completed laboratory and field experiments, which include tracer release methods, sampling and analysis techniques. Additionally, the use of CFD to optimize the design of tracer gas experiments is also presented. Finally, guidelines and recommendations are provided on the use of tracer gases in the characterization of underground mine ventilation networks.

Acknowledgements

This dissertation grew out of a set of papers that I have submitted to (or prepared for) conference proceedings and peer reviewed journals. The complexity of this study and the difficulties we have faced proved far more challenging than I had expected. Fortunately, this work benefited from suggestions and helps from many people including my committee members and my colleagues.

My advisor, Dr. Kray Luxbacher, provided vital help. She managed to find the time to edit almost every paper in this dissertation with great care. She also put forth a lot of effort during my laboratory and field experiments and provided numerous insightful suggestions on how to enhance the depth of this study. She provided many opportunities for me to present the work to other professionals as well.

I also want to thank my committee members for their encouragement and support. They are Dr. Greg Adel, Dr. Saad Ragab, Dr. Gerrit Goodman, and Dr. Michael Karmis. I'd like to especially thank Dr. Gerrit Goodman from the National Institute for Occupational Safety and Health (NIOSH), he traveled several times form Pittsburgh to Virginia Tech and provided valuable feedback on my research. He also created the opportunity for me to go to NIOSH and present this study.

Special thanks are given to Dr. Harold M. McNair for generously sharing his vast knowledge of gas chromatography.

Additionally, I appreciate Steven Schafrik for helping me set up and troubleshoot the high performance computer, which is an essential tool I used for CFD calculation. Thanks are also given to Hassan Fayed, who is from the department of engineering science and mechanics, for his assistances on CFD modeling.

I also want to thank our research group members: Edmund Jong, Rosemary R. Patterson, John R. Bowling, Susanne Underwood, Mike Devlin, and Kenneth Griffin for their help and background work.

Most of the field experiments in this study were conducted at Kimballton mine. I want to express my great appreciation to Mark Luxbacher, who provided great help and support to our tests at Kimballton mine.

I would like to thank my wife, Yufeng Yuan, for her love and support. She is a great wife and mother, and she did so much taking care of my little daughter, Danielle. I know that I haven't been much fun to be around lately.

Finally, this publication was developed under Contract No. 200-2009-31933, awarded by the National Institute for Occupational Safety and Health (NIOSH). The findings and conclusions in this report are those of the authors and do not reflect the official policies of the Department of Health and Human Services; nor does mention of trade names, commercial practices, or organizations imply endorsement by the U.S. Government.

Attribution

Beside my committee members, one professor and three colleagues provided technical and editorial input to different chapters in this dissertation. A brief description of their contributions is included here.

Harold M. McNair is an emeritus professor in the chemistry department at Virginia Tech. He is a co-author on Chapter 7 in this dissertation. He provided lots of technical support on gas chromatography and edited this chapter.

John Bowling was a graduated master student in the department of mining and minerals engineering at Virginia Tech. He is a co-author on Chapter 3 in this dissertation. He provided technical and editorial input for this chapter.

Steve Schafrik is a Ph. D. student in the department of mining and minerals engineering at Virginia Tech. He is a co-author on Chapter 4 in this dissertation. He provided technical support on the high performance computer that was used for the CFD modeling and edited this chapter.

Edmund Jong is a Ph. D. student in the department of mining and minerals engineering at Virginia Tech. He is a co-author on Chapter 5, 6, and 7. He contributed editorial comments on these chapters and helped with some of the experiments in Chapter 6 and 7.

Table of Contents

List of Figures

List of Tables

1 Introduction

Following an unexpected event in an underground mine, it is important to know the state of the mine immediately, even with limited information, in order to manage the situation effectively. When part or the whole mine is inaccessible, remotely and quickly ascertaining the ventilation status is one of the critical pieces of information that can help mine personnel and rescue teams make decisions. While underground communications systems are rapidly improving and are designed for use post-incident, their survival cannot be guaranteed and it is necessary to develop other methods to ascertain the mine status. Some alternate methods can be used to gather information safely and remotely, including collecting air samples from bore holes, inserting video cameras into bore holes to visualize underground status, and utilizing rescue robots underground if possible. Most information is not clear before rescue personnel enter the mine and none of the methods mentioned above could be reliable and efficient enough to stand alone. In a word, in an emergency situation, any information is "gold", not only to effectively save miners' lives, but also to help decision makers manage the emergency effectively, to increase safety for the rescuers, and to advance the rescue operation.

To quickly characterize the ventilation system is one of the pieces of essential information that can help mine personnel and rescue teams make decisions that save lives and ensure the safety of responders. Especially in some incidents, such as an explosion, communication systems may be severely damaged and collapse may occur with very little information available at the surface. However, the airflow paths and ventilation patterns will change according to the level and the location of damage. Therefore, the ventilation characterization can be analyzed and predicted by monitoring and studying changes in the ventilation system. Due to the complexity of the ventilation system, the use of the tracer gas is an effective method and has been used in many situations where conventional techniques are inadequate or cannot be effectively employed [1], [2]. Numerical simulations using computational fluid dynamics (CFD) can be used to model the ventilation status, which can be compared with the data from tracer gas measurement to further analyze, predict and confirm the underground ventilation status.

The research described here aims to develop a new methodology that can characterize underground ventilation systems using tracer gas techniques and CFD modeling. The overview

of the methodology can be seen in the flow chart shown in Figure 1. After an unanticipated event that has damaged ventilation controls, the level of the damage and the possible ventilation changes need to be estimated based on the available information. Then CFD models will be built to model the normal ventilation status before the event, as well as possible ventilation damage scenarios. At the same time, tracer gas tests will be designed carefully and performed on-site. Tracer gas will be released at a designated location with constant or transient release techniques. Gas samples will be collected at other locations and analyzed using Gas Chromatography (GC). Finally, through comparing the CFD simulated results and the tracer on-site test results, the general level of ventilation damage can be determined.

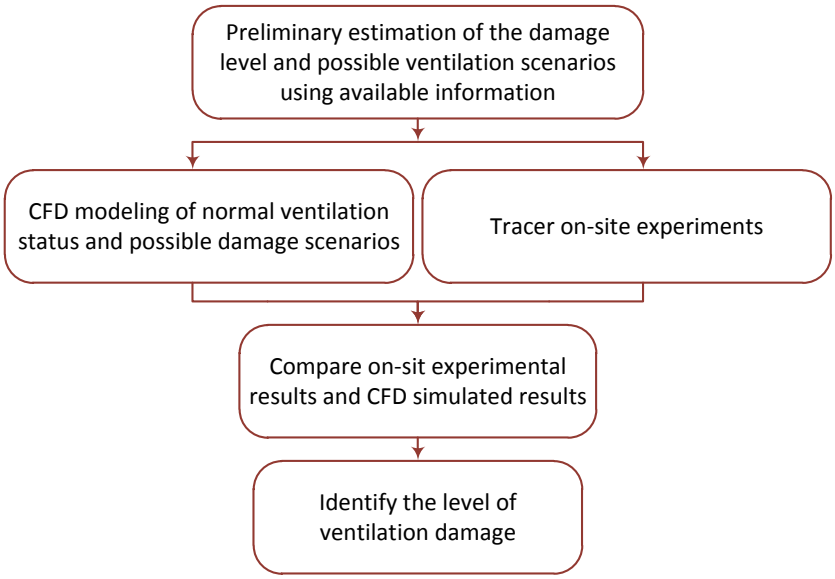

Figure 1. Flow chart of the methodology

This dissertation consists of eight chapters. Each chapter, excluding the first and the last, is a paper that is published in, or about to be submitted to, conference proceedings or peer reviewed journals. This information is provided at the beginning of each chapter.

Chapter 1 is an introduction to the research and an overview of the developed methodology. The literature review is detailed in Chapter 2 focusing on CFD applications in mining. It is a standalone review that will be formatted for journal publication. Chapter 3 describes a preliminary laboratory experiment and CFD modeling with the objective of evaluating the feasibility of CFD modeling of tracer gas in an experimental apparatus. Chapter 4 is a completed laboratory experiment with a detailed CFD modeling study. The aim of this study is to use the experimental data to validate the CFD model, study the relationship between the tracer concentration and the location of incident damages, and finally through analysis of air

samples and the CFD model results, determine the general location of ventilation damage. Chapter 5 is a CFD modeling study for an actual size conceptual mine developed based on the laboratory experimental mine model which primarily aims to review the best methodology for full CFD mine simulations and the potential useful information that the simulation results can provide. Chapter 6 describes the application of the developed methodology to an actual mine. It proved that the methodology is feasible not only in the laboratory, but also in the field. Chapter 7 discusses some common problems encountered when using tracer gases in underground mines, including tracer release methods, sampling and analysis techniques. Additionally, the use of CFD to optimize the design of tracer gas experiments, which played an important role in this study, is also presented. The aim of the chapter is to provide guidelines and recommendations on the use of tracer gases in the characterization of underground mine ventilation systems. Finally, chapter 8 contains the conclusions and discussions of this study. Highlights of this research and recommendations for future work are also included.

The following review paper will be submitted to a mining specific journal. It was entirely written by Guang Xu with editorial input from Dr. Kray Luxbacher and Dr. Saad Ragab, and may be compressed to meet journal requirements.

2 Review of CFD Applications in Mining

2.1 Introduction

The principles of fluid dynamics are widely applied to mine ventilation, including methane control, fire development, explosion, dust movement, and ventilation efficiency. Understanding of the mechanism of fluid dynamics is valuable for solving problems, especially safety and health problems, in the mining industry. Due to the complexity of the phenomena involved in mine fluid dynamics problems, Computational Fluid Dynamics (CFD) modeling has been increasingly applied to the mining industry in recent years to accurately predict the flow patterns, study the flow mechanism and results, and design equipment to improve the efficiency and safety of mine industry. CFD modeling is especially useful when the comprehensive analysis using physical experimentation requires expensive equipment, large amounts of time and understanding of flow in inaccessible areas.

CFD is a tool with which one can carry out numerical experiments with the purpose of determining indices that are impossible, or at least very difficult, to obtain from experiments. The numerical experiments can not only be used to help interpret physical experiments, but also to better understand phenomena that are observed during physical experimentation [3]. The computational cost of CFD is dropping as a result of increasing speed of computers, and with the cost of physical experiments generally increasing, these costs can be reduced considerably with the use of CFD that can be used to better design physical experiments and increase efficiency.

CFD plays a strong role as a research and design tool and is a well-established technique applied to a broad range of fields including aircraft, turbomachinery, automobile and ship design, and meteorology, oceanography, astrophysics, biology, oil recovery, civil and architecture. Many of today's mining problems need both analysis and visualization of fluid flow behavior in complex geometric domains making CFD a powerful application in both mining research and design.

Because of the success of CFD, there are many publications of CFD application studies in mining; however, very few include a comprehensive review detailing the current state-of-the-art in research and development. The purpose of this paper is to present such a review which provides current state-of-the-art information about the progress in CFD application in mining and

illustrates its capabilities by way of examples. The emphasis is on general-purpose commercial CFD code methodology rather than specialized CFD software development. Previous research into the area of CFD applications in mining is explored and summarized in this paper.

2.2 Principles of CFD

Computational fluid dynamics (CFD) is one of the branches of fluid mechanics. It began evolving in the early 1970's and employed physics, numerical mathematics and computer sciences to simulate fluid flows. CFD deals with numerical solution of differential equations governing the physics of fluid flow and the interaction of the fluid with solid bodies [4]. It uses numerical methods and algorithms to solve and analyze fluid flow problems. Flows of gases and liquids, heat and mass transfer, moving bodies, multiphase physics, chemical reaction, fluid-structure interaction and acoustics can be simulated through computer modeling [5]. The technique enables the user to predict what will happen under a given set of circumstances. The following section will give a brief introduction of the governing equations, along with the general methodology used in CFD.

2.2.1 Governing equations

CFD is based on the fundamental governing equations of fluid dynamics which express the fundamental physical principles of fluid dynamics. These governing equations have four different forms based on how they are derived: integral and partial differential form, conservation and nonconservation form. They are not fundamentally different equations but the same equation in four different forms [3].

The conservation of mass (The Continuity Equation) expresses the fact that mass cannot be created or disappear in a fluid system, the net mass transfer to or from a system during a process is equal to the net increase or decrease in the total mass of the system throughout the process [4]. The partial differential equation form of the continuity equation is shown in Equation 2-1 [3].

$$\frac{\partial \rho}{\partial t} + \vec{\nabla} \cdot \rho \vec{v} = 0 \qquad (2\text{-}1)$$

Where ρ is the density of fluid (kg/m^3); t is time (seconds); $\vec{v}$ is velocity vector (m/s);.

The conservation of momentum (Newton's second law), as shown in Equation 2-2, describes how the force action on the particle is equal to the mass of the particle times its

acceleration. When applied to the fluid element it states that the variation of momentum is caused by the net force acting on a mass element. The conservation form, partial differential equation, called the Navier-Stokes equation, is shown in Equation 2-3 [3].

$$F = ma \tag{2-2}$$

Where F is body force (N), m is mass (kg), and a is acceleration (m/s^2).

$$\frac{\partial(\rho\vec{v})}{\partial t} + \vec{\nabla}\cdot(\rho\vec{v}\vec{v}) = \vec{\nabla}\cdot p + \vec{\nabla}\cdot\vec{\vec{\tau}} + \rho\vec{b} \tag{2-3}$$

Where in addition to the variables defined in equation 1 and 2, $\vec{\vec{\tau}}$ is viscous stress tensor (newton) given by Equation 2-4, $\vec{b}$ is body force vector (newton), and μ is the molecular viscosity coefficient.

$$\vec{\vec{\tau}} = \mu\left(\vec{\nabla}\vec{v} + \left(\vec{\nabla}\vec{v}\right)^T\right) - \frac{2}{3}\mu\left(\vec{\nabla}\vec{v}\right)\vec{\vec{I}} \tag{2-4}$$

The conservation of energy (the first law of thermodynamics) states that energy can neither be created nor destroyed, but can only change forms. Specifically, it states that any changes in time of the total energy inside the volume are caused by the rate of work of forces acting on the volume and by the net heat flux into it [4]. The conservation form, partial differential equation is shown in Equation 2-5 [3].

$$\frac{\partial\rho e}{\partial t} + \vec{\nabla}\cdot(\rho e\vec{v}) = \rho\dot{q} + \vec{\nabla}\cdot\left(k\vec{\nabla}T\right) - \vec{\nabla}\cdot(p\vec{v}) + \vec{\nabla}\cdot\left(\vec{\vec{\tau}}\cdot\vec{v}\right) + \rho\vec{b}\cdot\vec{v} \tag{2-5}$$

Where $\dot{q}$ is the rate of volumetric heat addition per unit mass , T is temperature, e is internal energy per unit mass.

2.2.2 Steady and unsteady flow

The behavior of state of a fluid, such as velocity, pressure and density, generally vary with respect to space and time. A steady flow is one in which the state of the fluid may differ from point to point but do not change with time. Otherwise, if at any point in the fluid, the conditions change with time, the flow is described as unsteady [6]. Realistically, there is always slight variation in velocity and pressure in flow, but if the average values are constant, the flow can be considered steady to study the problems effectively [6].

2.2.3 Laminar and turbulent flow

If the particles of fluid move in straight lines even though the velocity with which particles move along is not necessarily the same, the fluid may be considered as moving in layers

and called laminar flow. Contrarily, if the paths of fluid particles are in a random and disorderly manner and a thorough mixing of fluid takes place, the flow is considered turbulent [7].

Reynolds number (*Re*) is evaluated to determine whether the flow is laminar or turbulent. It is calculated using Equation 2-6. For internal flow where ρ is the density (kg/m^3), u is the mean velocity over the cross section (m^2/s), l is the pipe diameter or the hydraulic diameter for non-circular ducts (m) and μ is the dynamic viscosity of the fluid (Pa.s). Under normal engineering conditions, flow through pipes at $Re < 2000$ may be regarded as laminar, $Re > 4000$ may be taken as turbulent flow and $2000 < Re < 4000$ are treated as transitional flow, which is a mix of laminar and turbulent flow [6].

$$Re = \frac{\rho u l}{\mu} \tag{2-6}$$

The flow in mine gob is treated as laminar flow in porous media in many studies. However, the real flow inside gob is still not fully understood, and the laminar flow assumption may not be valid [8], [9]. For most CFD codes, the modeling of transitional flow is usually not provided. But since most times the transitional flow only covers a small region of the total flow domain, it could be neglected and still allow for acceptable results [10], [11].

In underground mine ventilation, most flow states in mine openings are turbulent, which allow for effective dispersion and removal of contaminants in the workplaces [12]. There are many turbulence models available; however, none of the existing turbulence models is universally accepted as being superior for all turbulent problems. Some of the well-known turbulence models are discussed below.

Direct numerical simulation (DNS) solves the Navier-Stokes equations directly and resolves all the scales of motion. It is the simplest approach and provides the most accuracy. However, DNS requires very high grid resolution, thus, it has extremely high cost, and the cost increases rapidly with the Reynolds number (approximately as Re^3). For this reason, the DNS approach was impossible until the 1970s when acceptable computational capability was achieved. The DNS approach can provide valuable information for verifying or revising other turbulence models, but the application is limited to fundamental studies, with low or moderate Reynolds numbers flows [13–15].

However, for most engineering applications resolution of turbulent fluctuations in detail is unnecessary. Therefore, some common turbulence models are based on the Reynolds averaged Navier-Stokes equations (RANS) model which solves the Reynolds equations for the mean

velocity field through time averaging. The RANS models are determined by either the turbulent viscosity hypothesis or modeled Reynolds-stress transport equations [13]. The turbulent viscosity hypothesis is also called eddy viscosity hypothesis, and was introduced by Boussinesq in 1877. It states that the deviatoric Reynolds stress $(-\rho\langle u_i u_j\rangle + \frac{2}{3}\rho k\delta_{ij})$ is proportional to the mean rate of strain [13], which is shown below,

$$-\rho\langle u_i u_j\rangle + \frac{2}{3}\rho k\delta_{ij} = \rho\nu_T\left(\frac{\partial\langle U_i\rangle}{\partial x_j} + \frac{\partial\langle U_j\rangle}{\partial x_i}\right) = 2\rho\nu_T\overline{S}_{ij} \quad (2\text{-}7)$$

Where ν_T is the turbulent viscosity.

Although the turbulent viscosity hypothesis has not been justified and has poor accuracy for many flows [13], many of today's most widely used turbulence models are based on it.

2.2.3.1 The standard *k*-*ε* model

The standard *k*- *ε* model is a two-equation model that computes the Reynolds stresses by solving two additional transport equations, which are for the turbulence kinetic energy, *k* in equation 2-8, and the dissipation rate of turbulence, *ε* in Equation 2-9 [16], [17].

$$\frac{\partial(\rho k)}{\partial t} + div(\rho kU) = div\left[\frac{\mu_t}{\sigma_k} grad\ k\right] + 2\mu_t E_{ij}\cdot E_{ij} - \rho\,\varepsilon \quad (2\text{-}8)$$

Where E_{ij} is the mean rate of deformation tensor.

$$\frac{\partial(\rho k)}{\partial t} + div(\rho\varepsilon U) = div\left[\frac{\mu_t}{\sigma_\varepsilon} grad\ \varepsilon\right] + C_{1\varepsilon}\frac{\varepsilon}{k}2\mu_t E_{ij}\cdot E_{ij} - C_{2\varepsilon}\rho\,\frac{\varepsilon^2}{k} \quad (2\text{-}9)$$

Finally the turbulent viscosity μ_t in Equation 2-10 is derived from both *k* and *ε* [16], [17]:

$$\mu_t = C_\mu\rho\frac{k^2}{\varepsilon} \quad (2\text{-}10)$$

The model coefficients in the standard k- ε model are shown below [16], [17]:

$$(C_\mu, C_{1\varepsilon}, C_{2\varepsilon}, \sigma_k, \sigma_\varepsilon) = (0.09, 1.44, 1.92, 1.0, 1.3) \quad (2\text{-}11)$$

The standard *k*- *ε* model is the simplest complete turbulence model and widely used in the modeling of mining turbulent flow in broad range of applications. Yuan used the standard *k*- *ε* model in the ventilation airways to study the flow path in the gobs [8], and the spontaneous heating behavior in the gobs [18–21]. Similarly Ren [9] used the standard two equation *k*- *ε* model to estimate the turbulent transport in his gob spontaneous combustion study. However, these study results were not validated. Greg et al. [22] used the standard *k*- *ε* model in a coal dust explosions study and the results were validated with test data from a coal dust explosion test facility. Toraño et al. [23] used the standard *k*- *ε* model and Shear-Stress-Transport (SST) model in their study to evaluate the wind erosion effect on different coal pipe. They finally chooses the

standard *k*- ε model with a certain wall roughness parameter due to its better agreement with the US EPA wind tunnel measurements. Another study Toraño et al. [24] conducted used six different turbulence models to simulate dust behavior in auxiliary ventilation in mining roadways and compared their results with field measurements data, and the standard *k*- ε model provided better results. Silverster [11] states that the standard *k*- ε model is a more general but computationally intensive method and is favorable to be used in the field of mine ventilation. This turbulence model was also successfully used in the CFD study of dust dispersion [25] and minerals processing [26–29]. Many studies also indicate it can provide precise and good correlation between the measured and the simulated results [30–34]. However, the standard *k*- ε model is reported may produce inaccurate results under certain circumstances, especially for flows with rotation, curvature, strong swirl, three dimensionality, and flows with strong streamline curvature [5], [35]. This is partially because the turbulent viscosity hypothesis is not valid if turbulence is not isotropic and the ε equation has many empirical constants which have adverse effect on the predicted results [13].

2.2.3.2 The RNG *k*-ε model

The RNG *k*- ε model is an improvement on the standard *k*- ε model and it is derived from the statistical methods used in the field of renormalization group (RNG) theory [36]. It is similar in form to the standard *k*- ε model but includes modifications in the dissipation equation to better describe flows in high strain regions, and a different equation is used for effective viscosity. The turbulent kinetic energy and the dissipation rate equation are shown below:

$$\rho U_i \frac{\partial k}{\partial x_i} = \mu_t S^2 + \frac{\partial}{\partial x_i}\left(\alpha_k \mu_{eff} \frac{\partial k}{\partial x_i}\right) - \rho\varepsilon \tag{2-12}$$

$$\rho U_i \frac{\partial \varepsilon}{\partial x_i} = C_{1\varepsilon}\left(\frac{\varepsilon}{k}\right)\mu_t S^2 + \frac{\partial}{\partial x_i}\left(\alpha_\varepsilon \mu_{eff} \frac{\partial \varepsilon}{\partial x_i}\right) - C_{2\varepsilon}\rho\left(\frac{\varepsilon^2}{k}\right) - R \tag{2-13}$$

Where $S \equiv \sqrt{2S_{ij}S_{ij}}$, $S \equiv \frac{1}{2}\left(\frac{\partial U_j}{\partial x_i} + \frac{\partial U_i}{\partial x_j}\right)$, and α_k, α_ε, $C_{1\varepsilon}$, $C_{2\varepsilon}$ are derived from the RNG theory [17].

2.2.3.3 The realizable *k*- ε model

The realizable *k*- ε model share the same turbulent kinetic energy equation as the standard *k*- ε model, but a variable C_μ as shown in Equation 2-14, instead of a constant, to calculate the turbulent viscosity using Equation 2-10 [17].

$$C_\mu = \frac{1}{A_0 + A_s \frac{U^* k}{\varepsilon}} \tag{2-14}$$

Where A_0=4.04, $A_s = \sqrt{6}\cos\emptyset$, $U^* = \sqrt{S_{ij}S_{ij} + \Omega_{ij}\Omega_{ij}}$, $\emptyset = \frac{1}{3}\cos^{-1}(\sqrt{6}W)$, $W = \frac{S_{ij}S_{ji}S_{ki}}{\tilde{S}}$, and $\tilde{S} = \sqrt{S_{ij}S_{ij}}$.

Also a new transport equation is used for dissipation rate, which is shown in Equation 2-15 [17].

$$\rho\frac{D\varepsilon}{Dt} = \frac{\partial}{\partial x_i}\left[\left(\mu + \frac{\mu_t}{\sigma_\varepsilon}\right)\frac{\partial \varepsilon}{\partial x_j}\right] + \rho c_1 S\varepsilon - \rho c_2 \frac{\varepsilon^2}{k + \sqrt{\nu\varepsilon}} + c_{1\varepsilon}\frac{\varepsilon}{k}c_{3\varepsilon}G_b \tag{2-15}$$

This model is better than other *k*- ε models for many applications, and has especially improved the modeling of planar and round jets, boundary layers under strong adverse pressure gradients or separation, and rotation and recirculation flows [17], [36].

2.2.3.4 Reynolds stress closure models (RSM)

The Reynolds Stress Model (RSM) is a higher level, elaborate model. The turbulent viscosity hypothesis is not needed in this model and individual Reynolds stresses $\langle u_i u_j \rangle$ are directly computed from the model transport equations [13]. The advantage of RSM is that it introduced terms accounting for anisotropic effects into the stress transport equations, which are critical for flows with significant buoyancy, streamline curvature, swirl or strong circulation [37]. More detail about this model can be found in Pope's book [13] or Durbin's study [38]. RSM can produce more realistic and rigorous solutions for complicated engineering flow, but it requires more execution time and memory, and it can be difficult to achieve good convergence behavior using this model[5].

2.2.3.5 Spalart Allmaras model (SA)

This model was developed by Apalart and Allmaras [39], and is a one equation model first used in aerodynamic applications. In this model, the turbulent viscosity ν_T is solved by a single model transport equation. The model equation is provided blow

$$\frac{\overline{D}_{\nu_T}}{\overline{D}_t} = \nabla \cdot \left(\frac{\nu_T}{\sigma_\nu}\nabla\nu_T\right) + S_\nu \tag{2-16}$$

Where $\boldsymbol{S}_\nu$the source term which depends on the laminar viscosity ν, turbulent viscosity ν_T, the mean vorticity $\boldsymbol{\Omega}$, the turbulent viscosity gradient $|\nabla\nu_T|$, and the distance to the nearest wall l_w [13]. This model is intended for aerodynamic flow, such as transonic flow over airfoils,

and its application to aerodynamic flows has proved successful [13]. For more detail about the model, one can refer to the original paper [39].

Wala et al. [40] used different turbulent models to simulate the air flow and methane distribution in a ventilation test gallery. The results from the shear-stress transport (SST) and the Spalart Allmaras (SA) model were presented. Both models were successful in predicting the methane concentration and the airflow distributions, while one may better than the other in different scenarios. Parra et al. [41] also applied the SA turbulent model in the study of deep mine ventilation efficiency. Good velocity agreement was achieved comparing to the experimental values.

2.2.3.6 Large eddy simulation (LES)

Large eddy simulation (LES) directly represent the larger three-dimensional unsteady turbulent motions [13]. A filter operation is applied to the Navier-Stokes equations to eliminate small scales of the solution. LES resolves large scales of the flow field solution and can be expected to be more accurate and reliable than alternative approaches such as RSM and RANS. It is especially much better suited to unsteady effects than RANS [42]. The computational expense lies between RSM and DNS models [13]. It is also a very computational expensive method and the prediction results may not improve for fully developed turbulent flow, compared with the k- ε model [43]. Because it is at a much earlier stage of development than RANS modeling, few applications were found in the mining related fields. One example is Edwards and Hwang [44] used the LES method in Fire Dynamics Simulator (FDS) to study fire spread in the mine entry. The results were compared with measured values and the differences were reasonably interpreted.

2.2.3.7 Summary

There is no clearly superior model which works well over different applications. For general engineering turbulent modeling, Bakker [17] recommend that start the calculation using standard k- ε model. For very simple flows that contain no swirl or separation, converge the calculation with second order upwind scheme. For flow involves jets, separation, or moderate swirl, converge the solution with the realizable k- ε model and seconder order difference scheme. If swirl dominates the flow, then RSM and a second order differencing scheme are

recommended. Other models should only be used if there is evidence from the literature proving they are especially suitable for the interested problem.

2.2.4 Numerical analysis

All methods in CFD use some form of discretization which can be classified as finite-difference, finite-volume, and finite-element. CFD can be approached using any of the three main types of discretization mentioned above [3].

Finite difference method (FDM) is among the first approaches applied to the numerical solution of differential equations and is widely employed in CFD. It is applied to the differential form of the governing equations. It uses Taylor series expansion for the discretization of the derivatives of the flow variables. Finite difference method is simple and allows for one to obtain high-order approximation to achieve high-order accuracy. However, the application is restricted because this method requires structured grids and can only be applied to simple geometries due to the reason that it cannot be applied directly in body-fitted coordinates. Thus, finite difference methodology is rarely used for industrial applications [4].

Finite volume method (FVM), which is derived from the finite difference method, directly satisfies the integral form of the conservation law and uses the integral form of the governing equations. It discretizes the governing equations by dividing the domain of interest into several arbitrary polyhedral control volumes, and then integrates the differential form of the governing equations over each control volume. Finite volume methods have two primary advantages which make popular for use in CFD codes, including CFX, FLUENT, and PHOENICS. The primary advantage is that the spatial discretization is accomplished directly in the physical space. It naturally achieves the coordinate system transformation between the physical and computational domain. Secondly, finite volume methods not only can be easily implemented on structured grids, but also do not require a coordinate transformation in order to be applied on unstructured grids. Therefore, the flexibility of finite volume methods are particularly suitable for treating complex geometries [4], [45].

The finite element methods (FEM) need the governing equations to transform from differential form to integral form and start with dividing the physical space into triangular or tetrahedral elements. It is popular because it uses integral form and unstructured grids, which are

preferable for complex geometries. However, the popularity in solving the CFD governing equations using these methods only started in the early of the 90's [4].

2.3 Commercial CFD codes

Tremendous progress has been made in the development of CFD codes since the 1990s; hence, the use of CFD codes has increased dramatically in the last few years. The commercial CFD codes are the primary source of tools in use by the mining industry and other engineering communities. The powerful application of these commercial codes to model complex flow in many research and design fields makes them much more attractive. Some of the common commercial codes are listed in Table 1. Most of the commercial CFD codes use the finite volume method due to the fact that it satisfies the integral form and allows for treatment of complex geometry. These codes employ graphical user interfaces and can be supported on the platforms of UNIX, Linux and Windows on workstations or PCs.

Table 1. Commercial CFD code

CFD code	Company	Web site
FLUENT	Anysys	http://www.ansys.com/Products/Simulation+Technology/Fluid+Dynamics/ANSYS+FLUENT
CFX	Anysys	http://www.ansys.com/Products/Simulation+Technology/Fluid+Dynamics/ANSYS+CFX
PHOENICS	CHAM	http://www.cham.co.uk/
CFD-ACE	ESI	http://www.esi-group.com/products/Fluid-Dynamics/cfd-ace-multiphysics-suite
CFD 2000	Adaptive	http://www.adaptive-research.com/cfd2000_software.htm

2.4 CFD commercial software analysis process

There are generally three stages to perform CFD analysis: preprocessing, solving and postprocessing. Figure 2 shows the flow chart of CFD analysis process.

Preprocessing is the first step in building and analyzing a CFD model taking place before the numerical solution process. The first step of the analysis process is to consider and understand the flow problem. The second step is to create the geometry of the problem. CAD geometries can be imported and adapted for CFD software. Approximations and simplifications of the geometry may be needed to analyze the problem with reasonable effort. Then a suitable computational mesh needs to be created and applied to the problem domain. After the mesh has been developed, boundary conditions and initial conditions should be specified according to the physical conditions which give the simulation a starting point. Finally, the flow problem is specified by the fluid parameters, physical properties and solving techniques.

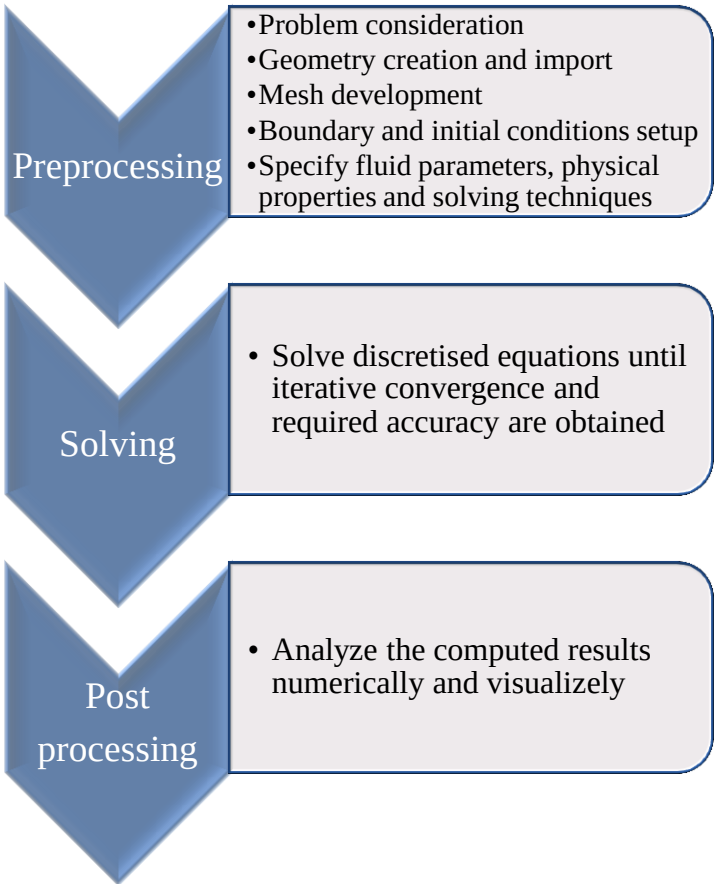

Figure 2. Flow chart of CFD analysis process

Iterative methods are usually used to solve the discretized equations until a predetermined convergence and required accuracy are obtained.

Postprocessing is the final step in CFD analysis. It organizes and interprets the data generated by the CFD analysis. The results can be analyzed both numerically and graphically. Some powerful commercial CFD software not only creates visualization graphs, including contour, vector, line plots and even animations, but also allows for export of CFD data to third-party postprocessors and visualization tools such as TechPlot. The illustrative presentation of the results allows the designer or researcher to have increased understanding of the interested problems, thus, understand how the system responds to a variety of different operating conditions [46].

After these three steps of processes, in order to better understand the possible differences in the accuracy of results and performance of the computation with respect to physical properties and important parameters such as flow conditions and boundary conditions, the process may need to be repeat in order to exam the sensitivity of the computed results.

Although the commercial softwares are user-friendly, the simulation process, especially analyzing the results, requires complete understanding of the underlying physics, and sometimes a model needs reasonable assumptions and improved boundary conditions to make it manageable. Therefore, dependable results cannot be achieved without specialized training and sound engineering skills [46].

2.5 Quality control of CFD

As aforementioned, CFD is increasingly used in the research and design of ventilation and other fluid systems with in the mining industry. Conscientious execution during the process of CFD studies is of paramount important to ensure quality CFD results because modeling and numerical errors and large deviations may occur in such studies. This section looks at the various techniques that are necessary to improve the quality of CFD calculations. Finally, guidelines for CFD quality control procedures are provided which are recommended in CFD-related studies.

2.5.1 Mesh quality and convergence

It is complicated work to discretize the computational domain into a suitable computational mesh. Mesh generation may account for the majority of time spent on a CFD study in order to generate a proper mesh that allows for a compromise between desired accuracy and computational cost [47]. The following discusses reasonable mesh quality, mesh size, and mesh convergence which ensure a high-quality computational solution.

2.5.1.1 Mesh convergence

It is important to conduct a mesh independence study before utilizing CFD results since the numerical solution may depend on the mesh size if mesh independence is not reached [48]. However, obtaining a mesh-independent solution is almost impossible due to computational expense. The mesh convergence, which is a relaxed criteria of mesh independence, states that the solution asymptotically approaches the exact solution of the governing equations [43]. This is the more practical method which requires the solution does not change significantly as mesh is further refined.

By comparing the results of different mesh sizes, mesh convergence should be studied considering different flow features and different representative locations. Flow features usually

used to check mesh convergence are velocity profile along a line, velocity contours and vectors at interested locations, temperature distribution, and contaminant concentration.

Grid Convergence Index (GCI) [49] can be used for uniform grid refinement studies in CFD. GCI provides a conservative estimate of the error between fine grid solution and the unknown exact solution [43]. GCI is expressed as

$$GCI_{fine\ grid} = \frac{F_s|\epsilon|}{r^p - 1} \tag{2-17}$$

Where F_s is the factor of safety and recommended by Roache for two grid comparisons; p is the formal order of accuracy; r is the grid refinement ratio (usually is 2) $r = \frac{h_2}{h_1}$, in which $h_1 and\ h_2$ are mesh size for fine and coarse grid, respectively. ϵ is the relative error which is shown below

$$\epsilon = \frac{f_2 - f_1}{f_1} \tag{2-18}$$

Where f_1 and f_2 are any solution of interest, such as velocity, contaminant concentration, temperature, of fine grid and coarse grid, respectively.

This approach is intentionally developed for uniform grids, and the calculation should be within the asymptotic range of convergence [49]. Refer to the original paper for detailed derivation and application of the method.

2.5.1.2 Near wall mesh size

The wall treatment in turbulent flow models is very important, because the wall is in the viscosity-affected regions which have large gradients in the solution variables. A successful prediction of wall bounded turbulent flows are determined by the accuracy of the near wall region [47]. A y^+ strategy can be used as guidance in selecting the suitable grid configuration and corresponding turbulence models.

The wall y+ is a mesh-dependent dimensionless distance from the wall expressed as in Equation 2-19:

$$y^+ = \frac{u_\tau y}{\mu} \tag{2-19}$$

There are three regions in the boundary layer [50]:

1. Laminar sublayer (y+ < 5)
2. Buffer region (5 < y+ < 30)
3. Turbulent region (y+ > 30)

A high degree of mesh refinement in the boundary layer is required for low Reynolds number turbulence models, because it solves it solve the governing equation all the way to the wall. The first grid normally should be located at $y^+ \leq 1.0$ [5]. While for high Reynolds number

models, an empirical law-of-the-wall relations for the flow regime of the boundary layer is used. It does not consider the damping effects of a wall and the computation must start at a point in the fully turbulent region. In this case, the mesh does not need to extend into the boundary layer region, and the number of computational cells is consequentially reduced [5], [43].

Different turbulent flow models require different ranges of y^+, and recommendations are usually available for different CFD code. For example, Ansys Fluent recommend using either very fine near wall mesh, on the order of $y^+ = 1$, or coarse mesh that $y^+ \geq 30$. These recommendations should be used when using a specific CFD code [43].

Ariff et al. [51], [52] conducted a series studies using the wall y^+ approach to compare the influence of different near wall mesh sizes and different turbulent flow models. The y^+ value (near wall mesh size) was chosen according to the Fluent User's Guide. The study provided guidance on selecting appropriate mesh configuration and turbulence model.

2.5.2 Solution convergence

The numerical solution is an iterative process. A steady-state solution requires the solution converge to an accurate approximation of the exact solution. In order to monitor how much the solution changes with each iteration, a residual is introduced, which is a quantity that measures the unknown error. One definition of the residual is shown in Equation 2-20 [15], [53].

$$R \equiv \sqrt{\frac{\sum_{i=1}^{N}(u_i - u_{i-1})^2}{N}} \tag{2-20}$$

Where u_i is the solution of this iteration, u_{i-1} is the solution of last iteration, and N is the number of grids or cell in the calculation domain. The scaled residual is shown in Equation 2-21.

$$R \equiv \left(\sqrt{\frac{\sum_{i=1}^{N}(u_i - u_{i-1})^2}{N}}\right) \Big/ \left(\frac{\sum_{i=1}^{N} u_i}{N}\right) = \frac{\sqrt{N\sum_{i=1}^{N}(u_i - u_{i-1})^2}}{\sum_{i=1}^{N} u_i} \tag{2-21}$$

The scaled residual is often used which is a relative measure to the average value calculated in the domain, rather than an absolute measure.

Commercial CFD codes usually provide default convergence criterion, such as stop the computation if the residual is reduced to a four-order-of magnitude. The solution is assumed converged when the residual is below the default criterion. However, the default convergence criterion is not always sufficient to ensure that the solution is converged. Some times smaller convergence criterion need to be apply to achieve an accurate solution [43].

Sometimes the residual may reached the convergence criterion, but the solution still changes with further iteration, which means a stable solution has not been reached. Therefore, in addition to monitoring the residual, the selected solution variables must be monitored until they no longer change with more iteration. A point monitor can be set up to monitor the solution (velocity, temperature, etc.). If the solution profile indicates no change as the iterations proceed, the solution is considered converged [15]. Monitoring selected variables at certain points is recommended after the residual monitor, as part of the solution convergence assessment [15].

2.5.3 CFD verification and validation

Verification and validation are essential processes required to achieve reliable CFD results. Verification and validation assess the credibility of the CFD results. Verification deals with the mathematical correctness of a numerical solution, whereas validation deals with the physical correctness of model. Verification and validation are extensive topics with much literature devoted to them. This section will only briefly discuss these topics along with their application to mining research.

2.5.3.1 Verification

Verification deals with the mathematical correctness of the CFD solution including two topics: code verification and solution verification. Mining engineering usually uses commercial CFD code or already developed and verified CFD code, which already ensures there are no unknown errors (or minimal errors) in the computer code. In this situation, code verification is not necessary. The main task in solution verification is error estimation. There are three sources of numerical errors in CFD: the round off error, the iterative convergence error, and the discretization error. The round off error is due to the finite precision arithmetic of computers. It isusually negligible compared to the two other sources of error and will not be further discussed. The iterative convergence error comes from the inexact solution of the algebraic system by some iteration method. The discretization error is due to the replacement of the differential equations by partial different equations. These two kinds of errors can be reduced by conducting the mesh convergence study and solution convergence study mentioned previously. Verification must take place before validation, otherwise the computed results may agree with the experimental results only by chance [54], [55].

2.5.3.2 Validation

Validation deals with the physical correctness of the CFD model. It usually conducted by comparing modeled data to experimental data [55]. Validation is very important in the field of CFD studies because it provides the degree of confidence necessary for the CFD results application. This section discusses different techniques that have been used in the validation of mining CFD models.

Laboratory studies have traditionally been used to study mine ventilation and other fluid problems in the field of mining. Jade [56] conducted a CFD study to estimate shock loss coefficients in two-way splits and junctions in mine airways. The CFD results are reasonably close to that of experiments conducted in a designed laboratory setup, which showed the potential of CFD in predicting airflow and shock loss in mine airways. Collecutt et al. [22] calibrated their CFD model by comparing to a laboratory scale experiment before modeling an actual dust explosion in a tunnel. The laboratory studies usually use physical scale models. In this case, the laboratory results are only valid when geometric and dynamic similarity are achieved between the physical model and its prototype. Geometric similarity requires the model to have the same linear scale ratio in three dimensions, and dynamic similarity requires the model and the prototype to have the same length, time, and force scale ratio. For incompressible flow with no free surface, this requires the Reynolds numbers (*Re*) to be the same; and if a free surface is exist, the Reynolds (*Re*), Froude (*Fr*), and Weber (*We*) numbers need to be the same. Compressible flow scenarios require the Mach number to be the same.[35]. However, the dynamic similarity is often difficult or impossible to obtain. Moloney [35] built a $1/10^{th}$ scale model for the purpose of validating the CFD model, but the model could not meet dynamic similarity, because it required a 62 m/s exit velocity, which is not practical in the lab. The same challenge was faced by Ndenguma [32] when a 15% scale model required an impractical exit air velocity of 152 m/s. Instead of meet the dynamic similarity, a percentage volume flow method was used to scale the air flow.

The experimental results found in the literature could also be used to validate a CFD model. In Toraño's CFD study [23], which focuses on the effect of wind erosion on different coal storage pile shapes, the numerical model was validated by the US EPA experimental reference study to ensure that the CFD model was accurate and valid for situation. The Root Mean Square values of deviation, shown in Equation 2-22, were used to quantitate the difference

between the CFD and the EPA experiment results, and a 3.75% deviation was found, which indicated the CFD model was accurate enough.

$$RMS = \sqrt{\frac{1}{N}\sum_{i=1}^{N}(y_i - \hat{y}_i)^2} \quad (2\text{-}22)$$

Another method used to validate a CFD model is to use the data obtained from field or on site full scale experiment. For example, Peng et al. [57] developed a 2D dense-medium separator CFD model to analyze the flow patterns and the mechanisms of particle separation in the separator. The in-plant test results, which showed a close fit to the simulated results, were used for the CFD validation. Similar validation can be found in Peng's other work detailing CFD studies of mineral separation [58]. Toraño et al. [59] used an anemometer and methane detector to obtain velocity and methane concentration data which were than used for the CFD model validation. The best CFD model was then chosen based on the least experiment and simulated differences. Parra et al. [41] conducted a detail ventilation measurement in a real mine gallery using an anemometer to validate the numerical model, and the grid size and the algorithm used for the simulation were guaranteed acceptable by achieving good agreement. The validated model was then used to simulate different combinations of blowing and exhaust ventilation methods. However, sometimes it is hard to conduct accurate field measurement, and it is common for the measured field data have error up to 20% [60].

The use of tracer gases started in the 1950s in building ventilation systems [61]. Tracer gas techniques have been used in many situations where the standard ventilation survey methods are inadequate [1]. The applications of tracer gases in underground mines include analyzing ventilation patterns, measurement of air leakage rates, and evaluating dust control methods [62]. For this reason, tracer gas is sometimes used for CFD model validation. Krog et al. [63] used CFD to study the airflow patterns around the longwall panels and used SF_6 as a tracer gas to validate the CFD model. Konduri et al. [64] used CO_2 as a tracer gas in their field experiment to determine effective ventilation air quantities when a jet fan was used for auxiliary ventilation, and the measured results were used to compare with the CFD simulated results.

Flow visualization has long been used in the fluid flow research, and can be used for CFD validation. A visual comparison of the results from the experiments and the CFD calculation provides effective means of CFD validation [65]. There are three basic visualization

techniques: adding foreign material, optical techniques, and adding heat and energy [65]. Moloney et al. [35] conducted an experiment using the laser sheet flow visualization technique, combined with the CFD studies to evaluate different ventilation methods. In another study, Wala et al. [66] utilized a Particle Image Velocimetry (PIV) system to visualize the airflow patterns in a physical scaled mine model and validate CFD models. PIV is an optical technique that can measure flow components in a plane. Highly reflective tracer particles need to be added to the flow field. The motion of the particles can be recorded by a camera and the tracer particles are illuminated twice within one camera shot. The processed results can display velocity vectors of the flow field and potentially be used to compare CFD velocity vectors in the same plane. Ndenguma [32] used smoke to visualize the flow patterns in a scale mine heading model ventilated by jet fan and scrubber. The flow patterns represented by the smoke which were recorded using a camera were similar to those presented from the CFD results.

Velocity agreement between experimental and CFD results is a major indicator of validated CFD model. Therefore it is necessary to accurately measure flow velocities. Moloney et al. [35] conducted a $1/10^{th}$ scaled mine auxiliary ventilated headings experiment to validate the corresponding CFD model. Laser Doppler Velocimetry (LDV), which can measure two components of velocity without disturbing the natural flow patterns, was used to measure flow velocities and validate CFD model. Hargreaves and Lowndes [67] used a Trolex TX6522 Multisensor unit and TX5924 vortex shedding anemometer, which are intrinsically safe devices, to measure and record air speed in an underground coal mine. However, because the anemometer can only measure airflow perpendicular to the measurement gate, and airflow in the mine is usually three dimensional, the measurement of the airflow and data interpretation is difficult. Therefore, a multi-directional intrinsically-safe anemometer is needed to adequately map the complicated flow patterns in mines. Taylor et al. [68] used an ultrasonic anemometer to measure three dimensional air flow velocities in a simulated mine entry. The results of the ultrasonic anemometer were used to generate the quantitative flow profile using vectors, which includes the direction and magnitude of flow. These results were later used for CFD validation purposes [40]. In addition, the advanced experimental methods, such as LDV and PIV, have been widely used to give detailed information on the turbulent flow field in stirred vessels and validation for the CFD studies in the process industry [26], [69–72].

2.5.3.3 Procedures in CFD study

In order to achieve high quality CFD results, certain procedures need to be followed. Figure 3 shows the basic steps in a complete CFD study.

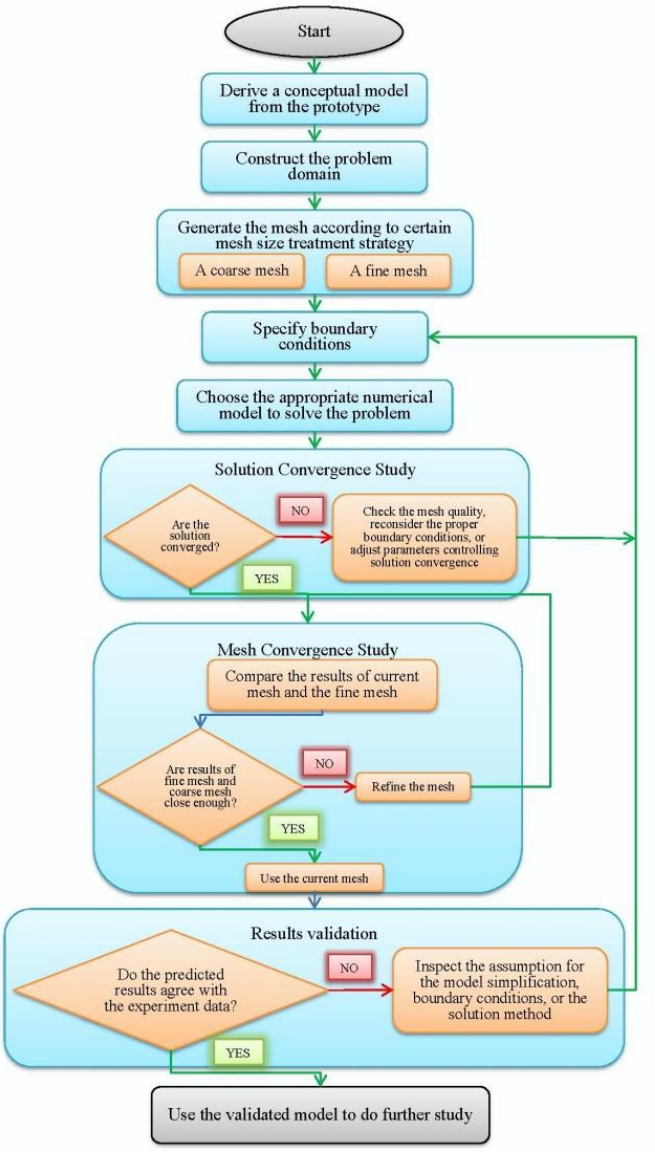

Figure 3. Basic steps in CFD study

2.6 CFD application in mining

CFD modeling has been used as a tool of research and design in the mining industry in many areas to assist understanding and analyze the mechanism of fluid flow in order to improve efficiency, safety, and health. This paper organizes mine ventilation related CFD applications into the following categories for convenience, although these categories are often interrelated.

2.6.1 Mine ventilation airflow

CFD is widely applied to the study of ventilation to improve the quality, quantity and control of ventilation, which can further assist in the improvement of gas, dust and climate control [67].

Wala conducted a series of studies aiming at validating CFD code by comparing the CFD results against mining-related benchmark experiment results [40]. He pointed out that although significant studies have been conducted using full-scale field tests or scaled physical modeling to evaluate the face ventilation system performance and have improved the ventilation effectiveness, there are still some doubts on the results due to the complexity of the ventilation and the limitation of experimental methods. Traditional theoretical and experimental methods can produce valuable results, but they are limited in completeness and accuracy. CFD is a promising tool which embraces a variety of technologies and can overcome the disadvantages mentioned above if the CFD solution has been validated. CFD 2000 was used to determine the optimum design of an upcast shaft and main fan ductwork arrangement [73]. The CFD model was first validated by existing experimental data available in other literature with reasonable agreement. Then the author designed four different shaft collar and shaft cover arrangements and simulated them with the validated CFD model. A best design was determined by analyzing the simulated results which could reduce the power cost due to less pressure loss. They took CFD validation studies a step further by performing several experiments in a scaled physical face-ventilation model and comparing a CFD model with the experimental results in order to validate the work [40]. Methane concentration and three-dimensional airflow were measured and compared with the CFD results. They conducted a grid independence study, used the SIMPLE algorithm to achieve pressure velocity coupling of momentum and continuity equations and compared two turbulence models: the Shear-Stress Transport (SST) model and the Spalat-Allmaras (SA) model. These two models can be both used to simulate methane concentration and airflow distributions, but the SST model achieved better results in the box-cut scenario, while the SA model showed better agreement with the experimental results in the slab-cut scenario. Furthermore, a CFD study was carried out to study the effect of scrubbers on the face airflow and methane distribution during the box cut mining sequence [74]. The SST turbulent model was used in the CFD simulation, and the methane concentration results were compared under four different scenarios for CFD and experimental results. The results showed that the

scrubber improved the face ventilation. However, they indicated further study was needed determine the reason for some of the differences between experimental and simulated data. Some other CFD studies carried out by the same group of authors were presented [75], which showed the great potential of CFD in studying the underground airflow and improving the health and safety of miners.

Jade used a laboratory experiment and CFD simulation study to investigate the shock loss at the 90 degree intersections of two-way splits and junctions [56]. The shock loss coefficients (SLC) results showed that the CFD models are validated well with the experimental data. The SLC results were compared with previous literature and found that the literature underestimates the SLC by 50% or more for two-way junctions, and 20% for straight branch, thus, concluding that the widely accepted methodologies significantly underestimate SLC of two-way splits and junctions. The study also conducted regression analysis and obtained various equations for two-way 90 degree splits and junctions.

Zheng studied the Diesel Particular Matter (DPM) in an underground metal/nonmetal mine using CFD [76]. The study investigated the airflow and diesel exhaust propagation patterns. The study assumed that DPM movement can be represented by the air flow pattern since a very small fraction of DPM exists in the air. A model was built, which represents part of a mine in Missouri with highly mechanized room-and-pillar mining. The main air flow was simulated with and without stoppings. The model showed that although the DPM conditions are much improved by stoppings, some places still need auxiliary ventilation for adequate dilution. These places are dead end headings, cross cuts, and downstream of the backfill block. The study also evaluated the effectiveness of both blower and exhaust system to reduce DPM problems. The CFD model simulated a single heading with a loader and truck operating in the immediate face. The results showed that with the blower system the DPM is distributed in a smaller space than the exhausting system, but the loader driver in both systems would be working in a high DPM environment. Therefore, they determined that other strategies are needed to improve the situation. Overall, this study showed that CFD method can be used to simulate the airflow patterns for the entire mine or part of it, the ventilation efficiency and different ventilation measures can be evaluated.

Parameters such as velocity and contaminant concentration are broadly studied to evaluate the underground ventilation system. However, the more restrictive parameters, such as

mean age of air, which are used for evaluating ventilation in public places, are not commonly used to evaluate underground ventilation efficiency. Parra [41] points out that the mean age of air and local levels of pollutants' concentration in risk areas are better factors to qualify the ventilation quality. He used a validated CFD model to evaluate the effectiveness of three ventilation systems in deep mines: exhaust, blowing, and mixed, by analyzing the dead zones and the local mean age of air. The Spalart-Allmaras turbulent model was used and Navier Stokes equations for a three dimensional, steady, incompressible and isothermal flow are solved in the model. Dead zones are regions where velocity is below the regulated minimum velocity, but the dead zone criterion does not take into account the flow recirculation. The local mean age of air, $\bar{\tau}_p$, is obtained by solving Equation 2-23, [41]

$$V_i \frac{\partial \bar{\tau}_p}{\partial x_i} = \frac{\partial}{\partial x_i}\left\{\left(\frac{v_t}{\sigma_t} + \frac{v}{\sigma}\right)\frac{\partial \bar{\tau}_p}{\partial x_i}\right\} + 1 \quad (2\text{-}23)$$

Where $\boldsymbol{V_i}$ is the *i* component of the mean velocity, v is laminar viscosity, v_t is turbulent kinematic viscosity, σ is laminar Schmidty number, and σ_t is turbulent Schmidty number. Low air mean age indicates fresh air. The global efficiency, as shown in Equation 2-24, is used to compare different ventilation systems. An efficiency value of 1 represents a perfect displacement flow, and a value of 0.5 represents a perfect mixing flow.

$$\varepsilon = \frac{\bar{\tau}_{p,\,exiit}}{2\bar{\tau}_{p,\,\text{total}}} \quad (2\text{-}24)$$

Where $\bar{\tau}_{p,exiit}$ is local mean age in the outlet section and $\bar{\tau}_{p,\text{total}}$ is total local mean age.

Xicheng et al. used the same criterion, the dead zone and age of air, to study the effectiveness of the push-pull auxiliary ventilation system [77]. They point out that the effective range of a semi-confined jet can be determined by an equation, but there is no theoretical or experimental equation available to calculate the effective range of an exhausting duct due to its complexity. Thus CFD modeling is an approach to study it. The air age was calculated using Equation 2-25, where u_j is velocity, τ_p is the average air age, ρ is density, μ is laminar viscosity, μ_t is turbulent viscosity.

$$\frac{\partial}{\partial x_j}\left\{\rho u_j \tau_p - \left(\mu + \frac{\mu_t}{\sigma_t}\right) \times \frac{\partial \tau_p}{\partial x_j}\right\} = \rho \quad (2\text{-}25)$$

By examining the percentage of dead zones and the mean age of air of four different models, it was concluded that once the forcing duct position is determined, there is an optimum position for the exhausting duct in order to achieve the best efficiency.

Aminossadati et al investigated the effects of brattice length on fluid flow behavior in the crosscut regions [78]. CFD-ACE (ESI Software) was used in their study and k-ε turbulence model was employed. The results were compared with the results of FLUENT. The study indicated that airflow into the crosscut region was improved due to the use of brattice.

CFD can also be used to evaluate the fan effectiveness. Konduri et al. used a two-dimensional CFD model to simulate a jet fan for auxiliary ventilation and obtained similar results with the experiments [64]. Ray et al. used CFD to simulate the performance of vertically-mounted jet fans in a ventilation shafts [79]. The simulated results were compared with the calculated results, with validation using field measurements left as future work.

Mining is a dynamic process and airflow changes are associated with advance and retreat and the subsequent changes in mine geometry. However, it is particularly difficult to model a time dependent mining step together with the airflow simultaneously using CFD. Hargreaves et al. [67] use a series of steady-state computational models to represent the different stages of a tunnel drivage cutting cycle in order to assess the effectiveness and ventilation flow patterns of the force and machine mounted scrubber auxiliary ventilation system. The cutting cycle was decomposed into several representative steady-state stages and 24 simulations were carried out to replicate the whole cutting cycle. The simulation results were compared with the full scale ventilation experimental data. This study shows that CFD modeling can improve the understanding of auxiliary ventilation systems during different stages of cutting cycles and the results can be used to improve the planning and operation of auxiliary ventilation systems. The results of this study were later in conjunction with Virtual Reality (VR) technology to develop an improved ventilation planning and training tool [11].

2.6.2 Spontaneous combustion

Spontaneous combustion often occurs in the gob areas where events are difficult to locate and extinguish [8], and large-scale field experiments for the purpose of studying spontaneous heating in underground mines are particularly difficult[80].

Yuan conducted a series of large-scale CFD numerical modeling studies on spontaneous heating. He studied spontaneous heating in typical long wall gob areas with bleeder and bleederless ventilation systems with a stationary longwall face [18], [21], [81]. The estimated gob permeability and porosity profiles from a geotechnical model were used as inputs for the

CFD model using FLAC (Fast Lagrangian Analysis of Continua). The Kozeny-Carman equation, as shown in Equation 2-26, was used to estimate the changes in permeability in the caved rock. In the equation, *n* is the porosity and *k* is the permeability. The flow in the gob area is treated as laminar flow while fully turbulent flow was applied to ventilation airways. The studies showed the flow patterns inside the gob, and the effect of gob permeability, pressure at the bottom of bleeder shaft, resistance at collapsed entries, nitrogen injection, apparent activation energy, coal surface area, and critical velocity zones for spontaneous combustion were studied. The results of the CFD studies were reasonable according to experience and data from previous experiments and studies.

$$k = f\left(\frac{n^3}{(1-n)^2}\right) \tag{2-26}$$

The effect of barometric pressure changes on spontaneous heating in longwall panels was presented in another article by Yuan and Smith [19]. The actual recorded barometric pressure variations were used in a bleederless ventilation model and the oxygen concentrations were quantitatively examined. Results showed that the barometric pressure change will influence the maximum temperature of the spontaneous heating in the gob, although the influence is not significant. However, the influence was affected by the gob permeability and the coal oxidation rate.

Another study by Yuan and Smith examined spontaneous heating in a coal chamber utilizing CFD [80]. The results were validated by comparing results with a test from U.S. Bureau of Mines experiments and the results indicated similar phenomena. Theydemonstrated that the CFD model has the ability to reasonably reproduce the major characteristics of spontaneous heating in agreement with experimental test results and that the model is useful for predicting the induction time, which is key for prevention of spontaneous heating fires.

2.6.3 Mine fire

Mine fire is another challenging underground mine safety issue. The toxic gases,low visibility, and open flame caused by fires create a hazardous environment underground. Miners can be seriously injured by inhaling toxic products-of-combustion (POC), and the fire heat can cause rib and roof collapse [44], [82]. Underground coal fires also produce large amounts of CO2; for example, in one study in China, nearly 100 to 200 million tons of coal affected by underground coal fires were calculated to produce 2-3% of the total world CO2 emission [83]. A

number of studies are related to the investigation of mine fire and its combustion products utilized CFD.

A CFD study was conducted by National Institute for Occupational Safety and Health (NIOSH) and Mine Safety and Health Administration (MSHA) to investigate the temperature characteristics of mine fire [84]. The model was built using Fire Dynamics Simulator (FDS), which is a CFD program developed by National Institute of Standards and Technology. The model was built according to the deep seated coal fire test and the results will be used in the follow-up fire experiments with remote fire suppression applications.

Edwards conducted some CFD studies to understand fire and smoke spread. A model was made using FDS to simulate the 1990 fire at Mathies Coal mine [44]. The coal lined tunnel flame spread rate was studied and they showed that it is not sensitive to the heat of pyrolysis but very sensitive to the coal moisture content. The model also studied the flame spread in a tunnel lined with Douglas Fir timber sets and along a conveyor belt.

Another model was built using CFD2000 to model buoyancy induced Product-Of-Combustion (POC) spread from experimental fires in the laboratory and to analyze smoke flow reversal conditions. The simulated POC spread rates and gas temperatures were higher than the measured values. The reverse flow condition model had lower predicted critical velocity than predicted by a Froude model analysis. The study illustrated the limitations of CFD models with incomplete experimental conditions [85].

Ventilation control is a recommended method for the control of POC and smoke reversal, but a quantified ventilation strategy is usually not available. Edwards conducted an experiment and computational model to determine the critical ventilation velocity required to prevent smoke reversal [82]. Fire smoke reversal experiments were conducted with different fire intensities and it was determined that the critical velocity to prevent smoke reversal is proportional to the fire intensity to the 0.3 power which is in agreement with the one-third law dependence theory posted by other researchers [86]. The CFD model using FDS showed good agreement with the experimental results, and provided a predictive method to simulate a range of fire intensities and mine entry dimensions which is difficult to achieve experimentally.

Huang and others presented a CFD method using a two-dimensional model which is based on the theory of natural convection and heat transfer in porous media to study the flow and temperature fields in underground coal fires [83]. The solutions compared well with limited

available field data. The results showed that the fractures or high permeability are important factors to enhance natural convection. In a uniform permeable stratum, air flows from the low temperature zone to the hot area, but in a non-uniform permeable stratum, air flows from the more permeable zone to the hot area and less permeable zone. The study also found that air convection influences shallow coal seam fires more than deep coal seam fire and the gas produced by secondary combustion in fractures can enhance the convection.

2.6.4 Methane flow and control

Methane in underground coal mining is a major safety issue. Methane is highly explosive under certain concentrations and requires constant monitoring and control to maintain a safe working condition. The gas flow in the gob and mine ventilation systems are complex and difficult to measure. CFD can be used to better understand complex underground methane flow and design ventilation methods to reduce the methane risks[87].

Ren et al. presented a CFD modeling study of methane flow around longwall coal faces [88]. Due to the fact that methane to the working longwall face may be from source beds above or below the working seam, this study constructed a model that included a methane bearing seam 80 m above the working seam. Laboratory results were used for the permeability values of the roof strata, as well as the consideration of redistribution of stress field and the mining induced fractures. The pressure and velocity contours were provided, which related to the methane emission and migration. Although the CFD model provided practical results, validation from field data is needed.

Toraño conducted CFD analyses of methane behavior in underground coal mine auxiliary ventilation [59]. The conventional method calculates the average methane concentration without considering different methane content in different zones. The study aims to analyze the evolution of ventilation in different cross sections and in the roadway axis directions, and the influence of time. A CFD model using Ansys CFX 10.0 and field experiment were carried out to study the dead zone, airflow recirculation, and methane distribution. The study compared four different turbulence models and selected the k-epsilon model which agrees with the field measurement best. Both CFD and experiment results were compared with those calculated by conventional methods. The study shows that it is necessary to analyze auxiliary ventilation systems by CFD which helps identify potential dangerous zones and auxiliary ventilation design.

The coal mine production may be prohibited by the high methane content underground when the ventilation is not sufficient to lower the content with normal ventilation systems. Oraee used CFD to simulate a methane drainage system which can be used to reduce the ventilation and development cost in a gassy mine [89]. The study evaluated the methane drainage system with different vent hole spacing and the change of methane content with time. The study showed that the CFD model can be used to improve the drainage system design to more effectively manage methane underground. Balusu et al. presented an extensive study on the optimization of gob methane drainage system [90]. Several techniques were used during the course of the project, such as on-site monitoring, tracer gas tests, CFD simulations, and extensive field trials. The CFD method was used to analyze the gas flow and buoyancy mechanisms in the gob. The models were validated and calibrated using the field study results. The influence of different parameters, such as face flow rate, drainage hole position and spacing, are extensively investigated. The CFD results, in combination with other field investigations were used to develop optimum gob gas control strategies. The gas drainage strategies developed by this study gained about 50% gas drainage improvement compare to the traditional gob gas drainage strategy and greatly enhanced the safety and productivity of underground coal mines.

2.6.5 Gob gas flow

It is important to understand the mechanics of gas flow inside the gob in order to develop effective gas management and ventilation strategies [91]. It is hard to measure the air flow inside the gob because much of the gob area is inaccessible. Therefore, the CFD modeling technique is one reasonable way to investigate the ventilation in gob areas [18].

Permeability distribution in the gob is a key element of the gob gas flow model [91]. Esterhuizen and Karacan developed a methodology for calculating permeability variations in the gob suitable for reservoir models or CFD models and simulated the leakage flow into the gob, methane distribution within and effects of gob vent boreholes on flow patterns [92]. The permeability changes were determined using FLAC3D numerical modeling program and the results are used as input into the reservoir model. The simulated results were compared to empirical experience and measurements and are consistent with empirical observations and measurements reported in the literature.

A similar study was conducted by NIOSH [8]. The flow patterns inside the gob under one-entry and two-entry bleederless systems, and a three-entry bleeder system were studied using CFD. The gob permeability data were from the results of FLAC geotechnical modeling. The study also discussed the possible location of critical velocity zones which support spontaneous combustion.

2.6.6 Inertisation

The goal of gob inertisation is to lower the risk of potential explosions during longwall panel sealing off periods. Gob inertisation has been widely used around the world to control fires and spontaneous heating in underground coal mines. Effective inertisation can suppress the development of potential gob heating and maintain a normal coal production rate [93]. High wall systems have also effectively utilized inert gas to maintain safe methane levels [94].

Balusu et al. and Ren et al. presented their work using CFD to study the optimum inertisation strategies which can achieve gob inertisation within a few hours of the sealing the panel [93], [95]. The CFD model was first calibrated based on previous inertisation studies and gob gas monitoring. The gob porosity parameter was from the results of geomechanics models. The gob conditions before sealing off period were modeled by steady state modeling and then the sealed gob atmosphere was modeled by transient modeling. The validated model was used for parametric studies such as inert gas injection locations, inert gas flow rates, seam gradients, and different inertisation strategies such as injection of inert gas through surface gob holes. Results show that the inert gas composition is not the major factor in an inertisation process and that injection of inert gas at 200m behind the face is more effective than at the location right behind the face line. Several recommendations were provided to improve the inertisation strategy and the strategy developed by this study was implemented and demonstrated in the field. The new practice showed significant improvement by converting the gob into an inert atmosphere in a few hours instead of two to four days by traditional methods.

Trevits and others conducted CFD modeling using FDS to study the effects of increased inert gas (N_2) injection [96]. The results of the model achieved good correlation with the field test which used the pressure swing adsorption (PSA) N_2 generation technology to inert a mine sealed area. The results showed that the relationship between N_2 gas injection rate and the time needed to reduce the O_2 level is not linear and the benefit of inert gas decreases as the injection

rate increases. The CFD results also showed that injection of N_2 at two ventilation seals is more efficient than at one seal location with double the injection rate.

Mossad et al studied the effectiveness of high wall mining inertisation using CFD [94]. The study focused on improving mine efficiency with regard to safety and production rates by using inertisation to maintain methane concentrations within safe working limits. The model is a 2-D k-ε realizable turbulent model and the Semi-Implicit Method for Pressure-Linked Equations algorithm was chosen for the velocity pressure coupling. The study indicated that applying the inert gas at high angles of injection is more effective and CO2 is the most effective gas, when applied at a 60 degree angle, compare to N2 and Boiler Gas. This work was described in detail in Vella's dissertation [97].

2.6.7 Dust dispersion and control

The amount of dust generated during mining is another major concern. Dust can cause respiratory disease, contribute to the risk of underground explosion, and impede productivity [98]. The airflow and dust dispersion are very complex and the standard mine ventilation network analysis is not sufficient to analyze the detailed airflow patterns and dust distribution. CFD is an attractive approach to develop and evaluate dust control methods.

Heerden and Sullivan completed a CFD study to evaluate the dust suppression of continuous miners and roadheaders [98]. The study showed the steps during the CFD model constructions, and plotted the velocity vectors and contours of the results. The dust particles are assumed to follow the flow in the flow field, and the slow lines were used for qualitative assessment of dust movement. The model was used to evaluate dust suppression under different machine parameters and dimensions, such as the position of the continuous miners, the volume of the flows, and different models of roadheaders. The effect of drum rotation, water sprays, and air movers were also investigated. The methane concentration was added to the model later. The authors indicated that the model was validated by comparing with the experimental data, but no details were provided for the validation.

Srinivasa et al. studied airflow and dust dispersion at a typical longwall face using CFD [99]. The study evaluated the air curtains, semi-see-through curtain and air powered venturi scrubber dust control techniques. The effect of support legs and the shearer were also modeled with simplified geometry. The dust is assumed inertialess and follows the air flow streams. The

dust was added in the model as a dust source at the model inlet and was assumed to be constant and uniform across the inlet. The simulations were performed using Fluid Dynamics Analysis Package (FIDAP) program. The flow field equations were solved independently from the pollutant equation. The dust particles were calculated using Equation 2-27, where F refers to fluid phase and P to the particle phase.

$$\rho^P \frac{\partial u_i^P}{\partial t} = F_D(u_i^F - u_i^P) + (\rho^P - \rho^F)g_i + (\rho^P - \rho^F)f_i \quad (2\text{-}27)$$

Where: ρ = density, t = time, u = velocity, f = body force, g = gravity force, F_D was given as:

$$F_D = 18\frac{\mu_F}{D_P^2}C_D \quad (2\text{-}28)$$

Where μ_F = dynamic viscosity, C_D = drag coefficient, D_P = particle diameter.

The trajectory equation was given as the follows:

$$\frac{\partial x_i}{\partial t} = u_i^P \quad (2\text{-}29)$$

The advection-diffusion equation for the dispersed phase of dust particles was given as:

$$\rho\left[\frac{\partial c}{\partial t} + u_i c_j\right] = (\rho\alpha c_j)_j + Q \quad (2\text{-}30)$$

Where, c = dust concentration, α = mass diffusivity, Q = source term.

The air velocity results and the dust concentration values using air curtain were compared with field measurement. The predicted dust concentration was within 10% of the field values. The simulation indicated that the air powered venturi scrubber is the most effective means to control dust, with a 40-50% reduction within a distance of 3-4 m from the scrubber at 2.1 m/s face air velocity. The study concluded that CFD can be used to model underground dust dispersion and design dust control techniques [99].

Skjold et al. reported a CFD code DESC (Dust Explosion Simulation Code) which is a simplified empirical based CFD code that can be used to simulate the dust lifting phenomenon [31]. The empirical approach was used for the DESC code since the detail dust lifting mechanisms, such as the Magnus forces, Saffman forces, and particle collisions, cannot be feasibly modeled and is suitable for industrial applications. The DESC code is similar with the CFD code FLACS (Flame Acceleration Simulator). The dust particles are assumed to be in dynamic and thermal equilibrium with the fluid phase. The phenomena such as dust settling or flow separation in bends and cyclones cannot be modeled because slip velocity is not included in the code. The study simulated dust concentration for an experimental wind tunnel, as well as a set of dust explosion experiments described in literature. Although the experiment technical

details were limited, the simulated dust layer results agreed well with the experimental data. As a result of this study, Skjold et al. concluded that it is beneficial for the safety of coal mines or other industrial field to use a simplified dust lifting model.

Ren et al. presented their work using CFD to develop a new dust control systems [100]. The geometry of their models were comprehensive, including not only the coal face and the maingate, but also chocks, shearer, spill plate, BSL/crusher and conveyor, dust scrubbers, shearer clearer, venturi sprays, and curtains. One particular example they showed is the use of CFD modeling to design a new shearer scrubber system. By studying parameters such as the location of the inlet and outlet, the capacity of the scrubber, and the face airflow rates, the study indicated that positioning the scrubber inlet towards face ventilation can capture more dust particles. The CFD modeling results were used to design a new shearer dust system, which achieved 43% to 56% more dust reduction.

Silvester et al. [33] presented a CFD study on the influence of underground mineral tipping operations on the surrounding ventilation system and consequent dispersal of fugitive dust. It used a two-phase continuum approach to describe the interaction between the falling materials and the surrounding air. The standard k- ε model was used and wall roughness effects were not considered since they were proven to have negligible impact on subsurface mine ventilation modeling [101]. Different scenarios were modeled to investigate the influence of different factors. A Lagrangian particle tracking algorithm was used to represent the dust flow and plume dispersion. The CFD results were validated against experiments using scale models, which used water as a substitutefor air to achieve adequate dynamic scaling, and used a dye injection system to visualize the flow. Good qualitative agreement was achieved between the experiment and the CFD results. However, the use of continuum dynamics to represent the material as a granular fluid medium restricted the CFD model because they could only achieve an approximation of the actual process and could not reveal the mechanisms of the process. Another CFD study conducted by Silvester et al. on the dust control aspect was presented in [102]. The dispersion and deposition of fugitive mineral dust generated during mining at a surface quarry were studied. The influence of the mineral dust emission location, the wind direction, and the in-pit ventilation flows were investigated, and the results can be used to assist future quarry planning and blast operation to better control the dust emissions. However, the CFD models were not validated.

Torno et al. developed a CFD model to simulate the dispersion of dust generated in blasting in limestone quarries [25]. The standard k- ε model was used for turbulence modeling and a Lagrangian particle tracking method was selected to model the air and dust multiphase problem. The CFD model was validated by the experimental data using a trial-error method on the value of dust injection. It has been proved that the use of a barrier placed downstream of blasting can create 4.5% of dust emission retention.

2.6.8 Minerals processing

CFD has also been extensively used in recent years in the process industry for the research and development of new and existing processes. CFD modeling results can help researchers to gain detailed understanding of flow during minerals processing that can be used to design and modify equipment to improve separation performance. Numerous studies are available in the literature, but only two representative examples are shown here.

An initial study was presented by Lichter et al., which use the combination of CFD and Discrete Element Modeling (DEM) to evaluate the performance of flotation cells [103]. The CFD was used to simulate a flotation machine with different parameters, such as the size of the flotation cells and inlet velocities. Slurry was treated as single phase newtonian fluid with specified viscosity. The model did not include the air in the slurry system, but the author states that it still can be used to compare one cell design with another. The CFD results were then imported to a DEM simulation, which makes it possible to produce residence time distributions as a function of size and evaluate the metallurgical performance. No final conclusion was made on the relationship between parameters and the performance of the cell. However, this study showed the potential of the combination use of CFD and DEM modeling to determine the flotation cell operating and design parameters.

Peng used CFD to model the hindered-settling bed separator, which is used for size classification or relative density separation [58]. Most studies of the separation mechanisms are based on density and size difference without the particles-liquid interactions. Peng used the Euler-Lagrange CFD approach in her study can model the physical effects influencing the particle motion and predict liquid velocity profiles and solid particles movement. The 2-D model was validated by comparison of the CFD results and the actual plant test. The flow pattern, effect of feed system, and effect of operation parameters were investigated and discussed which

provided valuable information to better understand the detail separation mechanisms and to predict and optimize the separation process.

2.7 Other applications

Applications of CFD have been found in other design and research areas of mining industry, and some of them are reviewed here.

Torañ o [23] used CFD to model different shapes of open storage systems for bulk materials, such as coal and iron ore, to study the best operational and investment parameters to reduce the airborne dust. The US EPA established a methodology to estimate the level of airborne dust generated from an open pile. However, sometimes the existing methodologies or standards do not match the way materials are actually stored due to reasons like area restrictions and stacking means, and it is also not easy to carry out experiments to evaluate the level of airborne dust to compare to the standards. Therefore, CFD could be used to predict the different environmental impacts of various storage piles. Torañ o used the commercial CFD software Anysys CFX 5.7 to conduct the simulation. The model was validated by comparing results for cone and flat top oval piles with the US EPA study, and then a semicircular pile model was built and analyzed. Reynolds Averaged Navier–Stokes method and medium complexity turbulence models were used. The model showed good agreement with the US EPA study with low root mean square values. The semicircular pile model showed a lower emissions and wind erosions level, but the wind direction is an important factor that would influence the results.

Berkoe et al. [46] presented several projects they have done which applied CFD to the mining and metals field. These include quench cooler design to reduce process gas temperature, solvent extraction settler design to achieve uniform flow, plume capture performance prediction for different configurations of a fugitive emissions collection system, effect of wind on operations facilities, performance of a ferronickel smelting furnace, and slurry flow distributor design. Most of the models used the FIDAP software analysis package, except the slurry flow distributor design used the FLUENT CFD and the discrete phase model. They especially highlighted that the CFD study requires deep understanding of the underlying physics, and usually needs to apply simplified assumptions and improve boundary conditions. Therefore, it is important to have an person who can interface between the field engineering and the CFD modeling functions to obtain reliable results.

CFD has also been used to study the water pollutants associated with mining. Doulati et al. [104] used PHOENICS to study the acid mine drainage generation and subsequent pollutants transportation. The chemical reaction process model was implemented to PHOENICS by subroutines. Close agreements were achieved between CFD model and filed data. This study illustrated the ability of CFD to study the groundwater pollution problems and better understand pollution transport mechanisms.

CFD is also a promising method in the field of carbon capture and storage (CCS) technology. Mazzoldi et al. [34], [105] presented a risk assessment study for CO_2 transportation using a commercial CFD software Fluidyn-PANACHE. In this study, models were built to simulate an accidental release of CO_2 from high pressure transportation facilities within CCS projects. The results were compared with those using Gaussian/dense-gas models and they demonstrated that CFD models are more reliable and produce more precise results, thus can provide improved risk analyses. A similar study conducted by Dixon et al. [106] used the CFD code CFX to predict the consequences of releases of CO_2 from a liquid inventory. The concentration of CO_2 particles was modeled using both scalar equation and Lagrangian particle tracking methods and good agreement with experimental data were observed.

2.8 Conclusions

The CFD concept, its application in the mining industry, specifically in ventilation, and challenging issues have been discussed in order to provide insight into the current CFD research activities in mining. It is evident in this review that the scope and the level of sophistication of CFD studies in mining are increasing, especially with the continued high rate of advancement in computer power. The application of CFD in the mining industry will allow for improved understanding of the fluid problems that can enhance safety and optimize layout and equipment design.

Turbulence models are widely used since most flows in mining are turbulent. It is clear that the standard k-ε model has been commonly used as the most acceptable general purpose turbulence model. However, the quality of the solution is dependent on the turbulence model. Therefore the selection of turbulence models should consider physical models and flow features of specific problems.

Mesh independence studies must be included in the construction and analysis of a CFD model. This paper summarized the general procedures and methods to conduct the mesh independence study, which assure that solutions are not significantly dependent on the mesh.

Because CFD uses approximate approaches and some assumptions, validation of the CFD studies is necessary to ensure the simulated results are within an acceptable level of accuracy. The validation studies are generally conducted by comparing the results obtained from laboratory or full scale experiments with the simulated results. Several techniques were used in the cited work for CFD validation, such as tracer gas, 3D velocity measurement, and flow visualization. Accurate measurement of flow features may be difficult due to the complexity of the flow domain, such as underground mine working faces and flow in the gob. General agreement with the experimental data was reported in many validation studies, whilst discrepancies were also noted in some studies, which indicated a requirement for model improvement and accurate measurement of experimental flow parameters.

Overall, this paper reviewed the current state of research of CFD modeling in mining. Examples discussed in this paper and numerous studies that can be found in the literature showed that the potential benefits from the CFD simulations are enormous if the problem setup is addressed carefully and proper model verification, such as mesh and solution convergence, and model validation are conducted.

This paper was presented at the 2011 SME annual meeting in Denver, and is included in the meeting preprints (Feb. 27-Mar. 02, 2011, Denver, CO, Preprint 11-121). Guang Xu conducted the majority of the experimental and CFD modeling work and wrote the paper with technical and editorial input form coauthors: John R. Bowling, Dr. Kray D. Luxbacher, and Dr. Saad Ragab. Please cite this article as: Xu, G., Bowling, J. R., Luxbacher, K. D., & Ragab, S. (2011). Computational fluid dynamics simulations and experimental validation of tracer gas distribution in an experimental underground mine. 2011 SME Annual Meeting (p. Preprint 11–121). Denver, CO (USA).

3 Computational Fluid Dynamics Simulations and Experimental Validation of Tracer Gas Distribution in an Experimental Underground Mine

3.1 Abstract

Following a disaster in a mine, it is important to understand the state of the mine damage immediately with limited information. Computational fluid dynamics can be used to simulate and ascertain information about the state of ventilation controls inside a mine. This paper describes a simulation of tracer gas distribution in an experimental mine with the ventilation controls in various states. Tracer gas measurements were taken in the lab experimental apparatus, and used to validate the numerical model. The distribution of the tracer gas, together with the ventilation status, was analyzed to understand how the damage to the ventilation system related to the distribution of tracer gases. This study will be used in future research in real mine measurements to compare collected and simulated profiles and determine whether damage to the ventilation system has been incurred during an emergency situation, the nature of the damage and the general location of the damage.

3.2 Introduction

There is a lack of knowledge about the state of ventilation controls in a mine following the event of a significant incident such as a roof fall, bump, or explosion which requires immediate action. Currently, some information may be gathered safely from the surface, but most information regarding the state of the ventilation controls cannot be known before rescue personnel enter the mine. Having quick access to more information will help decision makers to more effectively manage a mine emergency and increase safety for rescue personnel.

It is essential to model ventilation patterns and the mine environment following an incident in a mine. Tracer gas techniques and numerical simulations using computational fluid dynamics (CFD) can be used to ascertain and simulate information about the state of ventilation controls inside a mine. Tracer gas measurement is an effective method to detect air flow routes

and estimate air flow quantity and the rates of dilution and dispersal of contaminants in underground mine ventilation systems [107], [108]. Air flow directions and quantities can be estimated by analyzing the tracer gas concentration. Dispersion of tracer gas in underground ventilation system may be very different depending on the location of damage after incident.

The use of tracer gases started in the 1950s in building ventilation systems [61]. Tracer gas techniques have been used in many situations where the standard ventilation survey methods are inadequate [109]. The applications of tracer gases in underground mines include analyzing ventilation patterns, measurement of air leak rates, and evaluating dust control measures [62]. Sulfur hexafluoride (SF_6) is widely used as a tracer gas and is ideally suited for use in the underground environment. SF_6 is not normally found in the underground environment and it is inert, nonflammable, nonexplosive and non-toxic which makes it safe for use in underground mining and other industrial environments. Most importantly, current technology makes it possible to detect very low concentrations of SF_6 (in the parts per billion or trillion range) [2], [110].

Computational Fluid Dynamics is a tool which can approximate numerical solutions in cases where experimental solutions are impractical or impossible. With the recent advances in computer technology and the success of CFD， the application of CFD has become increasingly attractive in modeling the ventilation systems in underground mines. It has been used in simulations of explosions [31], methane control [94], [111], ventilation system improvement [41] , gob inertisation methods [93], and spontaneous combustion and mine fires [20], [85].

A combination of experimental data and a CFD model of tracer gas dispersion has been used to study airflow and contaminant transport in indoor environments [112–114], pollutant dispersion [115], and other industrial applications. Little research has been done to simulate tracer gas dispersion in underground mines, especially using tracer and CFD simulation to predict the status after emergency in underground mines.

This paper presents both the experimental and numerical results of ventilation status and tracer gas (SF_6) dispersion in an experimental laboratory scale mine model with the ventilation controls in various states. Valves are used in the experimental mine model to simulate different ventilation statuses after “incidents” cause changes to the ventilation. Several passive area sources with constant emissions of a tracer gas (SF_6) were designed to simulate constant tracer injections in the experiment. The objectives of the experiment were to collect data for evaluating

the influence of different locations of damage after incidents and to validate the CFD model. This study indicates that tracer gas concentrations in a mine can be accurately modeled with prior knowledge of the ventilation system. It is the first step toward the research using tracer gas measurements to compare measured and simulated profiles and determine whether damage to the ventilation system has been incurred during an emergency situation, the nature of the damage and the general location of the damage.

3.3 Experimental measurements

3.3.1 Experimental apparatus

A simple typical mine layout was designed for experimental purpose. As is shown in Figure 1, it includes one gob panel, one active panel, one stopping, and two regulators. Three possible incidents locations are also designed including explosion damage to the stoppings and causing short circuiting of the airflow between the main entries, a roof fall in the active panel which will block the airflow across the working face, and an explosion in the gob which will block the airflow through the gob. Two boreholes are present: one rescue borehole on the tailgate of the active panel and another borehole in the gob. The normal air flow paths are also shown in Figure 4. The experiment is not set up to include flow through the gob, simply around it.

The experiments were conducted using the experimental underground mine shown in Figure 5, which is built according to the mine layout shown above. The experimental underground mine is composed of 2 inch (0.0508 m) inside diameter PVC pipes with the maximum dimensions of The PVC pipes were labeled with numbers for convenient reference. The experimental system has one intake and the exhaust is hooked up to an exhaust fan shown in Figure 6. Five valves (Figure 7) were used to simulate the stopping within the main entry, regulators, and roof fall/explosion damage.

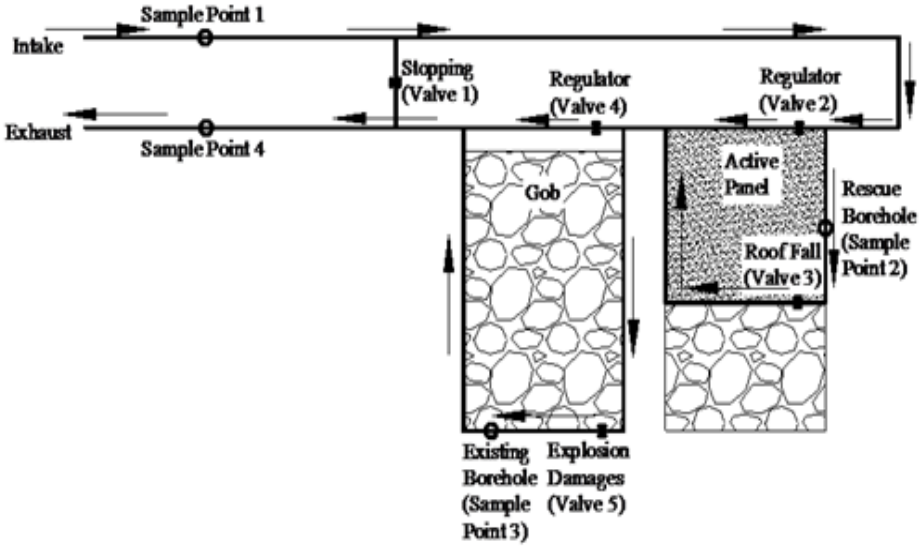

Figure 4. Simple typical mine layout

Figure 5. General view of the experimental system

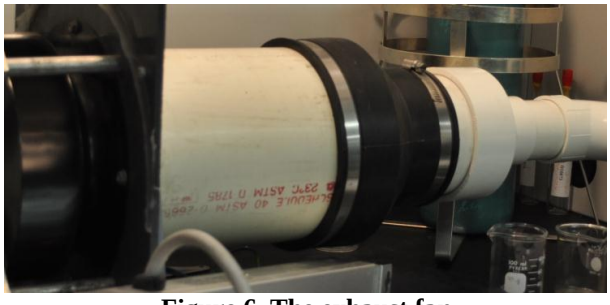

Figure 6. The exhaust fan

Figure 7. Valves used to simulate ventilation controls and mine airway damage

To continuously measure the velocity in the system, pitot tubes along with differential pressure transducers, connected to a data acquisition computer system were used (Figure 8). The difference between total pressure and static pressure from the pitot tube, which is proportional to the electrical signal, was measured by the differential pressure transducer. The velocity of air is then calculated by software using the follow Equation [116].

$$V = 44.72316 \times \sqrt{\frac{h_{kpa}}{d}} \qquad (3\text{-}1\ )$$

Where h_{kpa} is total pressure-static pressure in (kPa), and d is air density in kg/m^3.

Figure 8. Pitot tube and differential pressure transducer

A rotameter was used to measure the flow rate of tracer gas (SF_6) into the apparatus. Air samples were taken using glass syringe and Gas Chromatograph (GC) with electron capture detector (ECD) was used to analyze air samples and measure SF_6 concentration.

3.3.2 Experimental procedure

Although the five valves' states can be changed to simulate different situations and ventilation statuses, only two experiments were performed in this work. Case #1, defined as having only valve 1 closed, simulates normal ventilation status with the air flow paths shown in Figure 1. Case #2, with all the valves open, simulates the situation in which an explosion has damaged stoppings in the main entries. Air flow becomes short circuited due to the damage so that relatively little air reaches the panels, most intake air flows directly from the intake entry, through the crosscuts where stoppings were damaged, and is exhausted directly. The air flow paths in case #2 were shown in Figure 9.

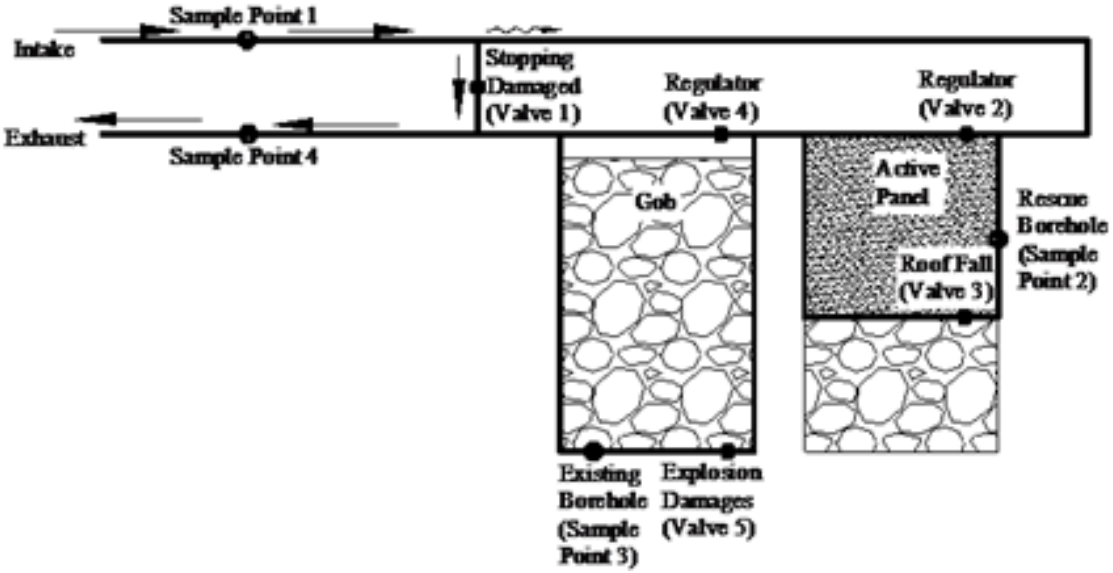

Figure 9. Flow path of case 2 after the stopping was damaged by explosion

Before releasing SF_6, the exhaust fan was turned on allowed to run until the flow reached a steady-state, marked by the air velocities no longer changing. The tracer gas was released just inside the inlet at a constant rate of 1 liter per minute. Air samples were taken after ten minutes had elapsed while tracer gas was released to ensure a stable airflow and tracer gas distribution. Air samples were drawn through septa at four different sample points which are shown in Figure 1 and for each location three measurements were repeated.

3.4 CFD modeling

3.4.1 Geometry and mesh

Auto CAD 2007 was used for three-dimensional modeling and the commercial software Ansys ICEM CFD, which is recognized as the fastest hexahedral mesh generation tool, was used to generate the mesh. An unstructured, hexahedral mesh was generated to represent the size and geometry of the lab experimental mine model. The "O" grid is used on the pipe cross section with fine mesh near the pipe wall and coarse mesh in the center. Figure 10 shows part of the mesh and Figure 11 shows the O grid mesh on the pipe cross section.

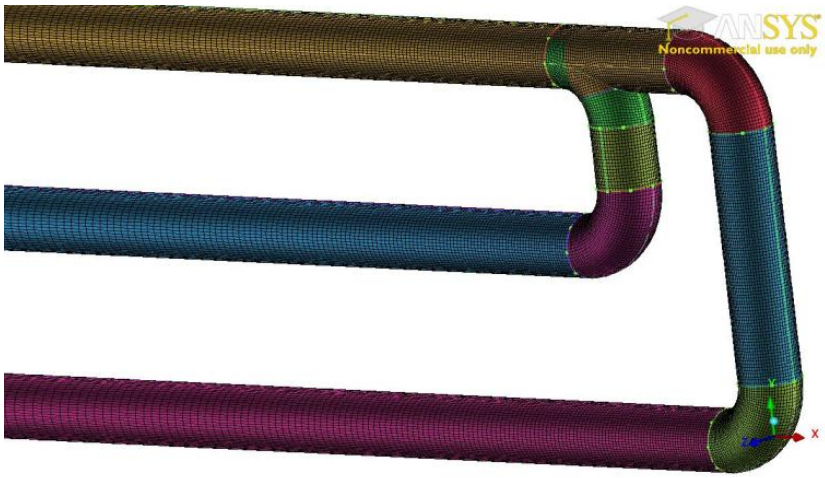

Figure 10. Part of the 3D model and meshing

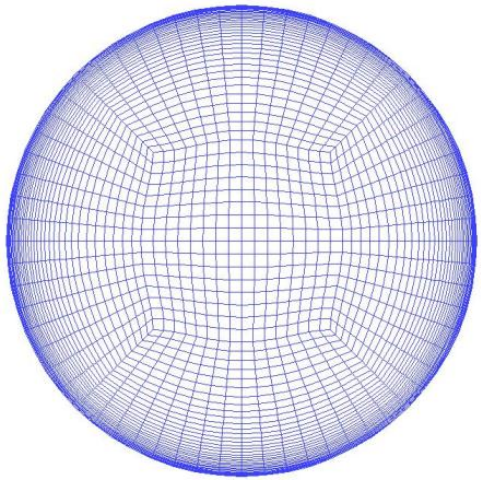

Figure 11. The "O" grid applied to pipe cross section

3.4.2 The turbulent airflow model

A proper turbulence model needs to be selected to simulate the pipe airflow and tracer gas dispersion. A steady state solution for the Reynolds averaged Navier-Stokes equations with

the standard k-ε turbulence model were employed to predict the incompressible turbulent airflow and user-defined scalar transport without chemical reaction and heat transfer was performed to predict tracer gas dispersion. The model was selected because it achieves reasonable accuracy over a wide range of turbulent flows in industrial flow simulations.

The inlet and the outlet of the model were specified as velocity inlet and pressure outlet, respectively. 403.38 Pa gauge pressure was applied to the outlet according to the experimental measurement. 18.0 ft/s (5.5 m/s) and 22.0 ft/s (7.0m/s) were applied to the inlet for Case #1 and Case #2, respectively. All of the other surfaces are treated as stationary walls with no slip. Both air and wall temperatures are assumed constant.

The numerical simulations in this study were conducted using the commercial CFD package, ANSYS FLUENT 12.1, to simulate the airflow and tracer gas dispersion for the same scenarios used during the laboratory tests. A first order upwind scheme was used for variables including pressure, momentum, turbulent kinetic energy and turbulent dissipation rate. Discretized airflow equations were solved with the SIMPLE algorithm in the CFD program to couple the pressure, velocity, momentum and continuity equations.

3.5 Results and analyses

Air velocities were measured at four sample points and were used to calibrate the CFD model. Table 2 shows the measured and simulated velocities. Generally the computed airflow velocity agreed qualitatively with the experimental data. However, obvious errors exist in quantitative comparison. For example, in Case #2, simulated velocities at Point 2 and Point 3 are less than the measured data at the respective points. As we know in this case, the airflow was short-circuited, so the velocities at Point 2 and Point 3 should be small. We can conclude that it is very possible the measured velocity is not accurate. The difference between measured and simulated data may be mainly caused by three factors: the precision and error of the differential pressure transducer, the leakage of the experimental model, and the boundary conditions of the computer model. Since the study is the first step of the project, the data are accepted for now before further improvements are made.

SF_6 was only used in Case #2. Air samples were taken three times at each sampling location and the average concentrations were calculated to compare with the simulated result. During the experiment, SF_6 was released at a constant rate of 1 L/min through a ¼-inch inside diameter tube and placed 10cm inside the air inlet. In the computational model, SF_6 was released

from a point source (¼-inch cube) at the same location as the experiment, with a mass flow rate of 401 kg/m^3*s which is equal to the 1L/min SF_6 flow rate. For Case #1 the measured SF_6 concentration is not available, but computer simulation was conducted.

Table 3 shows the measured and simulated SF_6 concentrations for Case #2, also shows the simulated SF_6 concentration for Case #1. There are differences between measured and simulated SF_6 concentration. The measured results are generally larger than the simulated results. This is probably due to absorption of SF_6 to the PVC pipes, although the parameters and boundary conditions used to simulate SF_6 also need calibration. Figure 12 shows the SF_6 distribution at a cross-section of Sample Point 1 in Case #1 and Case #2. From the contours one can see the CFD model can compute the diffusion of tracer gas and visualize the distribution. Because in Case #1 the velocity at the inlet is less than that of Case #2 (5.5 m/s and 7.0 m/s respectively), SF_6 was diffused less in Case #1 than in Case #2 and has a different distribution over the cross-section.

Table 2. Measured and simulated velocity at four sample points

		Point 1	Point 2	Point 3	Point 4
Case 1	Measured	6.9 m/s	3.8 m/s	3.7 m/s	7.0 m/s
	Simulated	6.8 m/s	3.6 m/s	3.5 m/s	7.0 m/s
Case 2	Measured	8.2 m/s	2.0 m/s	1.9 m/s	8.5 m/s
	Simulated	8.3 m/s	0.4 m/s	1.5 m/s	8.8 m/s

Table 3. SF_6 measured and simulated concentration

		Point 1	Point 2	Point 3	Point 4
	Test 1	3.00mg/L	7.41mg/L	6.81mg/L	9.61mg/L
	Test 2	3.67mg/L	3.00mg/L	4.80mg/L	6.31mg/L
Case 2	Test 3	6.33mg/L	6.65mg/L	6.65mg/L	6.96mg/L
	Average	4.67mg/L	5.69mg/L	6.09mg/L	7.40mg/L
	Simulated	3.60mg/L	4.00mg/L	4.00mg/L	4.00mg/L
Case 1	Simulated	4.60mg/L	5.10mg/L	5.10mg/L	5.10mg/L

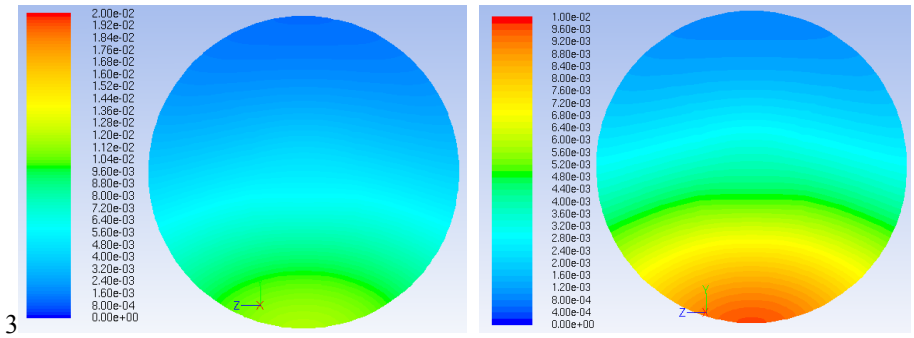

3

Case #1 Case #2

Figure 12. SF_6 Distribution contours in the CFD model in cross-section at sample point 1

3.6 Conclusions and future work

This study investigated airflow and SF_6 transport in an experimental coal mine through both experimental measurements and numerical simulation with CFD under two different cases (airflow patterns). An experimental coal mine, based upon a simple typical mine layout, was built using PVC pipes. Pitot tubes, differential pressure transducers, a computerized data acquisition system, and a gas chromatograph were used to measure the air velocity and tracer gas distributions throughout the simulated mines. The numerical simulations used CFD with the standard k-ε turbulence model and user-defined scalars to simulate airflow and tracer gas (SF_6) distribution.

Measured data were used to calibrate the CFD model and the simulated results were compared with the measured results. The velocities and the SF_6 diffusion results were acceptable while there are differences between the computed and measured results. Errors exist in both the physical experiment and the CFD model and further experimental improvement and validation of CFD model are needed.

The present study is the first step toward research intending to use tracer gas measurements to compare measured and simulated profiles and determine whether damage to the ventilation system has been incurred during an emergency situation as well as the nature and the general location of the damage. Results showed that the methods used are feasible although improvements are needed. Further work will include: (1) Experimental measurement validation and design improvement including calibrating the velocity measurement results, controlling and analyzing the errors from the differential pressure transducers, and improving the location of velocity measurement. (2) The PVC pipes may also need to be replaced with a material that is less prone to SF_6 adsorption. (3) Further calibrating the CFD model, especially the boundary conditions, diffusivity of SF_6, mass flow rate of SF_6. Also, it may be helpful to using the second order upwind scheme to achieve more accurate results. (4) Studying more cases under different airflow patterns to find the optimum location to release the tracer gas and techniques to release tracer gas which include the tracer dilution method, the constant injection method, or other methods will be constructive. (5) Finally, future experiments will use multiple tracer gases and comparing the efficiency over the use of single tracer gas.

This paper is published in the journal Tunnelling and Underground Space Technology. The experimental and CFD modeling work and writing was primarily completed by Guang Xu with editorial and technical input from coauthors: Dr. Kray D. Luxbacher, Dr. Saad Ragab, and Steve Schafrik. Additionally, Steve Schafrik was instrumental in the logistical details associated with running CFD on a high performance computer (HPC). The paper can be found at the link: http://www.sciencedirect.com/science/article/pii/S0886779812001551. Please cite this article as: Xu, G., Luxbacher, K. D., Ragab, S., & Schafrik, S. (2012). Development of a remote analysis method for underground ventilation systems using tracer gas and CFD in a simplified laboratory apparatus. Tunnelling and Underground Space Technology, 33, 1–11.

4 Development of a Remote Analysis Method for Underground Ventilation Systems using Tracer Gas and CFD in a Simplified Laboratory Apparatus

4.1 Abstract

Following a disaster in a mine, it is important to understand the state of the mine damage immediately with limited information to manage the emergency effectively. Tracer gas technology can be used to understand the ventilation state remotely where other techniques are not practical. Computational fluid dynamics is capable of simulating and ascertaining information about the state of ventilation controls inside a mine by simulating the airflow and tracer distribution. This paper describes a simulation of tracer gas distribution in a simplified laboratory experimental mine with the ventilation controls in various states. Tracer gas measurements were taken in the laboratory experimental apparatus, and used to validate the numerical model. The distribution of the tracer gas, together with the ventilation status, was analyzed to understand how the damage to the ventilation system related to the distribution of tracer gases. Detailed error analysis was performed and the discrepancies between experimental and simulated results were discussed. The results indicate that the methodology established in this study is feasible to determine general ventilation status after incidents and can be transferred to field experiment. Because it is complex to simulate the actual condition of an underground mine in a laboratory, the model mine used is simplified to simulate the general behavior of ventilation in a mine. This work will be used to inform planned on-site experiments in the future and the proposed methodology will be used to compare collected and simulated profiles and determine the general location of ventilation damage at the mine scale.

4.2 Introduction

After a severe underground mine incident, such as a roof fall, outburst, water inrush, or explosion that may cause tunnel collapse, underground information must be gathered immediately to estimate the extent of damage for rescue and recovery operations. In these

situations, communications between underground miners and rescuers on the surface may be tenuous at best, because very few commercially available communications systems have been proven to meet the basic requirements for emergency communication [117]. Some alternate methods can be used to gather information, such as collection of air samples from boreholes, utilization of a video camera via borehole to visualize underground status, and utilization of rescue robots underground if possible. However, none of these methods are reliable and efficient enough to stand alone. In an emergency situation, accurate information regarding the mine status is invaluable not only to save miners' lives, but also to help decision makers manage the emergency effectively, and to increase safety for rescuers.

In some incidents, such as explosions, all the communication lines maybe damaged and collapse may occur with the location difficult to pinpoint from the surface. However, the airflow paths and ventilation patterns will change according to the location of damage. Therefore, the location of damage can be approximately determined by remote measurement of ventilation parameters. Due to the complexity of the ventilation system, employment of the tracer gas method is an effective means and has been used in many situations where conventional techniques are inadequate or cannot be effectively employed [1], [2]. Numerical simulations using Computational Fluid Dynamics (CFD) can be used to model the ventilation status and the data from tracer gas measurement allow for further analysis, prediction, and confirmation of the underground ventilation status together with the location of the damage.

Tracer gas was first used in the building ventilation systems in the 1950s [61] and has been widely used for ventilation analysis both in buildings and underground mines [118]. Tracer gas based ventilation measurement is an effective method to detect air flow routes, estimate air flow quantity, and other complex ventilation problems [119], [120]. Sulfur hexafluoride (SF_6) is widely accepted as a standard mine ventilation tracer [118], because it can be detected in low concentrations, is nontoxic, odorless, colorless, chemically and thermally stable, and does not exist naturally in the environment [1]. The applications of tracer gases in underground mines include measurement of turbulent diffusion [107], methane control [121], study of mine ventilation recirculation of return into intake air, transit flow times through stopped areas, effectiveness of auxiliary fans, and estimation of volumetric flow rates [1], [122] air leakage investigation, and evaluation of dust control measures [62].

In recent years, Computational Fluid Dynamics (CFD) has become a powerful tool and has been commonly used to model the underground mine air flow behavior and solve relative problems [67], [100]. It has been used in a number of areas, including modeling ventilation airflow patterns [67], [98], study and control of coal spontaneous heating and underground fire [9], [20], [83], optimization of gob inertisation [95], dust control [98], and methane management [91]. The combination of experimental measurement and CFD modeling of tracer gas has been used to study airflow and contaminant transport in indoor environments and other industrial applications [114], [123], but little research has been done to model underground tracer gas applications, especially the use of these techniques to model and analyze the ventilation and mine environment following an incident that alters the ventilation system.

CFD has also been used in many studies to investigate underground tunnel risks. Hua et al. [124] used CFD model to develop an optimal smoke control strategy for tunnel fire. The model was validated using the test results from a similar tunnel and an optimal smoke control strategy was found based on the model results. Se et al. [125] used CFD model investigated the effect of active fan group on the airflow structure and temperature distribution in a tunnel with varied fire source. Gao et al. [126] used Large Eddy Simulation to study the dispersion of fire-induced smoke in a subway station and the influence of natural and mechanical ventilation was investigated. Risks challenging underground mine are also faced by underground tunneling and constructions, particularly the methane explosion described in [127], the fires scenarios mentioned above, flood, and earthquake. The proposed methodology can also be potentially applied to those situations to better understand the ventilation status remotely, and thus manage the emergency effectively with significant impacts on safety. Also, the tracer gas test, sampling, and analyze techniques used in this study can be applied to underground tunnel ventilation survey to investigate ventilation efficiency, flow path, and other related issues.

A CFD approach was used in this study due to the relative simplicity of the experimental apparatus. CFD can resolve details of flow features and tracer distributions. These will help, when we move our test to the field scale, to determine the optimum method and place to release and sample tracer gas. However, it is not practical to apply CFD to the entire mine due to its heavy demand on computational time. Ventilation network modeling is more practical in this situation, but it cannot resolve the detail of tracer gas behavior at the micro scale. Although the

focus of this study is CFD modeling, a hybrid scheme will be investigated when this work is applied to the field, which combines the benefits of CFD and network modeling.

In this study, tracer gas (SF_6) was used in an experimental laboratory simplified model mine which was built according to a conceptual mine layout. A CFD model was developed to simulate the laboratory apparatus. Various states of ventilation patterns were controlled by valves in the experimental mine to simulate different ventilation scenarios after incidents. Tracer gas was released to the model mine at a constant rate. Air samples were analyzed to test the tracer concentration at different locations. The aim of this study is to use the experimental data to validate the CFD model, study the relationship between the tracer concentration and the location of incidents, and finally, through analysis of the air sample and the CFD model result, determine the general location of the ventilation damage. A preliminary version of this study was presented by Xu and others [128].

4.3 Experimental setup and measurements

4.3.1 Experimental apparatus

The laboratory mine model represents a simple conceptual mine shown in Figure 13, in which the arrows indicate the normal air flow path and this state is referred as Case 1. It has one active panel and one gob panel, two regulators (V2 and V4) regulating the air flow into the panels, one stopping (V1) between the main entries, and five boreholes (P1 - P5). Stopping damage at V1, a roof fall in the active panel at V3, and explosion damage in the gob panel at V5 are three possible incidents will be investigated in this study. The air flow to the gob was simplified in both the laboratory experiment and the CFD model in that the air simply flows around the gob; a permeable gob was not studied. It should be noted that this simplified experimental model mine was not used to represent a full scale mine, but rather to validate the CFD model, choose the best sample methods, and test the effectiveness of our methodology, which can later be used to conduct field experiments.

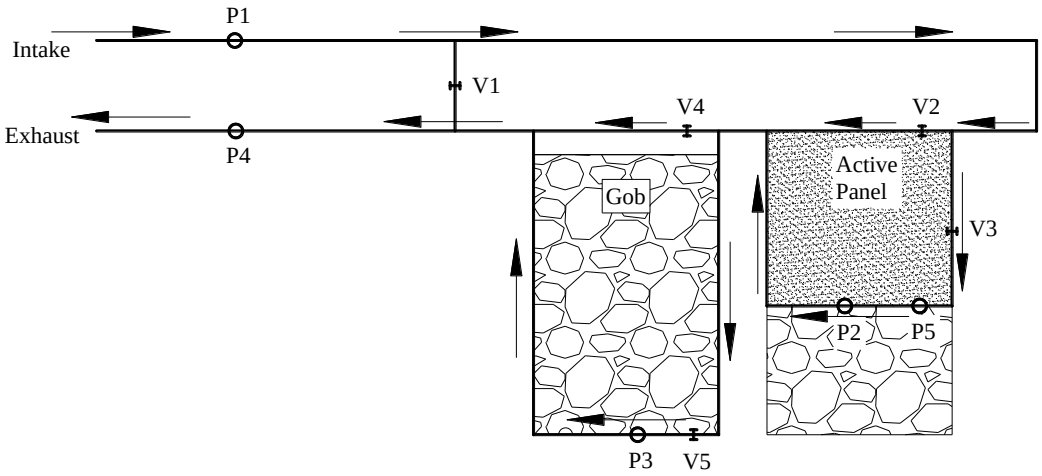

P1: velocity monitor point, P4: velocity monitor and sample points; P2: velocity monitor and tracer gas release point, represent a rescue borehole; P3: velocity monitor and gas sample point, represent an existing borehole; P5: velocity monitor and gas sample point, represent a borehole drilled specifically for gas sampling; V1:valve represents a stopping; V2 and V4: valves represent regulators; V3: valve represents roof fall; V5: valve represents explosion damage

Figure 13. Typical coal mine layout used in this study (Case 1)

The experimental mine model was built, as shown in Figure 14, using 0.05m (2 in.) inside diameter PVC pipes and allows for experiments representing general flow paths of a typical coal mine shown in Figure 1 under different ventilation statuses. The general dimension of the model is 6.63 m in length, 0.51 m in height, and 0.36 m in width. Air exhausts from the apparatus via a variable speed exhaust fan. Valves were used to represent stoppings, regulators, and damage due to incidents.

Figure 14. Configuration of the experimental underground mine model

Pitot tubes and an electrical manometer were used to measure differential pressure at points P1 - P4, and the results were used to calculate velocities at those points using the following equation [129]:

$$V = 44.723 \times \sqrt{\frac{h_{kpa}}{d_{COR}}} \quad (4\text{-}1)$$

Where h_{kpa} is differential pressure measured by pitot tube and manometer in kPa, and d_{COR} is corrected air density in kg/m^3, which can be calculated from the following equation [129]:

$$d_{COR} = 3.4834 \times \frac{P_B}{T_K} \times \left(1 - \left(\frac{0.3783 \times \frac{RH}{100} \times P_s}{P_B}\right)\right) \quad (4\text{-}2)$$

Where P_B is barometric pressure in kPa, T_K is absolute temperature in Kelvin, RH is relative humidity. P_s is partial pressure of water vapor at T_K, and can be calculated using the following equation:

$$P_s = 1.7526 \times 10^8 \times e^{-5315.56/T_K} \quad (4\text{-}3)$$

During this experiment, the measured barometric pressure is 94732 Pa, the temperature is 295 K, and the relative humidity is 29%. Therefore, using equations shown above, the calculated air density is 1.114 kg/m3. This value is used in the experiment velocity calculation and the CFD model input.

4.3.2 Gas release and sampling

There are basically two categories of tracer gas release techniques: transient techniques and the constant injection rate techniques [130]. Because of the small dimensions of the model mine and the high rate of air velocity, the air in the model mine will be totally replaced in 10 - 20 seconds. This makes it impractical to use transient release techniques since the sampling methods we investigated could not sample quickly enough to resolve a useful profile. Therefore, a constant injection rate technique was used when releasing SF_6. Tracer gas was released continuously at a controlled rate of 40 standard cubic centimeters (SCCM), into the model mine at point P2. In the experiment, tracer gas was released 10 min before sampling. An electrical mass flow controller was used to control and measure the tracer gas (SF_6) flow rate.

The experiment requires a sampling technique that is relatively simple with minimum leakage. Four sampling methods were considered including glass syringe, plastic syringe, vacutainer, and glass vial. The 50 µl gas tight glass syringe and 3 ml gas tight disposable syringe

are shown in Figure 15a and b. Glass syringes are expensive and relatively fragile, so they are not appropriate for large samples or transport underground. Experimentation showed that although plastic syringes are inexpensive and convenient, they yielded higher relative standard deviation (RSD) values, which measure the precision and repeatability of gas sample.

Blood collection vacutainers, shown in Figure 15c have long been used for sampling mine air and products of combustion because they are convenient and result in high precision even after one - two weeks of storage [131], [132]. The 10 ml vacutainer was chosen as the sampling method for the experiment. The vacutainers were re-evacuated in the laboratory to improve the sampling accuracy which improved the capability of vacutainers.

Crimp top vials, shown in Figure 15d, were also evaluated in a similar manner as the vacutainers. However, it was determined that the integrity was largely dependent on the crimping technique which was not consistent among vials.

Considering the observation mentioned above and comparison between different gas sampling methods, 10 ml blood collection vacutainers were chosen as a proper sampling method for the experiment.

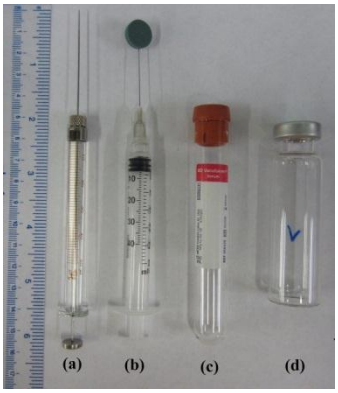

Figure 15. Gas sampling methods

4.3.3 SF_6 measurement

A gas chromatograph equipped with an electron capture detector (ECD) was used to analyze the concentration of SF_6 in collected samples. Calibrations are required before testing and the accuracy and precision of the calibrations are critical for quantitative analysis. A series of SF_6 standards were made, at concentrations of 10, 20, 50, and 100 ppm, to create a calibration chart that could be used for the analysis of SF_6 between 10 and 100 ppm. The standards were made by injecting 2.75 µl, 5.5 µl, 13.75 µl, and 27.5 µl pure SF_6 into a 275ml glass bulb which was full of ultra-pure nitrogen to make 10 ppm, 20 ppm, 50 ppm, and 100 ppm standards,

respectively. 20µl injections of those standards were made to the GC using the 50µl gas tight glass syringe shown in Figure 15a. The complete calibration chart is shown in Figure 16.

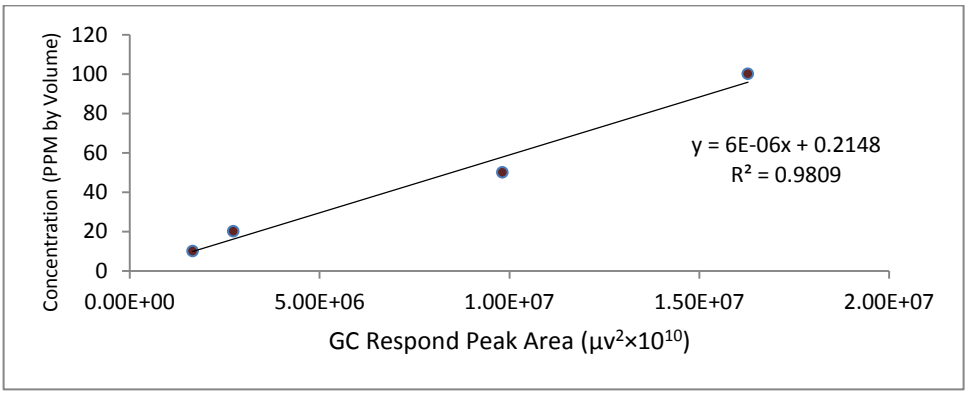

Figure 16. GC calibration chart for SF_6

As noted, units of ppm were used for the SF_6 concentration, indicating parts per million by volume or by mole, which are identical for an ideal gas, and it has the same value at both actual and standard conditions because the temperature and pressure changes affect the denominator of the ideal gas law proportionally [133].

After gas samples were collected from the laboratory apparatus using vacutainers, 20 µl of the gas sample was taken from the vacutainer, and injected to the GC using a 50 µl gas tight glass syringe. Three samples were taken at the same sampling location, and the average SF_6 concentration was used as the final result.

4.3.4 Experimental ventilation status

The experimental mine model was operated under four different conditions by closing and opening different valves, which represent the normal case, roof fall occurrence in an active panel, explosion in the gob panel, and stopping damage. These scenarios were chosen because they are likely to disrupt ventilation and have potential for remote characterization by tracer gas. The air flow path under normal case is shown in Figure 13 while other cases are shown in Figure 17. For convenience, the normal ventilation condition, roof fall in active panel, explosion in the gob panel, and stopping damage, will be referred as Case 1, Case 2, Case 3, and Case 4, respectively.

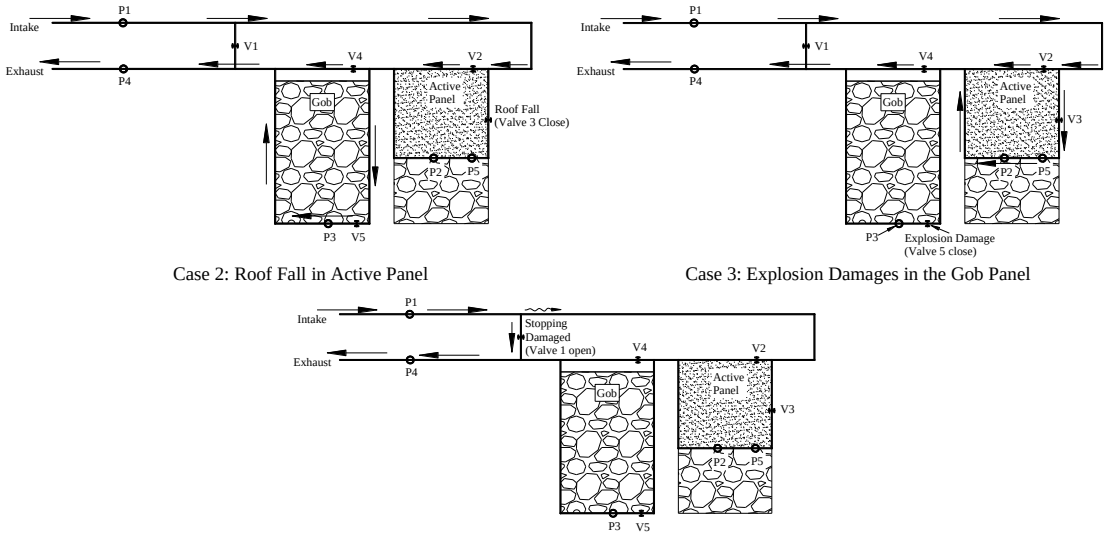

Figure 17. Air Flow path of different ventilation conditions

As can be seen, air flow paths under the four ventilation conditions are different and should result in varied distribution of SF_6. Although ventilation parameters, such as velocity and pressure, are different for each case, it may be difficult to measure those parameters after an incident in the field. However, air samples are routinely taken from boreholes when a mine is inaccessible and the tracer concentration can be analyzed.

4.4 CFD model setup

4.4.1 Hypothesis

Approximations and simplifications of the actual problem are needed to construct the CFD study, which allows for analyzing the problem with reasonable effort. The following assumptions are made in this study:

1) No leakage in the model mine.
2) Mine air is incompressible.
3) PVC pipe surface is smooth.
4) The flow in the model mine is fully turbulent.
5) No heat transfer during the procedure and the wall and air temperatures are constant.
6) The gravity influence on SF_6 is not considered.
7) Introduction of SF_6 will not influence the final steady state of the air flow.

These assumptions are made based on our preliminary study focuses. For example, assumption 1 is not realistic because small leakage could exist at the connections of the pipes. But the influence of this small leakage on the final experimental results is minor or predictable.

A better understanding and interpretation of the actual problem and the results also make the assumptions reasonable. Take assumption 7, for example, the influence of releasing small amount of SF_6 to the air flow is very minor compared to the quantity of air flowing through the model mine.

4.4.2 Governing equations

CFD is based on the fundamental governing equations of fluid dynamics, including the continuity equation, momentum equation, energy equation, and transport equation, which express the fundamental physical principles of fluid dynamics. The energy equation was not used in the model since the modeling fluid was assumed to be incompressible and there is no heat transfer. The governing equations can be expressed in the conservation form of transport equation [78]:

$$\frac{\delta(\rho_t \varphi_t)}{\delta t} + \mathrm{div}((\rho_t \overrightarrow{V_t} \varphi_t) - \mathrm{div}((\Gamma_{\varphi_t} \rho_t \mathrm{grad} \varphi_t) = S_{\varphi_t} \quad (4\text{-}4)$$

Where, $\varphi_t$is general variable of interest, ρ_t is air density, Γ_{φ_t} is diffusive coefficient, and S_{φ_t} is source term [78].

In the CFD model, SF_6 was released at a constant rate of 40 SCCM at a point corresponding to P2 in Figure 13, which is the same release rate and location as the laboratory experiment. It was simulated using user defined scalar, and scalar transport equation (Equation 4-4) was solved to calculate the velocity, pressure, and other quantities of SF_6. However, in turbulent flows, the diffusion, which is the third term of Equation 4-4, was programmed as a user defined function as follows [134]:

$$\Gamma_{\varphi_t} \rho_t = \Gamma_{\varphi_t} \rho_t + \frac{\mu_t}{S_{C_t}} \quad (4\text{-}5)$$

where $\Gamma_{\phi t}$ is the diffusion coefficient of SF_6 in air, μ_t is the turbulent viscosity, and S_{Ct} is the turbulent Schmidt number. Tucker et al. [135] provided an equation to calculate $\Gamma_{\phi t}$ of one gas in another gas resulting in a diffusion coefficient of SF_6 in air 8.96×10^{-6} m^2/s. Bai et al. [136] used a value of 9.7×10^{-6} m^2/s in their study; while Ward and Williams [137] reported the diffusion coefficient of SF_6 in air is between 5.9×10^{-6} m^2/s and 7.3×10^{-6} m^2/s. These values do not differ substantially, especially when considering the term μ_t / S_{Ct}, which determines turbulent diffusion, generally overwhelms laminar diffusion, which is determined by $\Gamma_{\phi t} \rho t$ [50]. Therefore, the final result is not significantly sensitive to the range of $\Gamma_{\phi t}$ cited in the literature.

This is also proved by the parameter sensitivity study in section 6. A value of 5.9×10^{-6} m^2/s is used in this study. The Schmidt number is a dimensionless parameter which is the ratio of diffusion of momentum to the diffusion of mass. For gases, it is approximately 0.7 [50].

4.4.3 Mesh and boundary conditions

Commercial drafting and meshing tools were used to generate the three-dimensional geometry and mesh. An unstructured, hexahedral mesh was generated to represent the size and geometry of the lab experimental mine model. The "O" grid is used on the pipe cross section with fine mesh near the pipe wall and coarse mesh in the center. This can help resolve the rapid variation of flow variables near the pipe wall with reasonable mesh size and compute time. Due to the complexity of the model, the whole geometry was divided into four parts before generating the mesh. Then four mesh parts were connected by interface boundary condition. Figure 18 shows the CFD model and the O grid mesh can be seen in Figure 19.

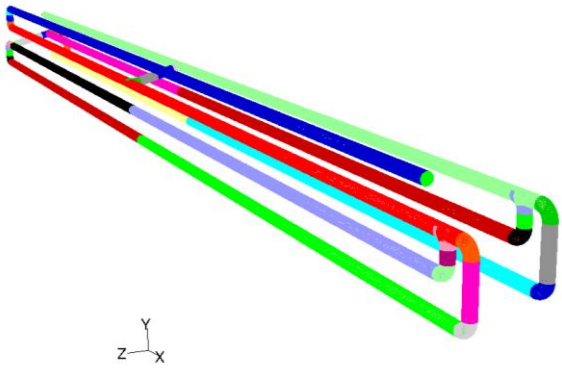

Figure 18. The 3D CFD model and meshing

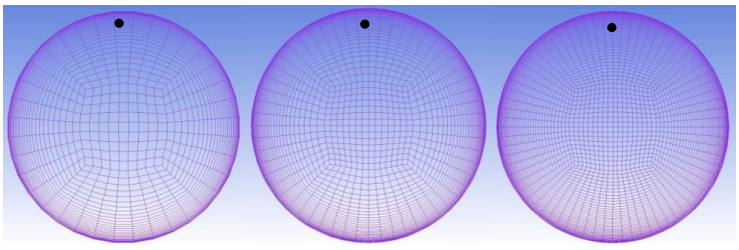

Figure 19. Cross section of different mesh size (from left: coarse mesh, medium mesh, and fine mesh)

The inlet and the outlet of the model were specified as velocity inlet and pressure outlet, respectively. The measured outlet pressures for the four cases were applied to the corresponding model pressure outlet boundary. However, because the pitot tube can only measure the maximum velocity when placed at the center of the pipe, the measured inlet velocities were calibrated so that the velocities at the other four measure points approach the measured value.

Table 4 shows the detail boundaries condition for all cases. All of the other surfaces are treated as stationary walls with no slip. Both air and wall temperatures are assumed constant.

Table 4. Boundary condition

Case Number	Pressure Outlet (Pa)	Velocity Inlet (m/s)
1	335	5.6
2	336	5.5
3	336	5.08
4	332	7.15

4.4.4 Numerical details

The numerical simulations in this study were conducted using the commercial CFD package, ANSYS FLUENT 12.1, to simulate the airflow and tracer gas dispersion. A standard two equations *k*- ε turbulence model was employed to simulate the air flow and SF_6 transport. The standard *k*- ε model is the simplest complete turbulence model and widely used in the modeling of mining turbulent flow in broad range of applications [8], [9], [22]. A second order upwind scheme was used for variables including pressure, momentum, turbulent kinetic energy and turbulent dissipation rate, which ensures the higher order of accuracy results. Discretized airflow equations were solved with the SIMPLE algorithm in the CFD program to couple the pressure, velocity, momentum and continuity equations.

4.5 Mesh independent study

4.5.1 Mesh quality and size

In order to achieve results that are independent of mesh size, three different mesh size models were developed and analyzed, including coarse mesh, medium mesh, and fine mesh. Two factors, determinant and angle, were utilized as a measure of the mesh quality. A determinant value above 0.3 is acceptable for most solvers and the minimum angle value above 18 degree is acceptable for Fluent [50], [138]. The generated mesh quality meets the criteria mentioned above.

The number of nodes are approximately doubled progressively, which is about 10 million, 20 million, and 40 million, for coarse, medium, and fine mesh, respectively. The meshes were generated to improve the node density both on the pipe's cross sections and along the pipe. Figure 19 shows the cross section mesh for coarse, medium, and fine mesh.

4.5.2 Solution convergence

Some criteria need to be met to achieve converged numerical solutions. Two criteria are used to check the solution convergence for each mesh [139]. The first criteria is residuals of each conservation equation, which is a specified tolerance defined by Fluent. The criterion used in this study is continuity residual value equal to or less than 10^{-5}.

Sometimes the residual may reach the convergence criterion, but the solution still changes with more iterations. Therefore, a second criterion is used, which monitors variables of the solution until it no longer changes with more iterations. In this study a point monitor was created on the outlet surface, shown as black dots in Figure 19, and the velocity at these points were monitored. The final velocity values for coarse, medium, and fine mesh size models at the monitor point are 6.716 m/s, 6.717 m/s, and 6.670 m/s, respectively. The velocity differences at the monitor point between medium and fine mesh is less than 1%, which is acceptable and indicates, from one aspect, that mesh independence has been achieved. The mesh independence will be discussed in further detail in the next section.

4.5.3 Mesh independence study

It is important to conduct the mesh independence study before using the CFD results since the numerical solution may depend on the mesh size if mesh independence is not achieved [48]. As the mesh becomes finer, the numerical solution will asymptotically approach the exact solution of the governing equations [43]. Mesh independences are studied considering different flow features and at different locations.

A line at the centerline 0.36 m away from the outlet was created for each case and three velocity profiles across the center line were plotted on Figure 20. It is apparent by comparing the shape of the profile and the predicted velocity that the solution is not changing with the mesh size since the profile points are practically on top of each other, which indicates that the solution is mesh independent. The result differences are within 1% as indicated by the calculation in the previous section. This also indicates that the medium mesh is sufficient for a robust solution and could be used for further modeling.

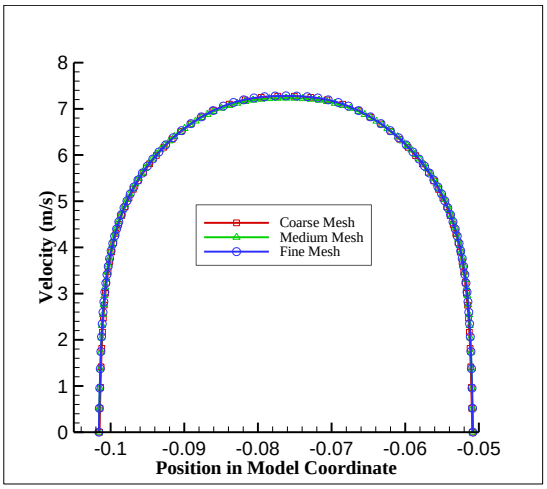

Figure 20. Velocity profile at the line monitor

Velocity contours and vectors are also used for visual comparison of different mesh size results. Due to limited space, they are not shown here. But the contours and vectors between different mesh sizes are generally the same with very small different, and the general high and low velocity zone are pretty similar.

The computed velocities at four velocity monitor points (P1 to P4) are compared with experimental results. The comparison is shown in Figure 21, which shows that the computed results for each mesh size are very close to the experimental results. Based on the comparison, the medium mesh can be chosen with 8.2% RMS (root mean square) deviation compared to experimental results. The differences between the computed and experimental results are due to errors, such as the accuracy of the measured velocity, which will be discussed in detail in section 4.7.

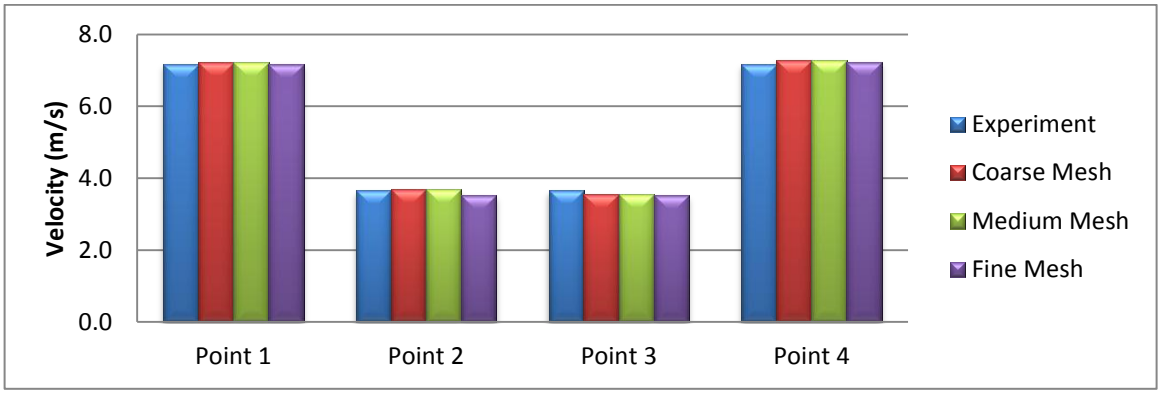

Figure 21. Comparison of computed and experimental velocity

4.6 Results and discussions

4.6.1 Velocity validation

The CFD models were first validated using the experimental velocity results before modeling the tracer. The comparisons with the errors are shown in Table 5. The CFD simulation data were taken at the same locations as the experimental data were measured. It can be seen that the simulated velocity in all cases are in good agreement with the experimental results with no more than 2% error. The differences are larger in Case 4 at points P2 and P3. This is because the manometer used in the experiment is limited in range at pressures equivalent to a velocity of less than 1.5 m/s. Generally, the comparisons indicated that the CFD models are valid and can be used to conduct tracer modeling.

Table 5. Velocity results comparison between experimental measurements and CFD simulations

		P1	P2	P3	P4
Case 1	Experiment	7.17 m/s	3.66 m/s	3.66 m/s	7.17 m/s
	Computed	7.23 m/s	3.70 m/s	3.55 m/s	7.28 m/s
	Error	0.68%	0.74%	3.13%	1.46%
Case 2	Experiment	6.69 m/s	0 m/s	3.34 m/s	6.85 m/s
	Computed	6.73 m/s	0 m/s	3.29 m/s	6.78 m/s
	Error	0.58%	n/a	-1.52%	-1.1%
Case 3	Experiment	6.52 m/s	3.34 m/s	0 m/s	6.69 m/s
	Computed	6.58 m/s	3.36 m/s	0 m/s	6.63 m/s
	Error	0.89%	0.60%	n/a	-0.84%
Case 4	Experiment	9.10 m/s	0 m/s	0 m/s	9.34 m/s
	Computed	9.16 m/s	0.89 m/s	0.87 m/s	9.18 m/s
	Error	0.69%	n/a	n/a	-1.68%

4.6.2 SF_6 concentration results

SF_6 concentrations obtained from the experiments and from the validated CFD models are shown in Figure 22. Because the GC calibration curve is only valid when the SF_6 concentration is between 10 ppm to 100 ppm, results out the range only show approximate values, for example, results above 100 ppm only indicate the results are more than 100 ppm and the extent above it.

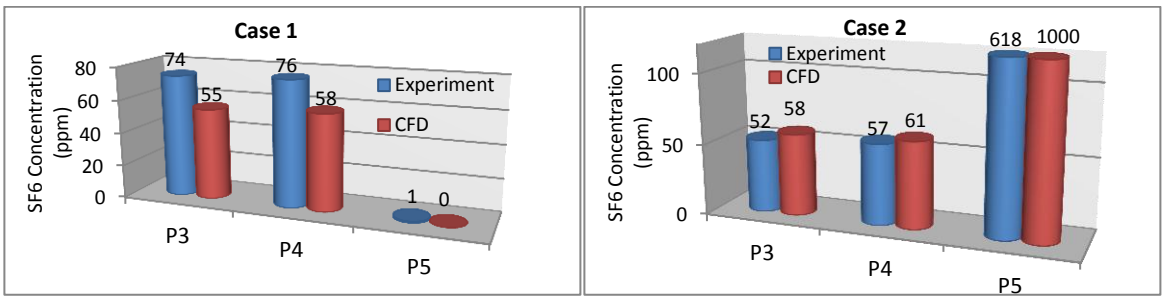

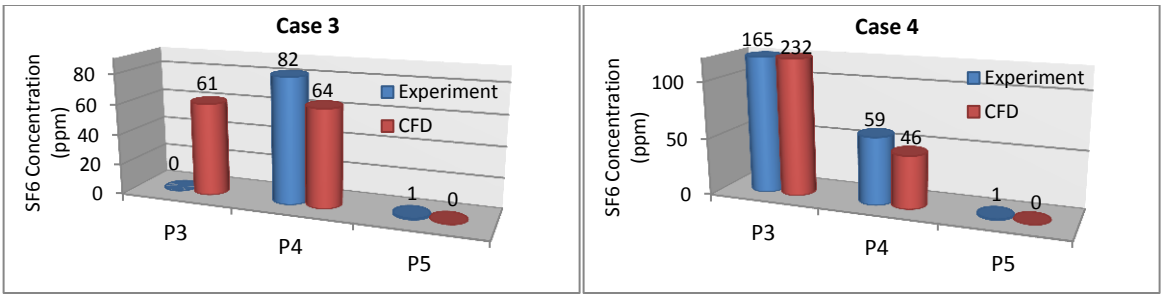

Figure 22. The comparison of experiment and CFD SF_6 concentration results (Values above 100 ppm do not indicate the exact value)

The largest difference is at point P3, Case 3. The CFD result shows 61 ppm while the experimental result is zero. This is under the situation that the explosion damage blocked the entry around the gob and theoretically no airflow exists in the entry. CFD calculations are based on ideal conditions of no air leakage and no flow in this entry. Due to the diffusion caused by the SF_6 concentration gradient between the main entry and the gob entry, the SF_6 concentration eventually reaches an equilibrium state where the concentration is very close to that of the main entry. Therefore, the CFD results showed that the main entry SF_6 concentration at point P4 is 64 ppm and the gob entry at point P3 is 61 ppm. However, the laboratory model mine is not under ideal conditions and it has minor leakage at the connections. Since a negative pressure is created by the exhaust fan in the laboratory apparatus, the leakage can cause fresh air leak into the gob entry and this purge effect overcomes the SF_6 diffusion and causes the experiment result at point P3 to be 0 ppm instead of a value close to that of point P4, which is 82 ppm. The same phenomena caused the CFD result for Case 2 at point P5 to be above 1000 ppm, although the experimental result at the same point is lower. The errors between the experiment and CFD results at other points will be analyzed in section 6. However, except for the large disagreement mentioned above, the experiment and CFD results at other points generally agree with each other, especially in that they display the same trend, as can be seen in Figure 22 (please note that values above 100 ppm do not indicate the exact value).

4.6.3 Ventilation status prediction

From section 4.6.2, one can see that the CFD predicted SF_6 results are in agreement with the experimental results if reasonable explanations are provided, meaning that SF_6 concentration results under different ventilation scenarios can be predicted ahead of time. Four different ventilation scenarios assumed in the experiment led to four dramatically different combinations of SF_6 concentrations at different sample points, as shown in Figure 23. This indicates that it is

possible to use the known SF_6 concentration at different sample points to predict the ventilation scenarios. For example, if we have a result that the SF_6 concentration at point P5 is very low (near zero), but point P3 is much higher than P4, using Figure 23 we can predict that the ventilation status is similar to Case 4, where the stopping between the main entries was damaged. The relationships between the concentrations and the ventilation scenarios are quite straightforward due to the relative simplicity of the mine model.

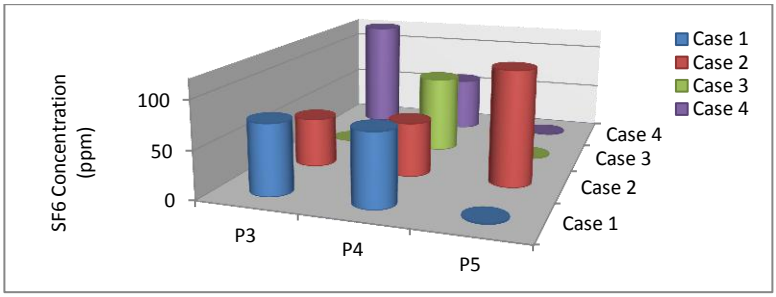

Figure 23. The comparison of SF_6 concentration under different ventilation scenarios

4.7 Error analysis

Velocity and SF_6 concentration are the two key parameters measured in the experiment and calculated in the CFD model. Because the CFD models calculate the results based on assumptions made in section 4.4.1 and measured parameter inputs, discrepancies exist when comparing with the measured results.

Part of the error results from the experimental instrumentation. First, the pitot tube is supposed to be installed against the airflow and at the center of the pipe, but this is not easy to ensure since the PVC pipe is not transparent. The displacement from the center pipe line will cause inaccurate differential pressure reading, resulting in an inaccurate velocity. Second, air density was used in the velocity calculation, but it was calculated based on barometric pressure, temperature, and relative humidity, all of which can introduce measurement error that result in the final velocity calculation error in the experiment. Third, the sensitivity and the accuracy of the manometer also can cause velocity error. The sensitivity of the manometer used is 0.005 in. of water, which corresponds to 1.5 m/s air velocity. The model mine leakage, although minimized by sealing of the apparatus, may also influence the velocities and SF_6 concentrations as well, especially at certain locations where the leakage overcomes the SF_6 diffusion in dead end scenarios. All of these errors may cause a final SF_6 concentration calculation error in the CFD model. Last, the GC calibration curve is a key factor to an accurate SF_6 concentration reading. The procedure described in section 2.3 may introduce error to the calibration curve that

affect the accuracy of the air sample analyses results although the RSD values for the GC work were well within acceptable range.

Parameters input into the CFD model, such as the air density, viscosity, and diffusion coefficient are chosen by the authors from calculation (air density) or from the literature. The air density error was mentioned in the previous paragraph. Air viscosity and diffusion coefficients also vary under different temperatures and in different literature. Therefore, parameter sensitivity studies were conducted using the Case 1 model, which is the normal ventilation status, with parameters chosen in this study, as the control model. Five more runs were calculated with different combinations of parameters, which can be seen in Table 6. From the comparison results, which are shown in Table 7, we can see that a 10% air density deviation has little influence on point velocities, but will cause about 10% SF_6 concentration deviation. The air viscosity deviation has little influence on either velocity or SF_6 concentration. The diffusion coefficient was increased 64% percent to another value found in the literature [136], but the subsequent influence on velocity was no more than 1.15% and SF_6 concentration no more than 4%. This is a minimal effect and this finding is consistent with the discussion about the diffusion coefficient in section 4.4.2. Overall, the three parameters studied: air density, air viscosity, and diffusion coefficient, cannot cause velocity results to err substantially. However, the SF_6 concentration is sensitive to air density, but not to air viscosity and diffusion coefficient.

Table 6. Parameters details for sensitivity study

	Air Density (kg/m^3)	Air Viscosity ($kg/(m•s)$)	Diffusion Coefficient (m^2/s)
Control model	1.1137	1.983×10^{-5}	5.9×10^{-6}
Run #1 (air density increased 10%)	1.2251	1.983×10^{-5}	5.9×10^{-6}
Run #2 (air density decreased 10%)	1.0024	1.983×10^{-5}	5.9×10^{-6}
Run #3 (air viscosity increased 10%)	1.1137	2.181×10^{-5}	5.9×10^{-6}
Run #4 (air viscosity decreased 10%)	1.1137	1.785×10^{-5}	5.9×10^{-6}
Run #5 (diffusion coefficient increased 64%)	1.1137	1.983×10^{-5}	9.7×10^{-6}

In conclusion, the CFD model results can be improved by reducing the instrument errors and providing more accurate parameters for the CFD input. These include precise placement of the pitot tube in the center of the pipe, use of manometers that have higher sensitivity and accuracy, reduction of human errors introduced when calibrating the GC by using accurate tracer gas standard. Also since the tracer gas concentration results are very sensitive to air density, ensuring accurate measurement of barometric pressure, temperature, and relative humidity, can improve the accuracy of the CFD calculated results.

Table 7. The results of models with different parameters

Monitor points		P1	P2	P3	P4
Control model	Vel. (m/s)	7.23	3.70	3.55	7.28
	SF_6 Conc. (ppm)	n/a	n/a	54.78	58.15
Run #1	Vel. (m/s)	7.20	3.68	3.54	7.25
	Error	-0.30%	-0.33%	-0.41%	-0.37%
	SF_6 Conc. (ppm)	n/a	n/a	49.61	51.77
	Error	n/a	n/a	-9.4%	-11.0%
Run #2	Vel. (m/s)	7.25	3.71	3.57	7.31
	Error	0.35%	0.43%	0.55%	0.41%
	SF_6 Conc. (ppm)	n/a	n/a	59.85	63.28
	Error	n/a	n/a	9.3%	8.8%
Run #3	Vel. (m/s)	7.25	3.71	3.57	7.31
	Error	0.31%	0.37%	0.52%	0.37%
	SF_6 Conc. (ppm)	n/a	n/a	53.87	56.95
	Error	n/a	n/a	-1.7%	-2.1%
Run #4	Vel. (m/s)	7.20	3.68	3.54	7.25
	Error	-0.33%	-0.42%	-0.43%	-0.41%
	SF_6 Conc. (ppm)	n/a	n/a	54.73	56.95
	Error	n/a	n/a	-0.1%	-2.1%
Run #5	Vel. (m/s)	7.23	3.65	3.56	7.28
	Error	0.06%	-1.15%	0.26%	-0.02%
	SF_6 Conc. (ppm)	n/a	n/a	52.64	56.95
	Error	n/a	n/a	-3.9%	-2.1%

4.8 Conclusions and discussion

A laboratory experiment and CFD studies were conducted in this study to examine the methodology using tracer gas in conjunction with CFD to determine the ventilation status after a mine incident. A laboratory model mine was built based on a conceptual mine layout which allows for changes to the ventilation status to simulate different ventilation scenarios after an incident. SF_6 was used as tracer gas and different gas sampling methods were evaluated and blood collection vacutainers were chosen to collect sample in the experiment. A gas chromatograph equipped with an electron capture detector was used to analyze the gas samples and the GC calibration method was presented.

CFD models were built and a detail mesh independence study was conducted. The CFD model was also compared with experimental results for validation purpose before it was used to model different ventilation scenarios. The velocity results agreed very well with the experimental results while discrepancies exist when compared to the SF_6 concentration results. However, the differences can be explained reasonably and the CFD results have the same trend as the laboratory experiment. A comprehensive error analysis was conducted focusing on measurement and instrument errors, which can contribute substantially to the errors in SF_6 concentration calculated by the CFD models.

The results indicate that the tracer gas concentrations can be predicted using CFD modeling. Different ventilation statuses will result in substantially different tracer gas distribution if tracer gas experiments were carefully designed. The methodology established in this study is feasible to determine general ventilation status after incidents in subsurface excavations. This requires that a detailed ventilation survey be conducted under normal status in order to establish and calibrate the CFD model. Tracer gas experiments need to be designed and performed carefully in order for ventilation status to be rapidly determined after an incident. CFD models can predict tracer gas distribution results under different ventilation situations and those results should be substantially different if the tracer gas release and sample locations are optimized. By comparing the tracer gas experiment and the CFD predicted tracer gas distribution results, the actual mine ventilation status should be the one with the similar CFD modeled results. Further studies are needed, especially field trial, utilizing the tracer gas method outlined in conjunction with CFD. The real mine experiment allows the use of transient tracer gas release techniques, which are expected to be more efficient and achieve more definitive results.

Due to the complexity involved in simulated the conditions of an underground mine in a laboratory, the model mine apparatus used in this study was simplified and built with PVC pipe. It should be noted that ventilation network modeling can serve the purpose of this study equally well at the macro scale and network modeling can be easily applied to full scale mines while CFD cannot mainly due to its heavy demand on computational time and initial boundary specification. However, network modeling cannot resolve the detail of tracer gas behavior, such as where tracer gas is fully mixed with mine air, layering effects of the tracer, and how a tracer concentration is distributed over entry cross sections. These factors are important for the tracer experiment regarding the best location to release and collect gas samples. The focus of this study is CFD modeling, but as this work is applied in the field, a hybrid scheme will be investigated. A hybrid scheme should combine the benefit of CFD and network modeling. CFD will only be used in critical areas where mixing and diffusion of the tracer gas within the airflow are questionable, while most parts of a mine will be modeled using network modeling to save computational time with equally effective results.

As stated earlier, the transient tracer gas release techniques will be used in the field experiments. The expected results should be similar to the CFD modeling results presented by Xu et al. at 2012 SME [140]. For the purpose of explanation, tracer gas's concentration profile

under assumed normal and roof fall ventilation scenarios from that paper's results are presented in Figure 24. As can be seen, different ventilation scenarios result in different tracer profile in terms of arrival time, number of peaks, and peak height. Because tracer gas field experiments may be time and resource consuming, such simulated results are valuable for on-site tracer experiments design since if the desired results are not achieved, it takes a period of time for tracer to be cleaned out of the mine so it does not interfere the next experiments. For example, the simulation can help to determine how much tracer gas needs to be released in order to achieve a concentration at the monitor point practically detectable, that is to say, we want the concentration fall into the range of the GC calibration curve so the gas samples can be directly injected to GC without dilution or concentration. The optimal time interval for gas sampling can also be determined before the experiment in order to adequately resolve each peak shown in the figure. Overall, the established gas sampling and analysis method in the laboratory can be used in the next stage field experiments. Numerical modeling with CFD or hybrid (CFD and network modeling) approach can not only predict the general ventilation scenarios but also helps the design of tracer gas tests to get the expected results and save time.

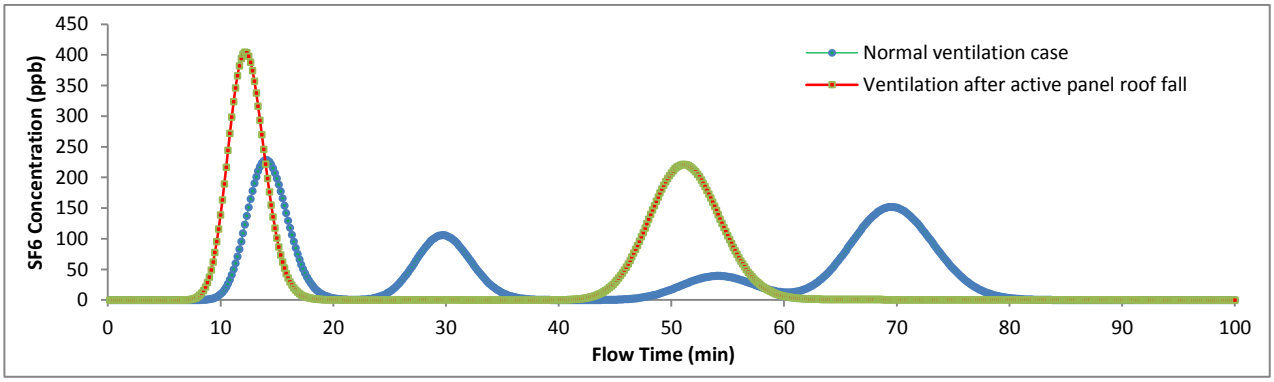

Figure 24. CFD simulated SF_6 concentration at a point monitor of different ventilation status

This paper was presented at the 2012 SME annual meeting in Seattle, Washington on February 22, 2012, and is included in the meeting preprints(Feb. 19 – 22, 2012, Seattle, WA, Preprint 12-051). Guang Xu conducted the majority of the work and wrote the paper with technical and editorial input form coauthors: Edmund Jong, Dr. Kray D. Luxbacher, and Dr. Saad Ragab. Please cite this article as: Xu, G., Jong, E., Luxbacher, K., & Ragab, S. (2012). Computational fluid dynamics study of tracer gas dispersion in a mine after different ventilation damage scenarios. SME Annual Meeting (p. Preprint 12–051). Seattle, Washington (USA).

5 Computational Fluid Dynamics Study of Tracer Gas Dispersion in a Mine after Different Ventilation Damage Scenarios

5.1 Abstract

Tracer gases are an effective method for assessment of mine ventilation systems, but their dispersion characteristics can differ substantially as ventilation parameters, such as flow path and velocity, vary. This research utilizes Computational Fluid Dynamics (CFD) to model a simplified full scale model mine, details a sensitivity study examining mesh size for an underground coal mine simulation, and examines gas dispersion parameters to determine the optimal model methods for simulation of tracer gases in underground coal mines. These models can be used to determine how a given tracer gas profile might be generated in a mine or areas of a mine that are not accessible, for example, immediately following a mine disaster. Accurate simulation scenarios can allow for the remote determination of the status of the ventilation network, but the sensitivity of the simulation at mine scale must be carefully examined.

5.2 Introduction

There is a need to immediately know the underground status right after severe coal mine incidents, such as roof falls, dust, and gas explosion, outbursts, and water inrush. In these situations, measurement of many parameters are necessary to estimate and evaluate the underground situation while organizing rescue operations, and managing the emergency situation. Several techniques can be used for information collection purposes, including collecting air samples from boreholes, inserting a video camera into boreholes to visually monitor underground status, and deploying specialized robots. However, none of these methods is sufficient to stand alone and more methods need to be developed in order to quickly and accurately gather information that could help decision makers manage the emergency effectively, increase safety for rescuers, and advance the rescue operation.

Tracer gas can be used to assess mine ventilation systems, and the dispersion of tracer gas will change according to changes of airflow paths and ventilation patterns, as a result of an incident. For this reason, tracer gas can be used to gather information, compare the results with

computational models and determine the general location of damaged ventilation systems. Numerical simulations using computational fluid dynamics (CFD) can be used to model the ventilation status and the data from tracer gas measurement can be utilized to further analyze, predict and confirm the underground ventilation status and the location of the damage.

The use of computational fluid dynamics (CFD) to simulate flow problems in the mining field has risen dramatically in recent years. CFD has become a cost effective research and design tool with the increasing speed of high performance computers and more advanced computational methods. CFD is applied to a wide range of industrial and research fields, such as aerodynamics of aircraft, automotive, pollution control, agriculture, food science, power plant, civil engineering, hydrology and oceanography, and medical science [3], [10]. It also has been used in a number of mining areas, including modeling ventilation airflow patterns [67], [98], study and control of coal spontaneous heating and underground mine fire [9], [20], [83], optimizing gob inertisation [95], dust control [98], and methane management [91].

An underground mine tracer gas test needs to be carefully designed before the release of any tracers. Knowing the expected results can help optimize the design of the tracer gas test, such as the release location and the rate, and the location and time interval for sample collection. This paper examines a simple full scale model mine CFD study, and primarily aims to review the best methodology for full CFD mine simulations and the potential useful information that the simulation results can provide. Although experimental data are not available to validate the model, several studies were carried out to control the quality of the numerical model results, such as the result convergence study and mesh convergence study. SF_6 was then introduced to the verified models which have different ventilation patterns due to different locations of damage. The SF_6 concentration at the outlet was monitored and compared for different models. The relationship between the tracer's concentration and ventilation status differences are also examined, which demonstrated the feasibility of our methodology to clearly determine different ventilation status after mine incidents using the tracer gas test and CFD simulated results.

5.3 The model mine

A full scale model mine was designed in this study based on the layout of a scaled experimental study presented in a previous paper [128]. As shown in Figure 25 (entries are represented by single lines), the designed mine model has one active panel and one gob panel. Two regulators are used to control the air quantity that goes to the active panel and the gob. The

cross-sectional dimensions are the same for all entries, as shown in Figure 26. The air velocity is defined as 4 m/s at the inlet. The mine layout has been simplified, and obviously does not represent the exact layout of an operating mine. Because CFD is such a computationally expensive technique it is likely that when this methodology is used in the field a combination of simplified mine layouts and less computationally expensive network simulation techniques will be used. Dimension and air quantity in this model are representative of operating mines.

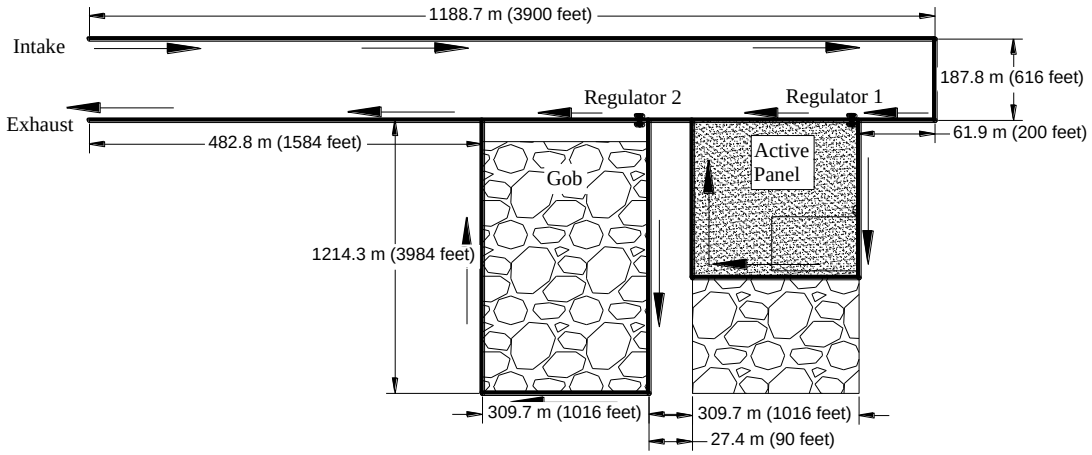

Figure 25. The layout of the full scale model mine

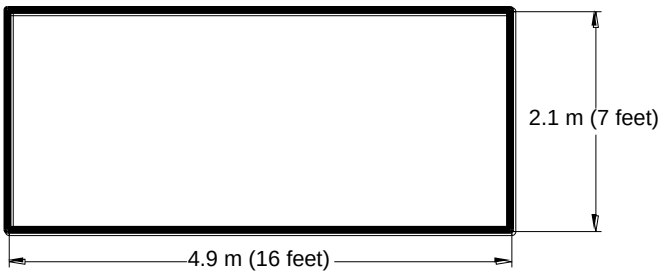

Figure 26. The cross section dimension of the model mine

5.4 CFD model setup

5.4.1 Assumptions

Approximations and simplifications of the actual problem are needed to construct the CFD study, which allows for analyzing the problem with reasonable effort. The following assumptions are made in this study:

1) No leakage in the mine;
2) Airflow is around the gob -- gob flow is not modeled at this stage;
3) Mine air is incompressible;
4) The flow in the mine is fully turbulent;
5) No heat transfer is considered, and wall and air temperatures are constant;

6) The gravity influence on SF_6 is not considered;
7) Introduction of SF_6 will not influence the final steady state air flow.

These assumptions are made based on our preliminary study focuses, which allows us to have basic ideas and data with reasonable effort. For example, assumptions 1 and 2 are not realistic, but this study does not focus on the air leakage and gob air flow, which are extensively being studied by other researchers [8], [92], [141]; this study is a simple and preliminary example of how to ascertain system damage remotely at the mine scale. However, some assumptions could be eliminated as our study progresses by improving our experiment and CFD model or incorporating the results of other study. Other assumptions may be constrained by the CFD model. These can be improved through a better understanding and interpretation of the actual problem and the result data. Take assumption 7 for example, the influence of releasing SF_6 to the air flow is very minor compare to the large space of the mine ventilation system.

5.4.2 Governing equations

CFD is based on the fundamental governing equations of fluid dynamics, including the continuity equation, momentum equation, energy equation, and transport equation, which express the fundamental physical principles of fluid dynamics [134]. The governing equations can be expressed in the conservation form of transport equation [78]:

$$\frac{\delta(\rho_t \varphi_t)}{\delta t} + \nabla((\rho_t \vec{V_t} \varphi_t) - \nabla((\Gamma_{\varphi_t} \rho_t \mathrm{grad} \varphi_t) = S_{\varphi_t} \quad (5\text{-}1)$$

Where, $\varphi_t$is general variable of interest, ρ_t is air density, Γ_{φ_t} is diffusive coefficient, and S_{φ_t} is source term [78].

5.4.3 Mesh and boundary conditions

Commercial drafting and meshing tools were used to generate an unstructured, hexahedral mesh representation of the geometry of the model mine.

The inlet and the outlet of the model were specified as velocity inlet and pressure outlet, respectively. The atmosphere pressure, which is 101.325 kilopascals, is applied to the pressure outlet boundary. A 4 m/s velocity was assigned to the mine inlet to achieve realistic air quantities to each panel. All of the other surfaces and regulators are treated as stationary walls with no slip.

5.4.4 Numerical details

The numerical simulations in this study were conducted using the commercial CFD package, ANSYS FLUENT 12.1, to simulate the airflow and tracer gas dispersion. A standard two equations *k*- ε turbulence model was employed to simulate the air flow and SF_6 transport. The standard *k*- ε model is the simplest complete turbulence model and widely used in the modeling of mining turbulent flow in broad range of applications [8], [9], [22]. A second order upwind scheme was used for variables including pressure, momentum, turbulent kinetic energy and turbulent dissipation rate, which ensures the higher order of accuracy results. Discretized airflow equations were solved with the SIMPLE algorithm in the CFD program to couple the pressure, velocity, momentum and continuity equations.

5.5 Mesh independent study

5.5.1 Mesh quality and size

In order to achieve results that are independent of mesh size, three different mesh size models were developed and analyzed, including coarse mesh, medium mesh, and fine mesh. The mesh quality and node numbers are shown in

Table 8. The mesh quality is considered very high since the determinants are 1 and angles are 90°. The node numbers are approximately doubled progressively from coarse mesh to fine mesh.

The meshes were generated to improve the node density both on the entries' cross sections and along the roadways. The mesh density is high near the roof, ribs and floor in order to resolve the rapid variation of flow variables near these regions. Mesh size is gradually increased toward the center of the roadway where the flow variation gradient is relatively small. The detail nodes number and size for each mesh are shown in Table 9. Figure 27 shows the cross section mesh for coarse, medium, and fine mesh.

Table 8. Mesh quality and nodes number

	Determinant 3×3×3	Angle	Nodes Number
Coarse Mesh	1	90^0	6,692,976
Medium Mesh	1	90^0	13,160,889
Fine Mesh	1	90^0	22,944,064

Table 9. Cross section mesh parameters

	With	Height	The first cell space near the wall (feet)	Increase ratio
Coarse Mesh	38	16	0.12	1.05

Medium Mesh	50	21	0.10	1.05
Fine Mesh	65	26	0.08	1.05

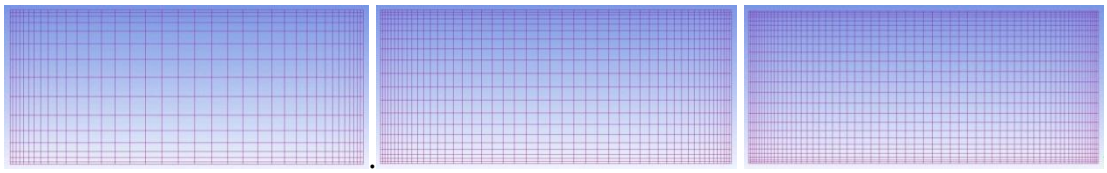

Figure 27. Different mesh of cross section (from left: coarse mesh, medium mesh, and fine mesh)

5.5.2 Solution convergence

Some criteria need to be met to achieve converged numerical solutions. Two criteria are used to check the solution convergence for each mesh [139]. The first criteria is residuals of each conservation equation, which is a specified tolerance defined by Fluent. The solutions are considered converged when the set residual tolerance has been reached. The criterion used in this study is the continuity residual reaches or less than 10^{-6}.

Sometimes the residual may reach the convergence criterion, but the solution still changes with more iterations. Therefore, a second criterion is used, which monitors the solution until it no longer changes with more iterations. In this study a point monitor was created and the velocity at this point was monitored. The point monitor was set 304.8m away from the outlet, in the middle of the roadway center line, and 0.15 m below the roof as shown in Figure 28. More iterations are applied until the velocity is stable. Figure 29 shows the velocity change with iterations for each mesh size model. The plot shows that the solution for each model at the monitor point stabilized and reached a steady state with further iterations, so the results are considered converged. One can notice that differences exist between different mesh size models. The final velocity values for coarse, medium, and fine mesh size models at the monitor point are 3.8396 m/s, 3.9347 m/s, and 3.9871 m/s, respectively. The percentage change value can be used to compare the results changes with mesh difference. The percentage change equation is given by the following equation.

$$Percentage\ Change = \left|\frac{A-B}{A}\right| \times 100\% \qquad (5\text{-}2)$$

Where A is fine mesh result and B is medium or coarse mesh result. Using equation 2 to compare the velocity differences with mesh difference, we get:

$$Velocity\ Percentage\ Change_{Coarse\ to\ Fine} = \left|\frac{V_{Fine}-V_{Coarse}}{V_{Fine}}\right| \times 100\%$$
$$= \left|\frac{3.9871-3.8396}{3.9871}\right| \times 100\% = 3.70\%$$

$$Velocity\ Percentage\ Change_{Medium\ to\ Fine} = \left|\frac{V_{Fine} - V_{Medium}}{V_{Fine}}\right| \times 100\%$$
$$= \left|\frac{3.9871 - 3.9347}{3.9871}\right| \times 100\% = 1.31\%$$

Where V is the velocity result of each mesh. These calculations indicate that the velocity differences at the monitor point between medium and fine mesh is less than 2%, which is acceptable, and the conclusion can be made that mesh independence has been achieved, which will be discussed in detail in the next section.

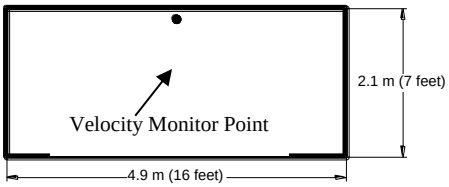

Figure 28. Point monitor location

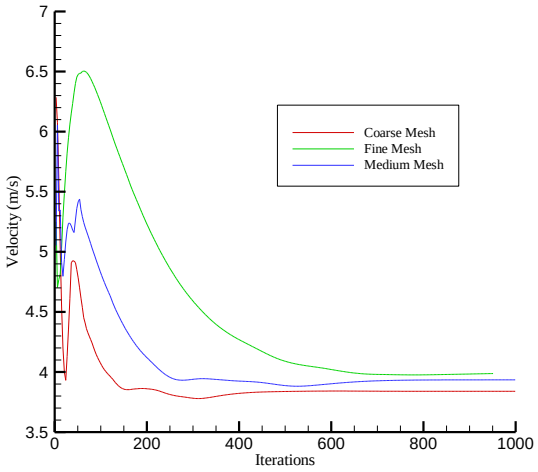

Figure 29. Velocity convergence history for different mesh size

5.5.3 Mesh independence study

It is important to conduct the mesh independence study before using the CFD results since the numerical solution may depend on the mesh size if mesh independence is not achieved [48]. As the mesh becomes finer, the numerical solution will asymptotically approach the exact solution of the governing equations [43]. Mesh independences are studied considering different flow features and at different locations. The following section shows the details of the comparison.

With the purpose of comparing the final result profile of different mesh size models, a horizontal center line 45.7 m and 304.8 m away from the outlet was created for each case and three velocity profiles across the center line were plotted on Figure 30 and Figure 31. From

Figure 30 we can see that as the mesh becomes finer, the results are changing but asymptotically approaching a profile which is the actual results. Figure 31 also indicate that the results of different mesh size are very close.

In this study, the solution is considered mesh independent since the result of medium mesh and fine mesh are very close as can be seen in Figure 30 and Figure 31. The result differences are within 2% as indicated by the calculation of previous section. This also indicates that the medium mesh is sufficient for a robust solution. However, fine mesh will provide more precise solution with longer computation time. In this study fine mesh is used since its computation time is still acceptable.

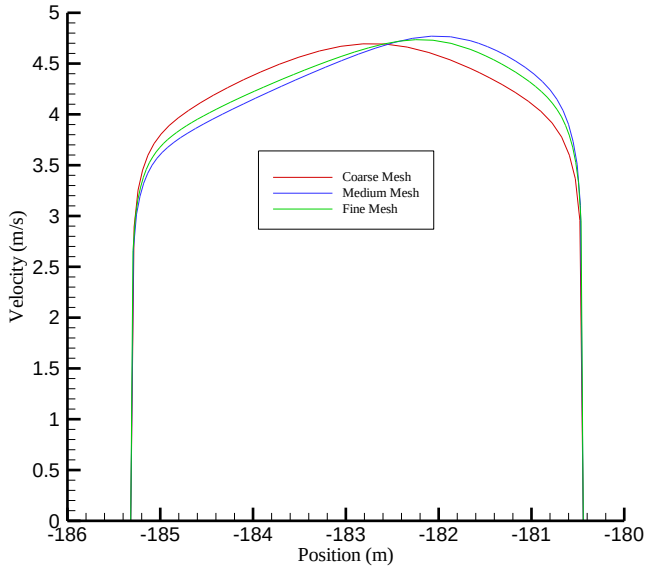

Figure 30. Velocity profile at the line monitor 45.7 m away from outlet

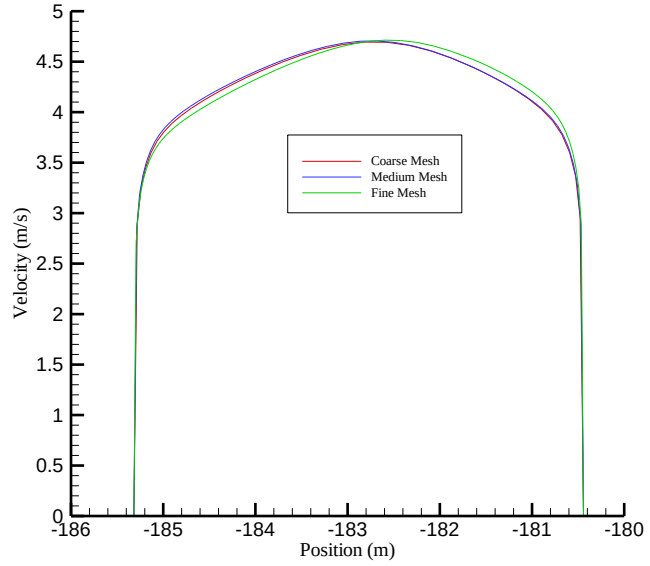

Figure 31. Velocity profile at the line monitor 304.8 m away from outlet

5.6 SF_6 transport simulation

5.6.1 Ventilation status

Beside the normal ventilation status which is shown in Figure 25, two more ventilation statuses are designed, which represent an airway totally blocked under two different conditions: a roof fall occurrence in active panel (Figure 32) and an explosion in the gob panel (Figure 33). The former case reduces air flow to the active panel while the latter case reduces air flow to the gob panel.

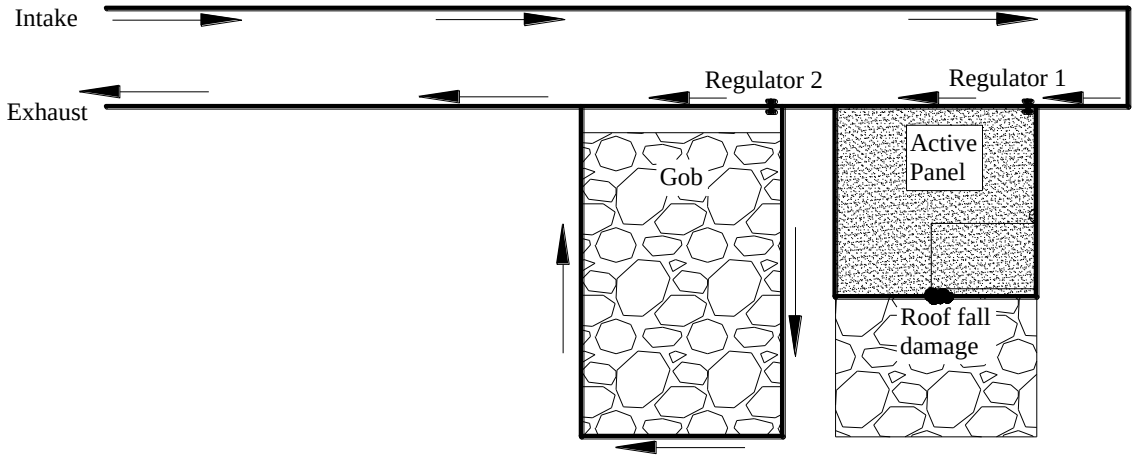

Figure 32. Airflow path after roof fall damage in the active panel

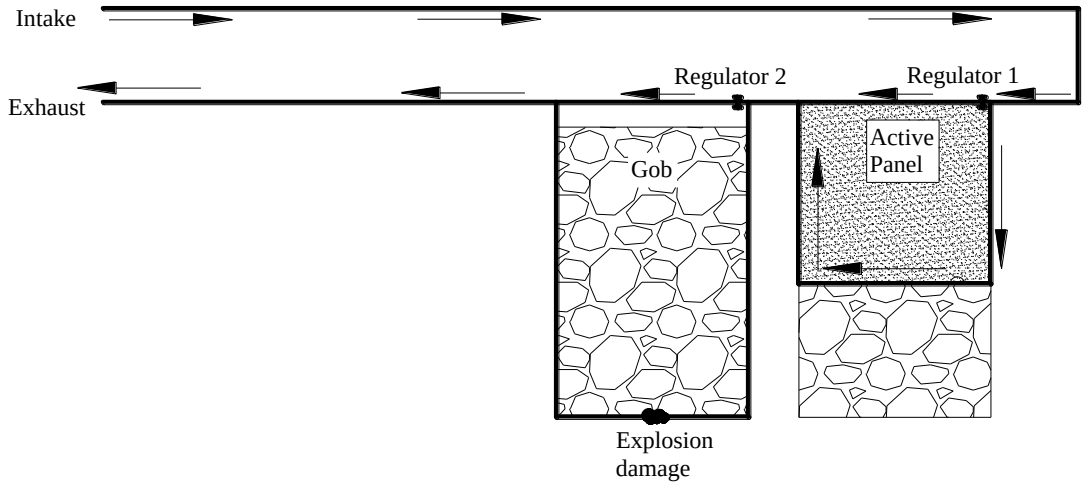

Figure 33. Airflow path after explosion damage in the gob

5.6.2 Tracer gas simulation

SF_6 is released at 4.6 m (15 feet) away from the inlet. The tracer is released at the constant rate of 10 L/min for 1min. A user defined scalar was used to simulate the tracer, and the scalar transport equation (Equation 1) was solved to calculate the velocity, pressure, and other

quantities of SF_6. However, in turbulent flow, the diffusion, which is the third term of Equation 5-3, was programmed as a user defined function as follows [134]:

$$\Gamma_{\varphi_t \rho_t} = \Gamma_{\varphi_t \rho_t} + \frac{\mu_t}{S_{C_t}} \quad (5\text{-}3)$$

Where Γ_{φ_t} is diffusion coefficient of SF_6 in air, μ_t is the turbulent viscosity, and S_{C_t} is the turbulent Schmidt number. Tucker et al. [142] provided an equation to calculate Γ_{φ_t} of one gas in another gas resulting in a diffusion coefficient of SF_6 in air 8.96×10^{-6} m^2/s; Bai et al. [136] used a value of 9.7×10^{-6} m^2/s in their study; while Ward et al. reported the diffusion coefficient of SF_6 in air is between 5.9×10^{-6} m2/s to 7.3×10^{-6} m2/s. These values do not differ substantially, especially when considering μ_t, the second term in Equation 3, which is three orders of magnitude larger than Γ_{φ_t}; the final results is not significantly sensitive to the range of Γ_{φ_t} cited in the literature. Therefore, a value of 5.9×10^{-6} m^2/s is used in this study. The Schmidt number is a dimensionless parameter which is the ratio of diffusion of momentum to the diffusion of mass. For gases, it is approximately 0.7 [50].

5.6.3 Results

SF_6 concentration was monitored at the outlet and plotted over time, as shown in Figure 34. Four possible tracer gas travel paths are plotted in Figure 35, which are numbered from 1 to 4. As can be seen from Figure 34, different ventilation scenarios have totally different SF_6 profiles at the outlet. Four peaks are observed for the normal ventilation status, which represents the tracer gas going through all four paths showed in Figure 35 (from inlet directly to outlet, from inlet to active panel then to outlet, from inlet to gob panel then to outlet, and from inlet to active panel then to gob panel to outlet). Two peaks show up for active panel roof fall and gob explosion scenarios, but the peak height and arrival times are different. In both scenarios, the first peak represents flow path #1, in which SF_6 flows from inlet directly to the outlet. In the active panel roof fall case, the air path also goes from the inlet to gob panel then to outlet (flow path #2); and in the gob explosion case, the second air path is from the inlet to active panel then to outlet (flow path #3). The flow path #3, which going to gob panel is longer than flow path #2 that to active panel, therefore the second peak of active panel roof fall case shows up later than that of gob explosion case.

The peaks can also be grouped according to the arrival time, which is directly related to the flow paths. The arrival time of each flow path in the three different ventilation status are

approximately in the same time range due to the fact that the total quantity of mine air is not changed. Figure 34 shows the simulated peaks for each scenario relative to each other, with the scenario flow paths in Figure 35.

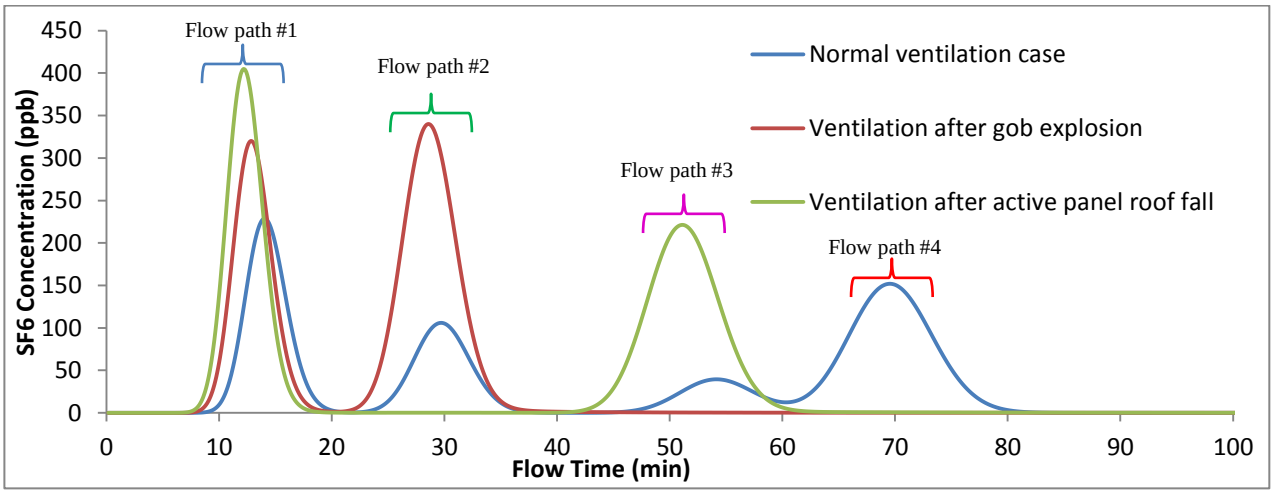

Figure 34. Simulated SF_6 concentration at a point monitor on the outlet VS flow time

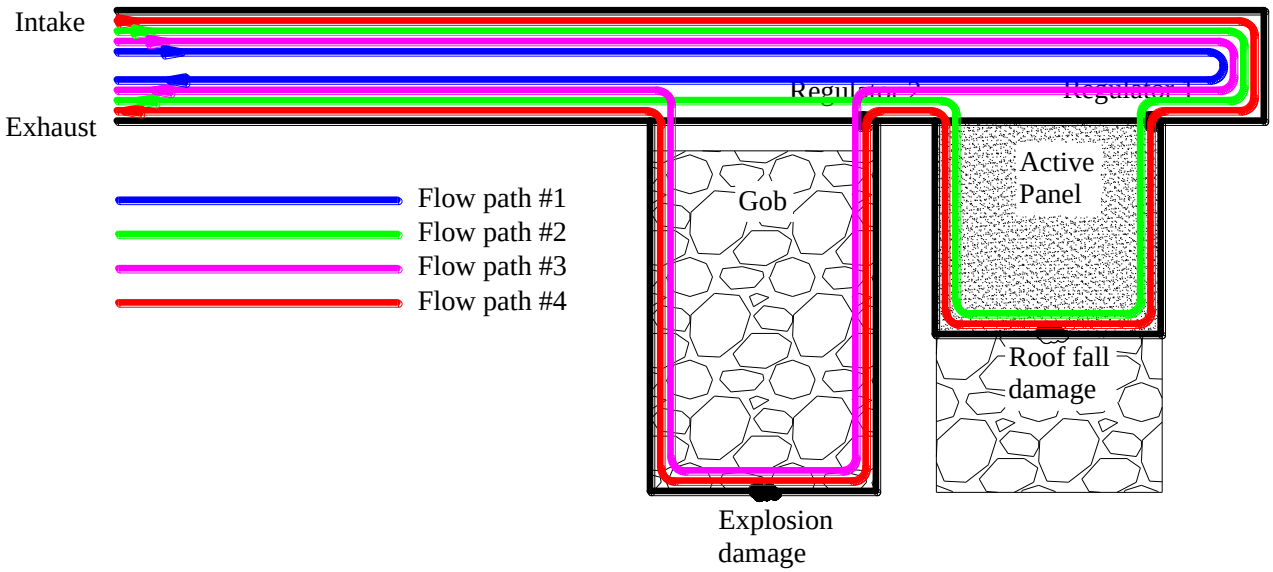

Figure 35. Tracer gas flow paths

5.7 Conclusions and discussions

This study conducted a full scale simplified model mine CFD simulation. Solution convergence and mesh independence studies were performed in order to obtain results independent of the model mesh size. The mesh size used in this study can be utilized as a guide when constructing field scale CFD models in underground mines. Additionally, this paper details the methodology for conducting convergence and mesh independence studies which are necessary for generating robust solutions with CFD.

Pulse injection of tracer gas (SF_6) was simulated for three different ventilation scenarios, which are the normal operating scenario, ventilation after roof fall in the active panel, and ventilation after gob explosion. SF_6 concentration was monitored at the outlet and plotted over time. The SF_6 concentration profile is obviously different for the three different ventilation statuses, which indicated that this method can be used to analyze and predict the ventilation status underground.

The simulated results are also valuable for the design of on-site experiments. For example, the results can be used to determine how much tracer gas needs to be released in order to achieve a concentration at the outlet that is practically detectable; how long the tracer gas should be released in order to generate the peaks for each airflow path, which is a key factor in identifying separate peaks for various ventilation scenarios; and the optimal time interval for sampling in order to adequately resolve each peak (in this study the smallest peak width is 10 minutes, which requires 1 minute sample interval to capture 10 points on the peak).

Further field experiments studies are needed to validate the CFD mode. Nevertheless, this study illustrates the potential of CFD to model tracer gas and its use in determining underground ventilation status. The CFD model and the predicted results in this study provided valuable guidance for further real mine CFD model and tracer gas field experiments design. Tracer gas experiments may be time and resource consuming. Therefore, carefully field tracer experiment design is very important in terms of efficiency and effectiveness. The CFD methods used in this study allows the researchers to determine release rates and volumes, expected profile shape and width allowing for design of best sample collection, and to anticipate profiles under various scenarios; all essential information for the experimental design.

The following paper will be submitted to a peer reviewed journal. The experimental and CFD modeling work and writing was primarily completed by Guang Xu with editorial and technical input from Dr. Kray Luxbacher, Edmund Jong, Dr. Saad Ragab, and Dr. Michael E. Karmis.

6 Remote Characterization of Ventilation Systems using Tracer Gas and CFD in an Underground Mine

6.1 Abstract

Following an unexpected event in an underground mine, it is important to know the state of the mine immediately, even with limited information, to manage the situation effectively. Especially when part or the whole mine is inaccessible, remotely and quickly ascertaining the ventilation status is essential to mine personnel and rescue teams for making effective decisions. This study developed a methodology that combines tracer gas and CFD modeling to remotely analyze underground mine ventilation systems. The study was conducted in an underground mine with four different ventilation scenarios created intentionally for this study. CFD models were built not only to simulate various ventilation scenarios, but also to optimize tracer test parameters to minimize the trial and error process. This minimization guarantees that the status of a ventilation system can be identified more rapidly in an emergency situation. The methodology was successful in identifying the experimental ventilation. This study showed that this methodology was effective in the field. Limitations of this study are discussed at the end of this paper.

6.2 Introduction

The remote collection of data is necessary when circumstances prevent people from entering an underground mine. Such situations include roof falls, outbursts, water inundations, or explosions. Communications between underground miners and rescuers on the surface may be tenuous at best because very few commercially available communications systems are capable of meeting basic requirements for emergency communications [117]. However, information regarding the status of the mine must be gathered immediately to estimate the extent of damage before determining rescue and recovery methods. Even with considerable improvement in underground communications systems, it is still necessary to remotely ascertain the mine's status using other methods. Some alternate methods can be used to gather information safely, such as collection of air samples from boreholes, insertion of video cameras into boreholes to visualize

underground status, and utilization of rescue robots if possible. However, none of these methods are reliable enough to stand alone.

Remotely and quickly ascertain the ventilation status is essential to mine personnel and rescue teams for making effective decisions. Especially in some incidents, such as explosions, communication lines may be damaged, roof may be collapsed, and stoppings may be destroyed. The post-incident status of these components are largely unknown. The airflow quantity, airflow paths, and ventilation patterns will change according to the nature of the damage. Therefore, the level of damage can be approximated by remote measurement of these ventilation parameters. Due to the complexity of the ventilation system, employment of the tracer gas method is an effective means of characterization ventilation systems where conventional techniques are inadequate or cannot be effectively employed [1], [2]. Computational Fluid Dynamics (CFD) can be used to model normal ventilation patterns as well as possible post-incident scenarios. By comparing the actual tracer test results and the modeled results under different ventilation conditions, the state of the ventilation system can be determined.

Tracer gas was first used in the building ventilation systems in the 1950s [61] and has been widely used for ventilation analysis both in buildings and in underground mines [118]. Numerous studies have utilized tracer gas techniques as a means to evaluate ventilation systems in underground metal/non-metal and coal mines. Sulfur hexafluoride (SF_6) is widely accepted as a standard mine ventilation tracer [118], because it can be detected in low concentrations, and it is nontoxic, odorless, colorless, chemically and thermally stable, and does not exist naturally in the environment [1]. Therefore, it was selected for use in this study. The applications for tracer gases in underground mines include measurement of turbulent diffusion [107], methane control [121], study of mine ventilation recirculation of return into intake air, transit flow times through stoped areas, effectiveness of auxiliary fans, and estimation of volumetric flow rates [1], [122], air leakage investigation, and evaluation of dust control measures [62]. However, most of these studies did not use CFD to design the tracer test in advance and usually were based on experience as well as trial and error.

CFD has become a powerful tool and has been commonly used to model underground mine air flows [67], [100]. It has been used in a number of areas including ventilation airflow patterns modeling [67], [98], study and control of coal spontaneous heating and underground fire [9], [20], [83], optimization of gob inertization [95], dust control [98], and methane management

[91]. The combination of experimental measurement and CFD modeling of tracer gas has been used to study airflow and contaminant transport in indoor environments and other industrial applications [114], [123], but little research has been done to model underground tracer gas applications, especially to optimize tracer test parameters and to remotely characterize ventilation systems after an unexpected event.

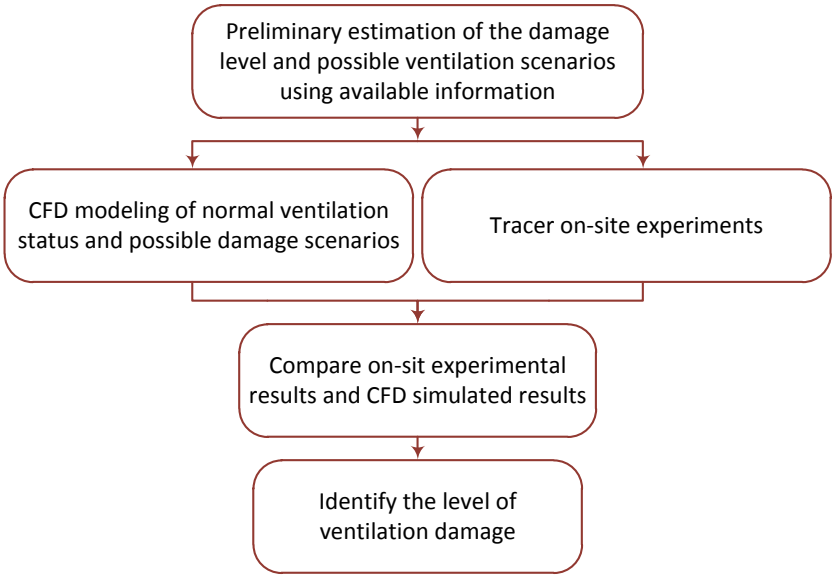

Figure 36. Flow chart of the methodology

The objective of the study presented in this paper is to develop a new methodology that can identify the general level of ventilation damage using a tracer gas and CFD modeling. An overview of the methodology can be seen in the flow chart shown in Figure 36. After an unanticipated event that has changed the ventilation controls, the level of the damage and the possible ventilation changes need to be estimated based on the available information. The CFD model can then be built to model the normal ventilation status before the event and possible ventilation damage scenarios. At the same time, tracer gas tests can be designed and performed on-site. Tracer gas can then be released at a designated location with constant or transient release techniques. Gas samples are collected at other locations and analyzed using a gas chromatograph (GC). Finally, through comparing the CFD simulated results and the tracer on-site test results, the general level of ventilation damage can be determined.

In this study, the tracer SF_6 was released in an area of a limestone mine with varying ventilation statuses intentionally created for this study. The scenarios included a stopping door open and closed and a booster fan turned on and off in various combinations. For this study, personnel were used inside the mine to conduct the experiments. However, in an actual event,

tracer gas release and sampling would be made through boreholes or other remote access. CFD models were built based on detailed mine entry measurements and ventilation surveys under the different scenarios. The CFD models were not only used for simulating tracer dispersion under the different scenarios, but also for tracer test design to optimize essential parameters, such as tracer release location, release rate and duration, and sampling location. The trial and error procedure is thus reduced or even avoided to achieve the desired results. According to the optimized parameters, SF_6 was released in the mine using the pulse release method. Gas samples were taken continuously using blood collection Vacutainers. The gas samples were analyzed by GC and the tracer concentration profiles were plotted over time for the different ventilation scenarios. The CFD model results agreed with the on-site tracer test results with reasonable errors. The experimental results showed that this methodology can help determine the ventilation system status. The developed methodology proved feasible in the laboratory in an earlier study [143]. This methodology provides an alternate way to gather information that can be used by mine personnel and rescuers to take safe and effective actions.

6.3 Onsite Experiments Description

6.3.1 Location of the onsite experiments

The experiments were conducted in the mine section shown in Figure 37. It is a 250 m belt entry, which is connected to a 40 m crosscut. The average cross sectional dimension of the belt entry is 5×2.8 m and 5.87×3.82 m for the cross cut entry. However, the cross sectional dimensions of both entries were measured every ten meters, and the results were used to construct the CFD model so that the actual dimension of those entries could be more accurately represented in the model. Three steel water pipes and one conveyer belt were present within the entries. They are considered large enough to influence the air flow, so their dimensions and positions were also measured and included in the CFD model as solid impermeable regions. There are two velocity inlets, one is at the lower end of the belt entry, and the other one is the stopping door at the end of the crosscut. Airflow directions are shown as red arrows in Figure 37.

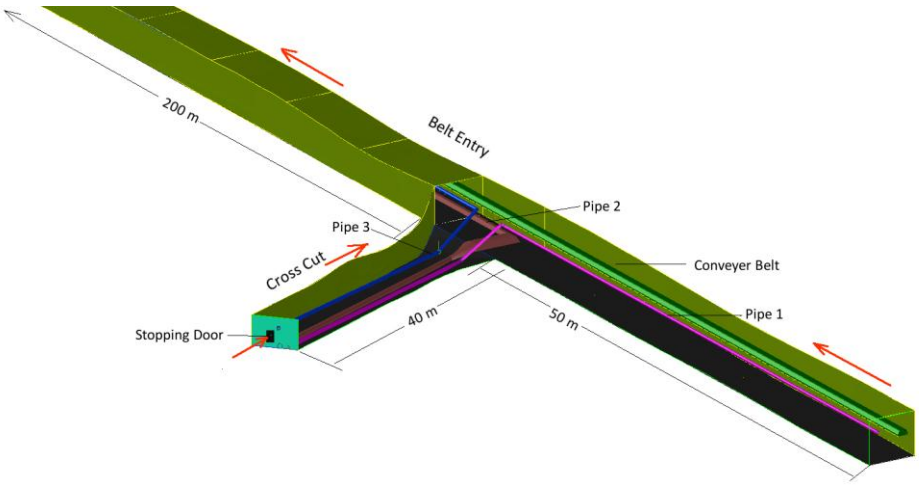

Figure 37. Layout of the entry section (red arrows show the air flow)

There is a booster fan at the bottom of the belt entry (not within the measured and modeled domain shown in Figure 37) that can be turned on or off causing total air flow change in the belt entry. Therefore, the different ventilation scenarios could be created intentionally by opening and closing the stopping door, and turning the booster fan on and off. A combination of four different ventilation scenarios from manipulating these parameters is presented in Table 10. Each scenario was assigned a case number and will be referred later in the paper for convenience. The velocity boundary conditions at the inlets are also shown in Table 10. The goal of this study was to design appropriate tracer gas tests and build CFD models to identify these four ventilation scenarios.

Table 10. Different ventilation scenarios

	Door velocity inlet (m/s)	Belt entry velocity inlet (m/s)
Case #1: Stopping door open, booster fan on	4.21	2.54
Case #2: Stopping door close, booster fan on	0.06	2.54
Case #3: Stopping door open, booster fan off	4.21	2.10
Case #4: Stopping door close, booster fan off	0.06	2.10

6.4 Tracer test design using CFD

Tracer gas experiments are time and resource consuming. Therefore, it is important to carefully design the experiments beforehand. Some essential parameters, such as the tracer release location, release rate and duration, sampling location, and the expected results, can be optimized using a CFD model before conducting the actual experiment. This makes it possible to reduce or even avoid the trial and error procedure to achieve expected results. CFD models were built in 2D to save computational time and in 3D to provide more accurate results.

6.4.1 CFD model setup

Approximations and simplifications of the actual problem are needed to construct the CFD study, which allows for an analysis with reasonable effort. The following assumptions are made in this study:

1) Mine air is incompressible;
2) The flow in the mine is steady and fully turbulent;
3) No heat transfer occurs during the study and the wall and air temperatures are constant;
4) The gravity is 9.81 m/s^2;
5) Introduction of SF_6 will not influence the existing steady state air flow.

The inlet and the outlet of the model were specified as velocity inlet and pressure outlet, respectively. The averaged velocity values, which are shown in Table 10, were applied to both of the velocity inlets in the belt entry and at the stopping door. These boundary conditions are based on the average measured air velocity readings by a hot wire anemometer using the fixed point traverse method. All of the other surfaces are treated as stationary walls with no slip. Both air and wall temperatures are assumed constant. A realizable two equation k-ε turbulence model was employed to simulate the air flow. A second order upwind scheme was used for variables including pressure, momentum, turbulent kinetic energy, turbulent dissipation rate and SF_6 transport, which ensures the higher order of accuracy results. Discretized airflow equations were solved with the SIMPLEC algorithm in the CFD program to couple the pressure, velocity, momentum, and continuity equations. A gravity of 9.81 m/s^2 was used to establish gravitational influence on the flow and SF_6 distribution. Steady state flow was calculated first for all cases and then SF_6 was released for a certain period at a designated location using the two species (air and SF_6) transport model. Two solution convergence criteria are used: the continuity equation residual reduced to 10^{-5} and the velocity at a pre-selected point achieved steady-state. A mesh independency verification was conducted for the CFD models to ensure that the results were independent of the mesh size. This verification is only presented for the 3D model in Section 6.4.3.

6.4.2 2D CFD model

A CFD model can be built in either 3D or 2D. A 3D model can provide more accurate results, but it is much more computationally intensive compared to the 2D model, especially when parameters need to be adjusted frequently during the optimization process. Therefore, a 2D

model was used first to provide results quickly, and after the optimized parameters were determined, a 3D model was used to obtain more accurate results. The 2D model schematic is shown in Figure 38.

The tracer gas release point was located in the crosscut entry in order to capture the flow changes in both the belt entry caused by the booster fan and the crosscut entry caused by the stopping door. Two locations were examined: one is 38 m from the door and is denoted as Release Point 1, the other is 2.5 m from the door and is denoted as Release Point 2. Both points are in the center of the entry. The sample points were chosen 10 m from the model outlet and 7 point monitors that are evenly distributed across the entry were created in the model to monitor SF_6 concentration change.

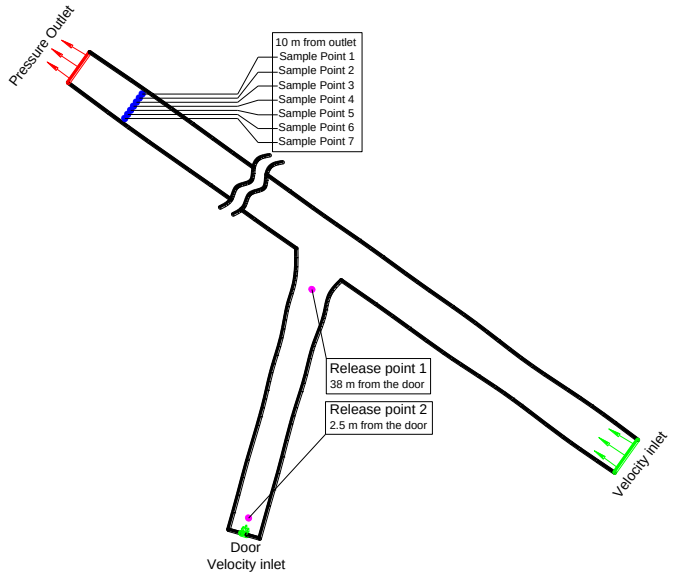

Figure 38. Tracer gas release and sample points

To design a tracer experiment, the first parameter that needs to be defined is where to release tracer. The two proposed release points in Figure 38 were examined under different cases. Point 1 was chosen as the release point because tracer concentration profiles can be captured within 10 min after release, while more than 20 min sampling time is needed to capture the tracer profile when the door is closed if released at Point 2.

The second parameter is the amount of tracer to release so that gas samples can be directly analyzed using GC at a concentration level within the detection limit. The amount of tracer released to the mine is controlled by the combination of the release rate and the release duration. The release rate is controlled by a flowmeter. After examining several different release

rates in the CFD model, it was determined 8.89 L/min was a reasonable rate to produce a concentration profile within the GC detection range.

The release duration not only determines the maximum concentration of the tracer profile but also the width of the tracer profile with respect to time. The profile time-width needs to be wide enough to allow enough samples to be taken. As can be seen in Figure 39, under Case 1 (door open, fan on) and release at the rate of 8.89 L/min, different release durations result in different profiles. If the release is too short, such as 10 s, the profile peak lasts only 30 s, which makes it hard to adequately sample to capture the peak. The concentration profile becomes broader as the release duration increases from 10 s to 2 min. Figure 39 also shows that the 30 s release increased the maximum concentration level compared to the 10 s release. However, increasing the release duration further, to 1 min and 2 min, did not increase the maximum concentration level. That is because the release duration is long enough that the maximum concentration leveled out under the fixed release rate. By comparing these profiles, releasing the tracer for 1 min was determined to be adequate for our sampling and analyses convenience. The expected concentration profile width is more than 80 s. This was wide enough to be captured by a 5 s sampling interval that we use in the field.

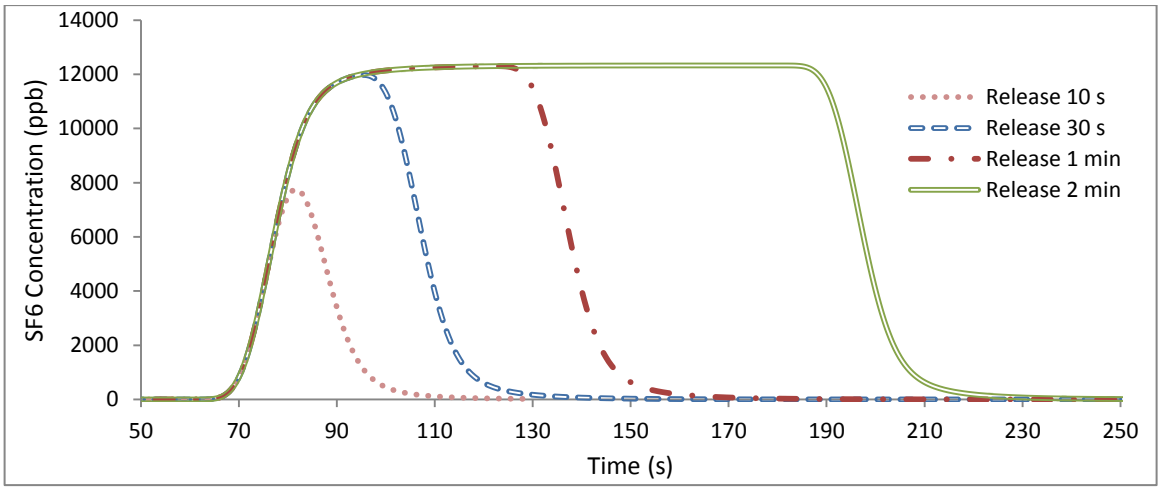

Figure 39. SF6 concentration profile under different release durations

The third parameter was where to take samples. Seven sample points, denoted as Sample Point 1 to 7 in Figure 38, evenly distributed across the entry were monitored. The final sample point was determined to be at Sample Point 7. The distribution of SF_6 in the belt entry was higher toward one side of the entry where Sample Point 7 was located and gradually lower toward where Point 1 was located, which can be seen in Figure 41. The tracer gas concentration profiles for these points were plotted in Figure 40. The maximum concentrations at the

monitored points were generally less than 12 ppm. At these concentration levels, a higher concentration can be analyzed relatively accurately. Therefore, Sample Point 7 was chosen to take air samples.

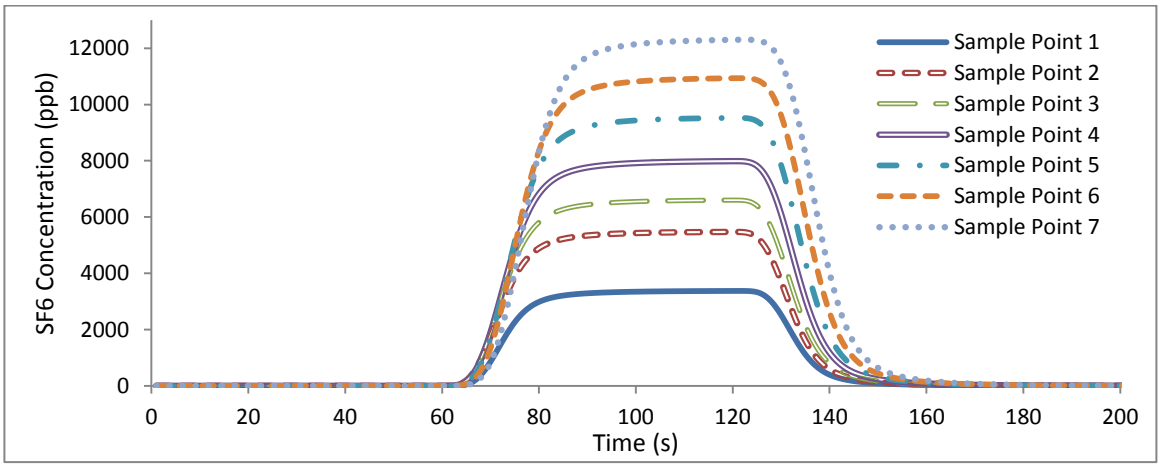

Figure 40. SF6 concentration profile on different monitor points

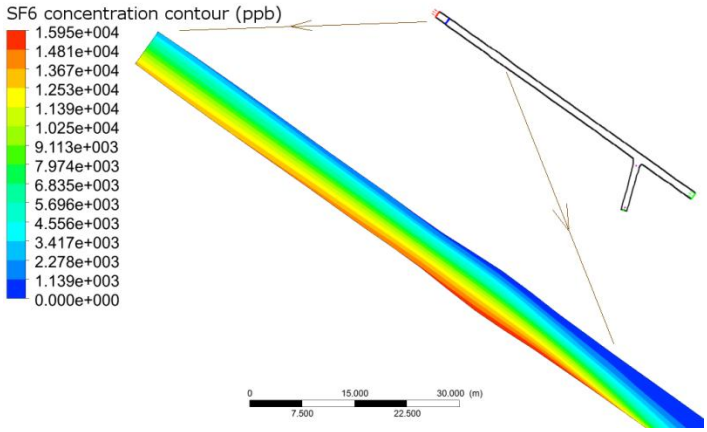

Figure 41. SF6 concentration contour after 170s release (Case 1)

It is always better to know the expected results beforehand. Based on the studies shown above, the optimized tracer test parameters are as follows: the tracer release location is located at Point 2 in Figure 38, the release rate is 8.89 L/min for one minute, and the sampling location is at Sample Point 7 in Figure 38. The SF_6 concentration profiles under the four ventilation cases, mentioned in Table 10, are shown in Figure 42. As can be seen, the profiles under the different ventilation cases are separated with each other based either on the differences in the peak arrival time or the peak height. The tracer profile shape is very different when the door is open and closed. This is because the flow features in the crosscut entry, especially at Point 1, are different, which is shown in Figure 43 as flow path lines. When the door is open, the tracer will go directly to the belt entry and to the outlet because the flow direction around the release point directly

goes to the belt entry. However, when the door is closed, there are circular flow directions around the release point causing the tracer to recirculate in the crosscut and flow to the belt entry very slowly.

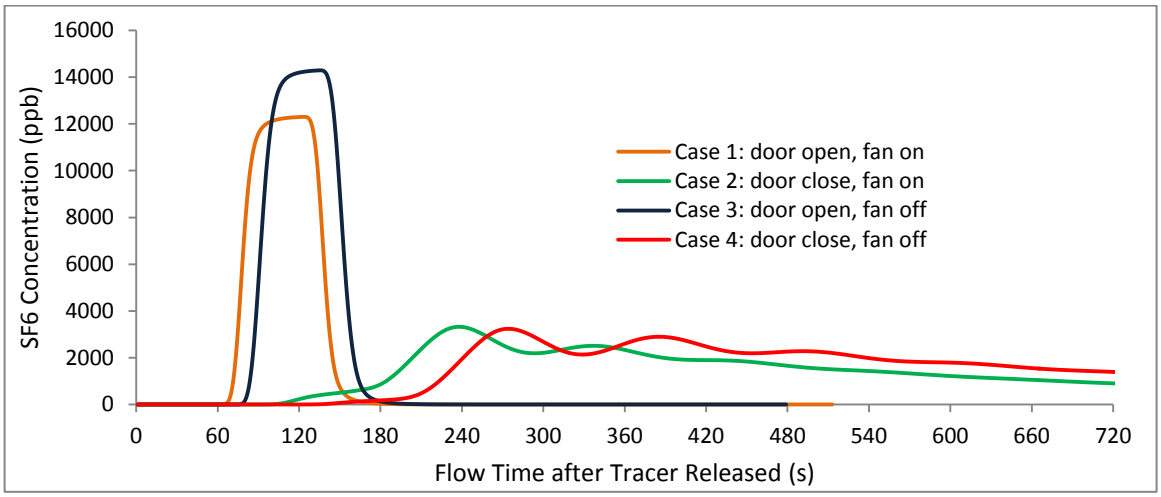

Figure 42. SF_6 profile comparison under different ventilation status

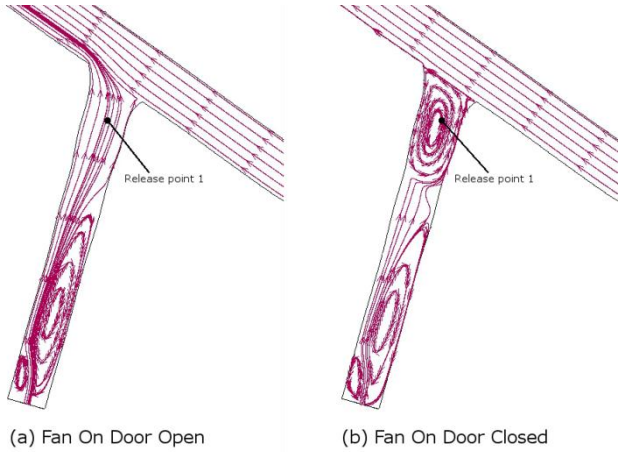

Figure 43. Flow feature difference in the cross cut entry when the stopping door is open and close

6.4.3 3D CFD model

2D flow is different from 3D flow. A 3D model provides more accurate results. Therefore, after the parameters were determined using a 2D model, a 3D model was used to validate and provide more accurate results.

The geometry of the 3D model is complex, mainly because of the existence of the water pipes in the entry. Meshes were generated using Ansys ICEM software and the cross section meshes are shown in Figure 44. A tetra-dominated mesh with prism layers was generated at the beginning of the modeling (Figure 44 (a)). However, the mesh quality is limited and difficult to

improve, which increase the difficulty for solution convergence. A hexa mesh (Figure 44 (b)) was generated later to improve the mesh quality, convergence behavior, and result accuracy. Due to the complexity of the geometry, it was divided into four parts. The meshes were generated separately in ICEM and combined together later in Fluent.

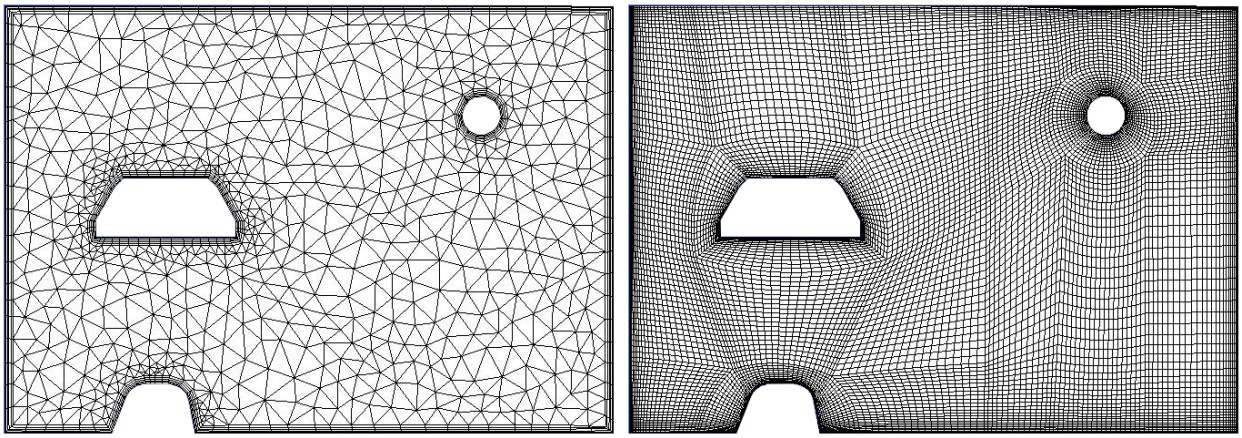

Figure 44. Mine entry mesh types

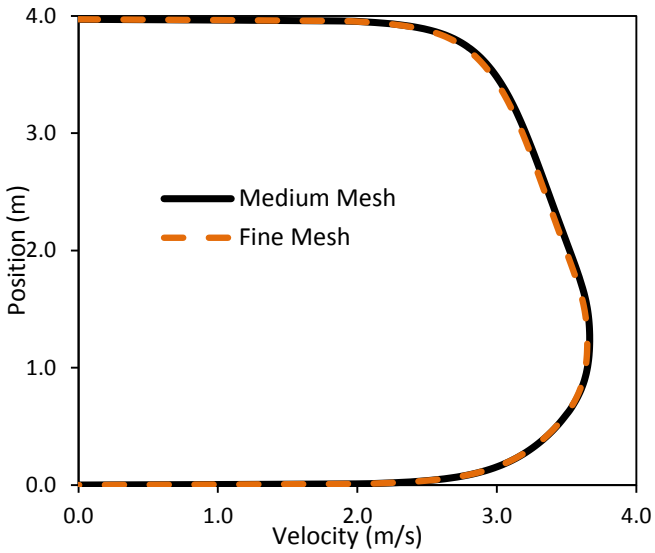

Figure 45. Medium and fine mesh velocity comparison

A mesh independence study was conducted by generating a medium and a fine mesh and comparing the results. This step is essential in CFD modeling because the numerical solution, such as velocity and tracer concentration in this study, may be affected by the mesh size if mesh independence is not achieved [48]. As the mesh becomes finer, the numerical solution will asymptotically approach the exact solution of the governing equations [43]. The total number of nodes for the medium mesh is about 20 million, and 40 million for the fine mesh. Since the focus

of this study was not to find the coarsest mesh that can achieve acceptable accurate results, the number of nodes chosen in this study was relatively large to guarantee a robust solution. The velocity profiles on the vertical center line of the cross section 10 m from the outlet are plotted in Figure 45. The profiles are nearly identical for medium mesh and fine mesh, which indicates that the solution is mesh independent. The medium mesh was chosen for further modeling in this study to save computational time.

For validation purposes, the modeled results were compared with the measured results. Nine points on the cross section 10 m away from the outlet were monitored and compared with the measured results. These points are numbered and shown on the contour in Figure 46(a). The actual velocities were measured using a hot wire anemometer at each point for one min. The average value was used as the measured value. Table 11 shows the velocity values at each point and the error compared to the measured values. As can be seen, the error can be up to 12%, but most of the errors are under 5%. The errors are acceptable since the flow in the mine entry was constantly changing due to factors such as truck movement. The flow variation can cause large measurement error as well. Thus, the CFD model is considered well agreed with the measured data, especially in the high and the low velocity regions. The contour shown in Figure 46(a) also indicates that the water pipes and conveyer belt have significant influence on the flow distribution.

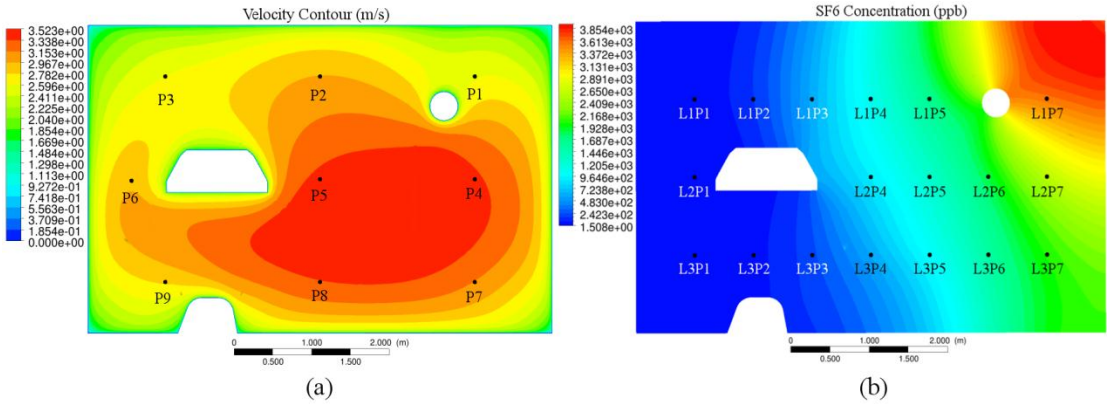

Figure 46. Velocity and SF_6 contour at cross section 10 m from the outlet (used case 2 as an example)

Table 11. CFD and measured velocity comparison

Point Number	P1	P2	P3	P4	P5	P6	P7	P8	P9
CFD Result	2.57573	2.97129	2.59509	3.36968	3.38794	2.92456	3.14654	3.32651	2.80662
Measured Result	2.63682	2.96578	2.34262	3.55174	3.22278	2.67142	3.14568	3.14054	2.50506
Error	2.3%	0.2%	10.8%	5.1%	5.1%	9.5%	0.0%	5.9%	12.0%

The validated model was used to model SF_6 transport. As discussed previously in Section 6.4.2, SF_6 was not evenly distributed over the cross section in the 2D model. Figure 46(b) shows the SF_6 contour from the 3D model 130 s after the tracer was released. Case 2 is used as an example in this figure, but the tracer distribution is very similar for all four cases. As can be seen, SF_6 concentration is higher at the top right corner and lower at the bottom left corner. This indicates that although SF_6 is heavier than air, it does not necessarily concentrate on the bottom since air flow features can overcome gravitational influences. This result also agrees with the 2D model. Several monitor points, which are shown in the figure, were set up to monitor the SF_6 concentration change with time.

Because monitor point L2P7 is the corresponding point with Sample Point 7 in the 2D model shown in Figure 38, the profile at this point was plotted as solid lines together with the 2D results in Figure 47 for comparison purpose. As can be seen, the 3D result profiles are generally lower than the 2D results, and the peak arrival times are also different. However, for different ventilation scenarios, they provide similar profile trends regarding the relative tracer arrival time and concentration level. As will be discussed later, the 3D results are more accurate compared to the field test measured results. Sample point L2P7 in Figure 46(b) is about 2 m high in the entry, which is not a convenient sampling point. The actual sampling point was chosen to be L3P7, which is about 1 m from the floor. The SF_6 concentration profile at this point is plotted in Figure 48 using dashed lines. Compared to the profiles at L2P7, they have a lower concentration level because the distribution of SF_6 is low toward the bottom part of the entry. The comparison to the actual measured profiles will be discussed in the next section.

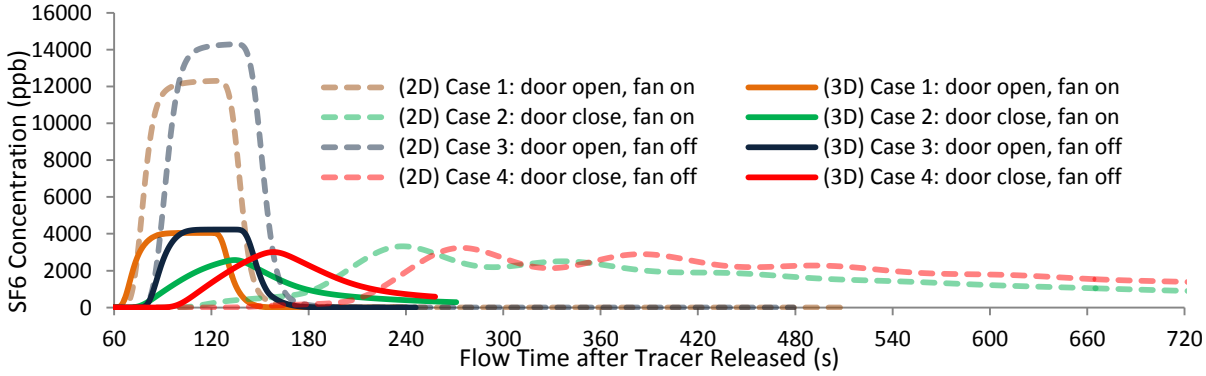

Figure 47. SF_6 concentration change with time

6.5 Onsite experiment

6.5.1 Tracer gas release, sampling, and analysis

The pulse release technique was used to deploy the tracer. Air samples were taken at 5 s intervals using the 10 ml blood collection Vacutainers. A Vacutainer is an evacuated glass tube-shaped vessel and is capped with a self-sealing rubber septum. It has been used extensively for sampling mine air and products of combustion because they are convenient and result in high precision even after one to two weeks of storage [131], [132]. These evacuated containers are not completely evacuated at the time purchased, so they were further evacuated in the laboratory to improve the sampling accuracy.

A GC equipped with an electron capture detector (ECD) was used to analyze the concentrations of SF_6 in the collected samples. After gas samples were collected using Vacutainers and brought to the GC laboratory, 20 μl of the gas sample were taken from the Vacutainer and injected to the GC using a 100 μl gas-tight glass syringe.

6.5.2 Onsite experimental results

The onsite experiments were conducted according to the tracer test parameters produced by the CFD model described in the previous section. These parameters are also summarized in Table 12. The measured tracer profiles are plotted in Figure 48. It shows that the profile for the different cases compared well with the CFD modeled results: the tracer arrival time is earlier and the maximum concentration level is lower when the booster fan is on compared to when it is off; the concentration profile is flatter and much broader when the door is closed compared to when it is open. However, the modeled concentration levels are generally 30% lower than that of the measured results, and the tracer arrival time differences are smaller for the measured results.

These errors can be caused by many factors, such as the model geometry not being exactly the same as the actual geometry due to measurement limitations and simplifications; the ventilation state was also constantly changing due to large vehicle movement or shift changes. However, there are two major factors that may contribute the most to the error: the first one is that the total flow quantity is about 13% less at the time of the field tracer test than the total flow measured earlier to build the CFD model, and the second one is that the flow quantity difference created by the booster fan is smaller than what was measured before. The first factor can lead to

the concentration level raising, and the second factor causes the tracer arrival time differences to become smaller with the booster fan on and off.

There are a couple of possible explanations for the first factor. During the time of the field experiments, a stopping door near another auxiliary fan located further away in the belt entry was kept open due to maintenance. This caused recirculation that reduced the total flow quantity. The CFD model was built in the summer of 2012, but the field experiments were conducted 6 months later in the winter. The barometric pressure change from summer to winter can reduce the total air flow quantity as well. The reason for the second factor is uncertain. It could be because the velocity measurements contained errors in the summer, the barometric pressure changed, or the mine configuration changed. The last two reasons could have caused part of the air quantity created by the booster fan to go to other places instead of the location where the experiments were conducted.

Table 12. Onsite tracer test parameters

Release Location	Release Rate	Sampling Location	Sampling Frequency	Total Sample Time
Point 1 in Figure 38	8.8 L/min	Point L3P7 in Figure 46(b)	5 s	500 s

Nevertheless, the CFD models were not adjusted according to the air flow quantities measured in the winter since any mine ventilation system is dynamic and would continue to change. The CFD model was also not updated because it is not practical to build the model and conduct the tracer test in the same day to account for changes. In the cases studied in this paper, although the total flow quantity was changed, the CFD model still successfully provided good results that can be used to design the tracer test and predict expected ventilation statuses. As can be seen in Figure 48, both the CFD and the field test results indicated that the tracer arrival time is earlier but maximum concentration level is lower when the booster fan is on compared to when it is off. The concentration profiles are much flatter and have a long tail when the door is closed compared to when it is open.

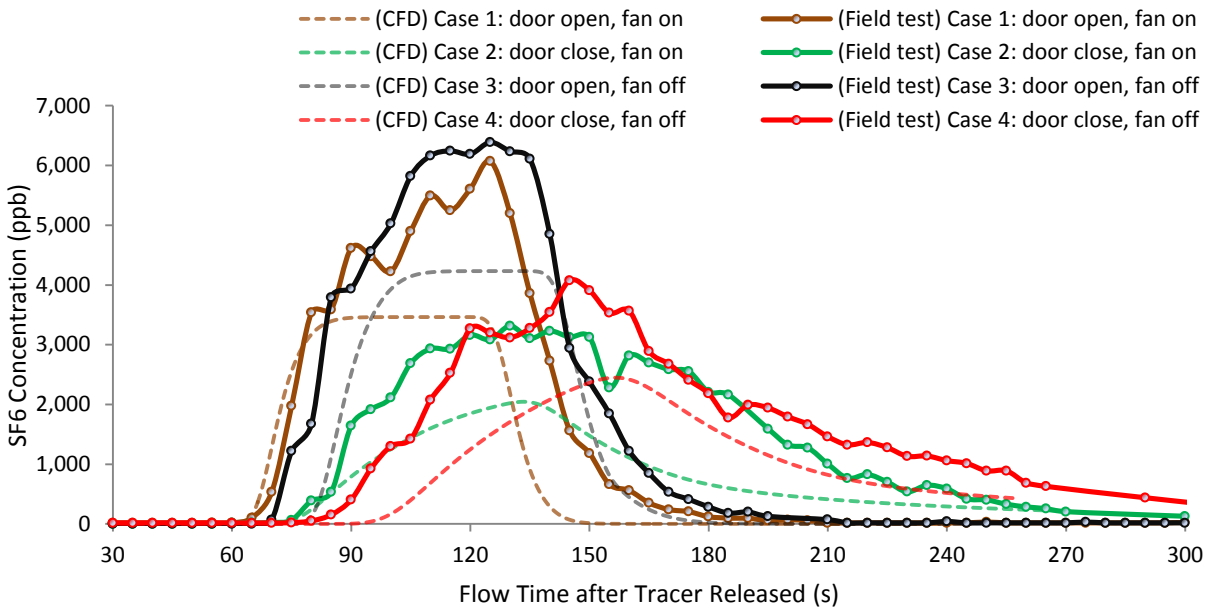

Figure 48. Modeled and measured SF6 profile comparison

6.6 Conclusions and discussion

In conjunction with the laboratory experiments conducted earlier [143], on-site experiments and CFD studies were conducted in this study to examine the methodology using tracer gas and CFD modeling to remotely analyze underground ventilation systems in the field.

A mine section with a 250 m belt entry connected to a 40 m crosscut entry was chosen. Four different test ventilation scenarios were created by opening and closing the stopping door, and turning the booster fan on and off. Ventilation surveys and mine entry dimension measurements were conducted before the tracer release experiments, which provided information for the 2D and 3D CFD models. The CFD models were used to determine the optimal tracer gas test parameters, such as the tracer release locations, rate, and duration, and the sampling locations. The 2D model was used to provide preliminary tracer gas test parameters. After these parameters were determined, the 3D model was used to obtain more accurate results.

The on-site tracer experiments were conducted according to the parameters determined by the CFD model. A flow meter was used to control the tracer release rate. Air samples were taken at 5 s intervals using the 10 ml evacuated containers. A GC equipped with an electron capture detector (ECD) was used to analyze the concentrations of SF_6 in the collected samples. The CFD model results compared well with the experimental results with acceptable differences, which are explained in the previous section.

This study indicates that different ventilation statuses will result in different tracer gas distributions. The developed methodology uses CFD modeling and tracer gas test to remotely analyze ventilation systems in subsurface excavations proved to be feasible both in the laboratory in another study [143] and in the field. However, detailed ventilation surveys and mine entry dimension parameters under normal conditions need to be available in order to establish and calibrate the CFD model. Tracer test results may be more sensitive to certain ventilation conditions than others depending on how the test is designed. CFD models played an important role in this study, not only in providing the expected tracer concentration profiles, but also in determining optimized parameters that would produce the best results and avoid the trial and error processes. This is extremely important because if the tracer test is not well designed and fails at first, more time will be squandered in subsequent tests.

This study also identified and incorporated errors that will occur as the result of the dynamic nature of a mine ventilation system. It is only practical to develop a model of a mine ahead of time and use it later, especially as applied to mine emergencies. This study demonstrates that even with the incorporation of these errors the methodology is still valid.

In an actual situation where the ventilation status needs to be determined using this methodology, only one tracer test could be conducted to produce one concentration profile which could then be compared to the possible scenarios modeled by CFD. As can be seen from Figure 48, the profile shape was more sensitive to the door status but less sensitive to the booster fan status. When the door was closed, the profiles have a very long tail that is obviously different from the bell shaped profiles when the door is open. This is easy to identify. However, if the door status is the same, the profiles when the booster fan was on or off were very similar. The major difference is found in the earlier tracer arrival time when the booster fan is on. In this case, it is hard to determine the booster fan status with the existing CFD model. It requires that the CFD model be built based on the most recent ventilation survey data and that the modeled tracer arrival time results are accurate enough to compare with the field tracer test results. Therefore, a more accurate ventilation survey data under normal conditions is needed for such a case. The tracer test could also be redesigned, for example by changing the release location, to capture the fan status more accurately.

In an emergency situation rapid tracer deployment is essential. In this study, tracer tests were designed using CFD, which eliminated the trial and error processes. The optimized

parameters obtained from the models proved to be very useful as tracer data was successfully obtained after only one release. Tremendous time and resources were saved by reducing such items as the number of trips to the mine and re-deployment of the tracer.

Estimating the level of damage and possible ventilation scenarios plays an important role in successfully identifying the actual ventilation scenario. If actual ventilation status was not accounted for in assumed scenarios, the methodology may fail to identify it. For example, in one of our blind field tracer tests, the result is shown as the purple dashed line in Figure 49. The result correctly indicated that the stopping door was open since the concentration profile does not have a long tail. However, the booster fan status matched Case 3 result the most but with a significantly lower tracer concentration level at the beginning of the profile. In this case, the best conclusion that can be made is that the ventilation status follows Case 3, in which the door is open and the fan is off. This conclusion was found to be inaccurate.

At the time of the blind test, the door was open and the booster fan was on. However, another booster fan in the belt entry had been turned off and on for maintenance purposes. This was not within the consideration of the modeled scenarios and therefore led to an inaccurate prediction. Although this is one limitation of the methodology, it is usually possible to narrow down the possibilities that are of the most concern. For example, certain booster fans being on or off may be more important to rescue efforts than others; certain stopping door statuses may also be more important than others to estimate the extent of an explosion. Therefore, it is still possible for this methodology to cover major possible ventilation scenarios with the help of experienced engineers.

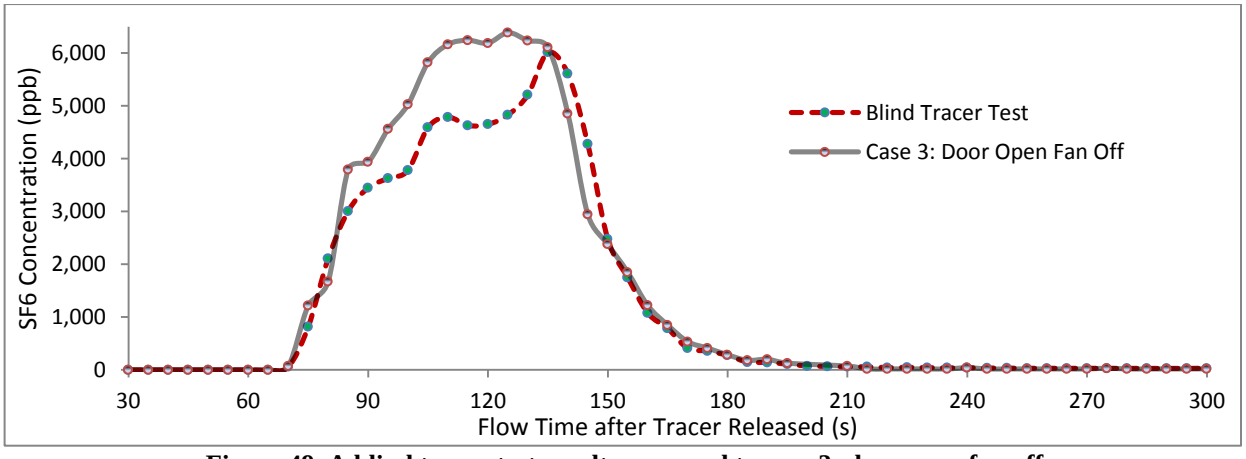

Figure 49. A blind tracer test result compared to case 3: door open fan off

It should be noted that robust CFD modeling is extensively time consuming, especially if a high performance computer is not available. Ventilation network modeling is more practical in simulating a full scale mine, but it cannot resolve the details of tracer gas behavior at the micro scale, such as how a tracer is distributed over entry cross-sections. Therefore, CFD is an important supplemental component of accurate tracer gas modeling and experimental design at the field scale. A hybrid scheme that combines CFD and network modeling will be investigated in future work. This hybrid would allow CFD to be used in critical areas where mixing and diffusion are complex while more generic areas of the mine could be network modeled to save computational time.

The following paper will be submitted to a peer reviewed journal. The experimental and CFD modeling work and writing was primarily completed by Guang Xu with editorial and technical input from Dr. Kray Luxbacher, Edmund Jong, Gerrit Goodman, and Dr. Harold M. McNair.

7 Preliminary Guidelines and Recommendations for Use of Tracer Gas in Characterization of Underground Mine Ventilation Networks

7.1 Abstract

Tracer gases are an effective method for assessing mine ventilation systems, especially when other techniques are impractical. Based on previously completed laboratory and field experiments, this paper discusses some common problems encountered when using tracer gases in underground mines. The discussion includes tracer release methods, sampling and analysis techniques. Additionally, the use of CFD to optimize the design of tracer gas experiments is also presented. Finally, guidelines and recommendations are provided on the use of tracer gases in the characterization of underground mine ventilation networks.

7.2 Introduction

Ventilation is a fundamental to the engineering of underground mines because it has considerable effects on health and safety. Measurements of airflow underground are usually carried out using traditional instrumentation such as vane anemometers, hot-wire anemometers, pitot tubes, and smoke tubes. However, these methods are not practical under certain circumstances in an underground mine. Examples include the measurement of recirculation and leakage, flow in inaccessible zones, and flow with very low velocities. Sometimes traditional instrumentation fails to provide accurate results. For example, in a study that investigated jet fan effectiveness in dead headings, tracer gas results were found to be more accurate than the results of smoke tubes [144]. Therefore, tracer gas techniques are a valuable tool for accurately measuring airflow in situations where traditional methods cannot be employed and providing information to characterize underground mine ventilation.

The tracer gas technique is a useful and versatile tool for studying mine ventilation systems with a long history of application. The Bureau of Mines [109] conducted a series of tracer gas tests using sulfur hexafluoride SF_6 and proved the usefulness of tracer gas techniques in measuring recirculation, air leakage, airflow in large cross section, low flow velocity, and transit air time. Grenier et al. [145] used tracer gases to analyze the spread of dust in a fluorspar

milling plant. The results indicated that tracer gases behave in the same physical manner as respirable dust and can be used to find patterns in dust movement within a ventilation system. Tracer gas has been accepted by the mining industry as a viable ventilation survey tool. More examples that used tracer gas to investigate various ventilation problems can be found in Timko and Thimons paper [144].

An ongoing research project that involves the selection of novel tracer gases for mine ventilation, the development of a methodology to use tracer gases and computational fluid dynamics (CFD) modeling to analyze, predict, and confirm the underground ventilation status together with the location of the damage, and finally validate the developed methodology in the laboratory and in the field are currently being conducted at Virginia Tech. Details of this work have been published in several forums [140], [143], [146], [147].

The focus of this paper is to provide preliminary guidelines and recommendations for use of tracer gas based on experience and practice. As this research progressed it was evident that there are few resources in the literature that provide the practical aspects of conducting tracer gas studies in mines. Some essential aspects of the tracer gas technique are discussed as well as new findings and recommendations, and studies in the literature are referenced as well. Using CFD modeling to design tracer gas experiments is also presented in this paper. Some modeling examples are provided to illustrate how CFD can help to determine the optimized tracer release and sampling locations, the release rate and duration, and eventually help to achieve desired results. Tracer gas experiments are time and resource consuming in underground mines, the guidelines and recommendations provided in this paper can be used by other researchers and industries for the design of tracer gas experiments more efficiently with less trial and error.

7.3 Tracer gas techniques

7.3.1 Choices of tracers

Sulfur hexafluoride (SF_6) is a widely accepted standard tracer gas that has been used in mine ventilation studies. SF_6 is non-toxic [148], and the Occupational Safety and Health Administration (OSHA)'s Permissible Exposure Limit (PEL) and the American Conference of Governmental Industrial Hygienists (ACGIH)'s Threshold Limit Value (TLV) for SF_6 is 1,000 ppm [149]. The amount of SF_6 released to a mine is generally much less than either the PEL or TLV limit. SF_6 can be detected accurately using gas chromatography (GC) in concentrations as

low as parts per trillion. It is also odorless, colorless, chemically and thermally stable, and not found in the natural environment. It is not measurably adsorbed on sandstone and coal. These are all desirable properties as a tracer gas [109]. Some alternative gases have also been used as mine ventilation tracers, such as nitrous oxide and helium. However, because they are not easily detected, large amounts need to be released thus causing transportation problems and difficulty in achieving stable flows [150].

It has long been realized that multiple tracer gases can add flexibility to ventilation surveys in many ways. Multiple gases not only allow the release of different tracers at different points without increasing the number of collected gas samples, but provide more information because the source of each tracer in one sample can be identified and air flows in different zones can be investigated simultaneously with multiple tracers. Once a tracer is released to the mine, it may take days to weeks for the tracer background to be reduced to a level that will not affect the next test. However, if multiple tracers are available, a different tracer can be used to conduct another test right after the previous test. Although the advantages are apparent, the use of the multiple tracer technique is still not common in underground mines. One key requirement for identifying other tracer gases is that the gas should be measurable by the same method being used for SF_6, which is the most commonly used tracer gas. SF_6 is commonly analyzed by GC, so it would be better if the other tracers were able to be analyzed by the same GC method. Using the same GC method, the additional tracers should have similar sensitivity to SF_6 as well as be able to be separated from SF_6. Kennedy et al. [150] investigated six Freons that are promising candidate tracer gases. They found that only Freon-13B1 ($CBrF_3$) and Freon-12 (CF_2Cl_2) were within two orders of magnitude of the sensitivity of SF_6 when analyzed using a GC with an electron capture detector. The other four Freon gases were several orders of magnitude less sensitive. $CBrF_3$ and CF_2Cl_2 were tested in the field and it was concluded that they perform well as mine ventilation tracer gases and are comparable to SF_6. Batterman et al. [151] used hexafluorobenzene (HFB) and octafluorotoluene (OFT) for indoor ventilation tracers. However, those two tracers were not simultaneously analyzed with SF_6. Patterson [152] researched the selection of novel tracer gases that can be used in mines together with SF_6. Freon 14 (CF_4), C_3F_8, and PMCH (C_7F_{14}) were tested on different columns using various GC methods. CF_4 and C_3F_8 were found to have much less sensitivity than SF_6 on the tested columns, with similar retention times to SF_6. PMCH was reported to be a appropriate tracer if used together with SF_6. A GC

protocol was developed that can be used to analyze SF_6 and PMCH concurrently on an HP-AL/S capillary column. One drawback of the protocol is the long 18 min analysis time. This process can potentially be optimized and shortened.

In summary, as for the choice of tracers in underground mines, SF_6 is no doubt the best choice. $CBrF_3$, CF_2Cl_2, and PMCH (C_7F_{14}) can be used together with SF_6. $CBrF_3$ and CF_2Cl_2 have both been successfully used in a mine. PMCH is a novel underground mine tracer gas. The author's research group is developing method to apply it as additional tracer that can be used together with SF_6.

7.3.2 Tracer gas release technique

Accurate and precise release of tracer gas is critical to conducting a rigorous study; there must be high confidence in the mass or rate of gas released to the system in order to achieve meaningful analysis of results. There are two commonly used tracer gas release techniques: pulse-injection, which is based on the injection of a short duration of tracer gas, and constant-injection, which is based on the continuous injection of tracer gas.

Tracer gases can be released in a controlled manner using various methods. For pulse injection, a known mass of tracer gas in a balloon or syringe can be used and injected to the mine. Or directly release tracer gas from a pressurized container and determine the weight loss of the container after release. However, it is hard for these methods to release in a controlled rate. Flow meters and permeation tubes serve as more accurate controlled rate tracer gas release methods, and they can be used for both pulse and constant injection.

Soap bubble flow meter (Figure 50 a), rotameter (Figure 50 b), and electrical flow meter (Figure 50 c) are commonly used flow meters that can be used to measure and to control the flow rate. The soap bubble flow meter measures the flow rate of tracer release, but accessory instruments are needed to control the flow rate of gas. For gases contained in a compressed gas bottle, a two stage regulator is often attached to the bottle. Capillary tubing may be used to connect the regulator and the soap bubble flow meter adding more resistance to achieve better gas flow control. The two stage regulator controls and maintains the delivery pressure to the flow meter as long as gas tank pressure is greater than the delivery pressure. Selecting different capillary tubing and adjusting the delivery pressure affects the flow rate. The described setup provides flow stability unaffected by atmospheric pressure [145].

Variable area flow meters, also known as rotameters, provide a different set of controls. The design is based on the variable area principle and indicates as well as controls the rate of flow. Positioned vertically, the gas flow lifts the float in the flow tube. For a constant flow rate, the float will be at a stationary position, which corresponds to a point on the measurement scale that indicates the flow rate. The flow rate can be changed by adjusting the delivery pressure or manipulating the valve on the flow meter. Although a specific meter can be purchased for a certain gas, the air flow meters are the most commonly found in the market. The air flow meter can be used for other gases with a correction factor provided by the manufacture.

An electrical mass flow controller can be used to accurately control the release quantity of a tracer. Using a mass flow controller, the flow rate can be adjusted using the digital control panel. It requires minimal adjustment to achieve the desired flow rate compared to the other types of flow meters.

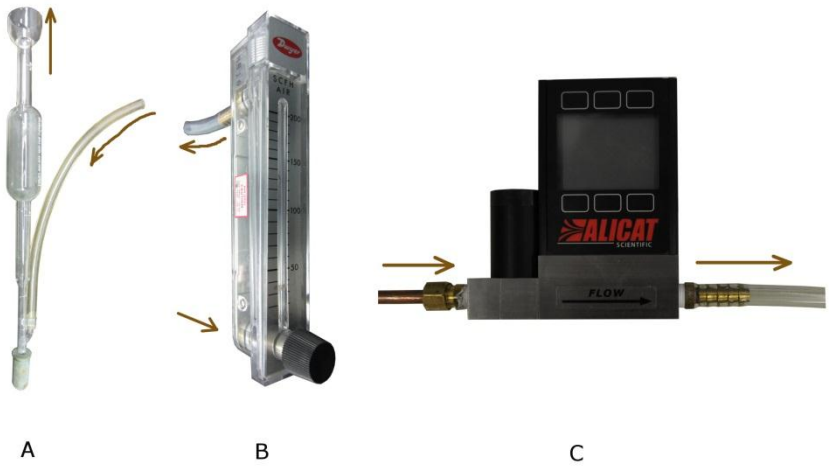

Figure 50. Different flow meters

The permeation device is a commonly used tracer release source for volatile compounds. The basic concept is to seal a certain amount of tracer in an impermeable tube with permeable material at one end. The emission rate can be determined by weighing the prepared tube at intervals of several days until equilibrium is reached. The emission rate is relatively stable if the temperature is constant. [153]. Dietz and Cote [154] described a perfluorocarbon (PFT) source in which a known mass of PFT is injected into a fluoroelastomer plug and crimped in a metal shell. PFT will diffuse from the end of the plug at a known rate that is inversely proportional to the square root of time for the emission of the first 50%-60% of the original amount of PFT. Johnson et al. [155] described the preparation of a permeation device they used for continuous and constant release of SF_6. It was constructed from brass rod, Teflon, a frit, and a swaglok nut.

Although their design was not used in a mine tracer test, the method can be used for the release of SF_6 and other tracer gases in mines. Batterman et al. [151] described an updated method for a constant injection technique with miniature PFT sources. The method was shown to be reliable for measuring indoor air exchange rates. The source was a diffusion controlled release of saturated vapor in the headspace of a PFT liquid container. A diffusion tube was inserted into the septum that sealed a glass vial partially filled with PFT. The emission rate was evaluated using a Fickian diffusion model and tested by experimentation. The described sources mentioned above can be easily modified for a wide range of applications. In general, the permeation device release methods are designed for very low emission rates over a long period of time, and this method has not been used in underground mines.

7.3.3 Tracer gas sampling methods

There are two categories of gas sampling methods: collecting samples for laboratory analysis and collecting samples for immediate analysis [156]. The first category is commonly used in underground tracer gas studies, which includes gas sampling bags, hypodermic syringes, and evacuated containers.

Gas sampling bags have been successfully used for a number of years to collect gas samples and make gas standards. Gas sampling bags are available commercially and come in a variety of sizes and shapes, and are made from a number of materials, such as PVC (polyvinyl chloride) or Tedlar (polyvinyl fluoride). One needs to pay special attention to the material of the sampling bag because the sampled gas may be reactive, adsorptive, absorptive, or diffusive with the bag materials [156]. There are many applications of using gas sampling bags for collecting gas and vapor samples [157]. It usually requires a pump to inject gas into the bag, so it is not a very convenient tool for dynamic gas sampling. Kennedy [150] tested the tightness of TEDLAR gas sampling bags and no detectable degradation of gas samples was found in a 24 hour period. The storage time is typically no more than 24 hours, so analysis should be conducted as soon as possible, unless storage experiments indicate a longer storage time.

Hypodermic syringes satisfy most underground sampling requirements. Syringes are inexpensive, easy to carry, and hard to break. However, their short storage time restricts their use. For example, in one study, gases such as carbon dioxide are lost rapidly due to permeation [131]. It is standard practice to fill and evacuate the syringe twice before drawing so that the gas

left in the syringe does not contaminate the gas sample. The syringe can be sealed with a vinyl cap [145]. The tightness of hypodermic syringes have been tested by Kennedy et al. [150]. In the study, six syringes were filled with certain concentrations of SF_6, $CBrF_3$, and CF_2Cl_2, and left for 24 hours. The concentrations did show a significant reduction, with a loss of 0.5-1 percent for SF_6, 2.5-3 percent for $CBrF_3$, and 6 percent for CF_2Cl_2. These syringes were emptied and refilled with the same standard gas, left for another 24 hours, and tested again for the tracer gas content. The loss of tracer was reduced to half of the original percentage after the first filling. This indicated that the loss was not only due to permeation through the walls or leaks in the seals but also due to adsorption of the tracer onto the syringes. Like sampling bags, samples generally should be analyzed on the same day they are taken.

Vacutainers have long been used for sampling mine gases. A Vacutainer is an evacuated glass or plastic tube-shaped vessel and is capped with a self-sealing rubber septum. Such containers are commonly used to take blood samples. The advantages of Vacutainers are that they are small, light-weight, economical, convenient, and simple to use [156]. The Bureau of Mines officially adopted the Vacutainers for taking mine gas samples because they are convenient and can obtain consistent results [131]. Freedman et al. [131] tested the 10 ml Vacutainers for use in mines. In their study, a device was described which can evacuate up to 56 Vacutainers to a few millimeters of pressure. It was found that for stored gas samples, CO_2 shows substantial loss in concentration over the 41 days due to permeation. The CO concentration level gradually increased up to 50 ppm over time in factory supplied or completely evacuated Vacutainers. This phenomenon is unexplained. They recommended that the storage of evacuated Vacutainers should not exceed 1 to 2 months if low levels of CO can cause interference. If precise CO_2 level is of interest in collected samples, the analysis should be done within 1 week after samples are taken.

The 10 ml Vacutainer was also chosen as the sampling method for our experiments. These evacuated containers are not completely evacuated at the time purchased and a small amount of gas (air) is still present. However, the containers are evacuated to a fixed and designated pressure [158]. The factory evacuation is designed to draw 10 ml of blood. Preliminary tests indicate they draw 9.5 ml of water. The left three Vacutainers in Figure 51 illustrate this result. It was noted that the capability of drawing water to be reduce slowly with time. The actual Vacutainer capacity measured by water displacement is 12.9 ml. Therefore, the

Vacutainers were re-evacuated in the laboratory to improve the sampling accuracy. The right three Vacutainers in Figure 51 show the result of laboratory evacuation, which improved the capability of Vacutainers of drawing 12.5 ml of water. This means 0.4 ml of air is left in each Vacutainer, which is 3.1% of the actual capacity. This will make the measured gas concentration 3.1% less than the actual gas sample concentration, but it is acceptable for most tracer gas analysis purposes.

Figure 51. Vacutainers factory evacuation and laboratory evacuation

The evacuation system used in the laboratory is shown in Figure 52. Basically it is a vacuum pump connected to several needles so that several Vacutainers can be evacuated at a time. Vacutainers are inerted onto each of the needles through the septum for about 30 s, and need to be pulled off very slowly, which allows enough time for the septum to re-seal for a high quality evacuation. Each needle connected to the system needs to be replaced after about 5 Vacutainer evacuations since it will dull and hard to penetrate the Vacutainer septa.

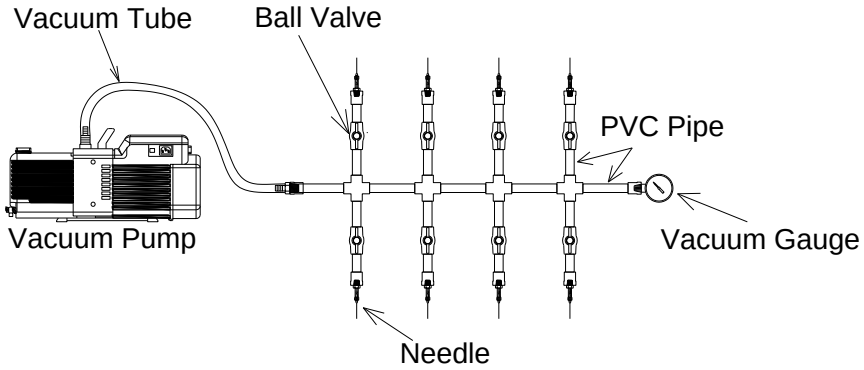

Figure 52. Evacuation apparatus schematic

Although the Vacutainer storage time is promising, an official time has not been reported in the literature. An attempt to test its storage time for SF_6 was conducted during a month period and no obvious SF_6 concentration changes were found. However, the method used introduced significant amounts of systematic errors that are difficult to control and quantify.

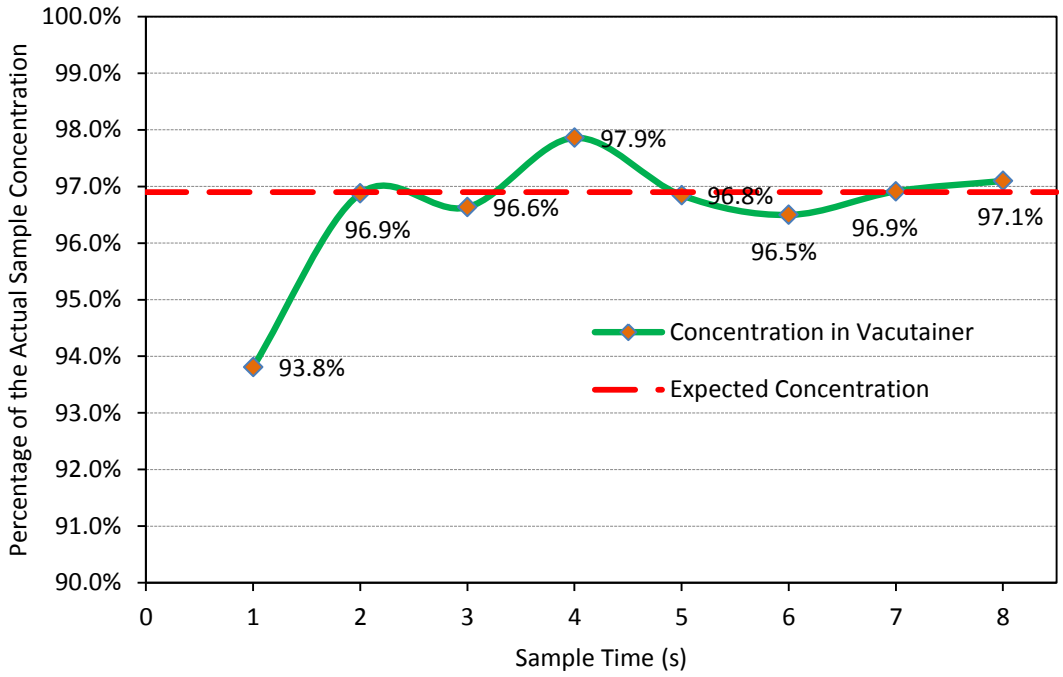

Figure 53. Vacutainer sample time

The Vacutainer sample time was also studied to determine how fast the gas sample will fill the Vacutainers. The sample time is defined as beginning when the rubber septum is punctured by a needle ending when the needle is removed from the septum. This is important, especially for dynamic sampling, because it determines the minimum sampling interval. As in the previous test, for each test, three samples were taken and the average concentration was used to compare with other results. The test results are shown in Figure 53. Given adequate time for the Vacutainer to draw sample, the expected concentration in the Vacutainer should be about 96.9% of the actual concentration, as mentioned before. The 96.9% concentration level is marked in the dashed line in Figure 53. As can be seen, the concentration in the Vacutainer reached the expected level with sampling times longer than 2 seconds. Variations exist which are likely due to error during Vacutainer evacuation and GC manual injection. Therefore, for the 10 ml Vacutainer, the least sample time is recommended to be 2 seconds. Dynamic SF_6 samples were successfully taken every 5 seconds during 8 minutes period in our underground tracer tests. In each 5 seconds, Vacutainer takes sample for 3 seconds and 2 seconds are needed for changing

to a new Vacutainer. This is the fast minimum sampling interval we can achieve if only one people takes samples manually.

7.3.4 Analysis of tracer gas

There are two main techniques for determining gas concentrations: infrared spectroscopy (IR) and gas chromatography (GC). This paper focuses on the GC method which is one of the most widely used analytical techniques for gas samples due to its selectivity and sensitivity. A wide range of compounds can be analyzed through the proper selection of columns and detectors.

Gas chromatographs need to be calibrated over its operating range to quantitatively measure a certain gas concentration. Thus, tracer standards are needed for the calibration. The standards can be prepared in the laboratory or purchased as a certified mixture. To make the standards in the laboratory, a gas-tight syringe can be used to inject a small, known quantity of tracer into a known volume of air or ultra-pure nitrogen in a sealed container. An example of one of these containers is shown in Figure 54. With both valves open, this container can be flushed using ultra-pure nitrogen and filled with it after both valves closed. To prepare standards for trace concentrations, a serial dilution technique can be used. Serial dilutions are completed by withdrawing a measured quantity of the mixture prepared in the first step and injecting it into another container. The procedure can be repeated until the desired concentration is achieved. This method is time consuming and errors can be introduced at each stage of dilution. Although this method can be used to produce useable calibration curves, the purchased certified gas standards can provide better accuracy and repeatability [159].

Figure 54. Glass bulb for tracer gas standard preparation

Split injection is a widely used injection technique for GC analysis. It automatically reduces the sample size to prevent the column from overloading by allowing only a fraction of the sample enters the column. This fraction is defined as a split ratio. A split ratio of 20:1 indicates that one part of the sample enters the column and 20 parts exit the GC system through the split vent [160]. Theoretically, this means 1/21 of the total sample is analyzed. Again,

theoretically, this makes it possible to compare two results with the same GC method but with different split ratio. For example, a sample analyzed with a split ratio of 50:1 could be corrected to 20:1 by multiplying a factor of 51/21. However, this split ratio calculation was found to be inaccurate due to the mechanical nature of the splitting control. Figure 55 shows the measured results of the same SF_6 sample with different split ratio but all corrected to the split ratio of 20:1. As can be seen, this correction method fails to provide accurate results. Although the accuracy of the split on different GC machines may vary, it is recommended that a single split ratio is chosen and that corrections to the data based on split ratio are avoided.

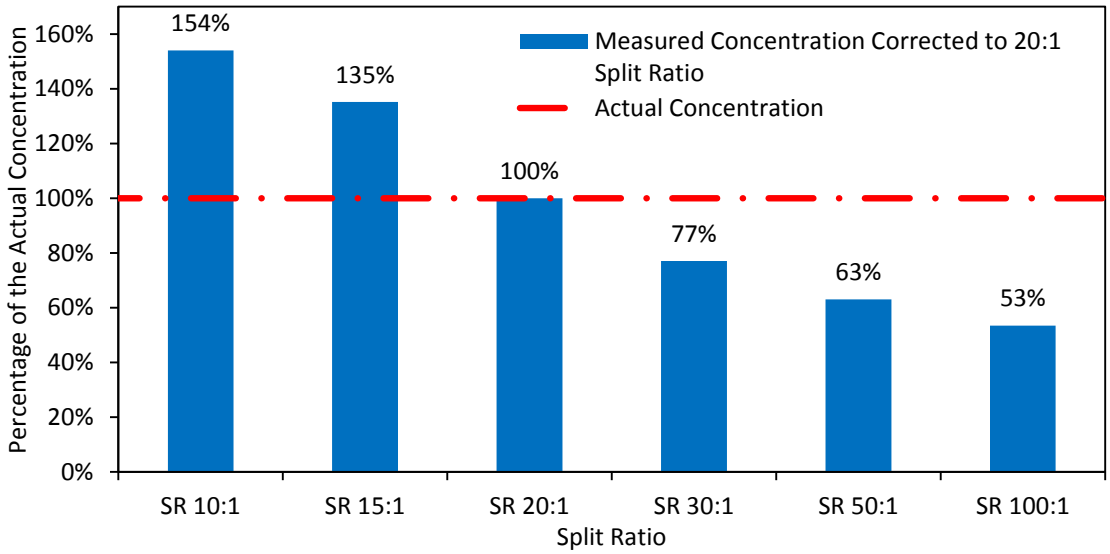

Figure 55. Same sample measured with different split ratio comparison

Since this correction method is not always reliable, the split ratio should be held constant for all calibration standards and gas samples. A calibration curve is used to quantify the concentration in collected samples. To create a calibration curve, the analysis concentration range needs to be determined first, and then start from a reasonable injection amount and split ratio for the calibration. It is better to inject the highest concentration standard first to make sure the column will not be overloaded. If it is overloaded, increase the split ratio or reduce the amount of injected sample. Afterward, inject the lowest concentration standard to ensure that the concentration is above the detection limit; otherwise, the split ratio needs to be decreased or a larger amount of sample needs to be injected. After the injection volume and split ratio are determined, these parameters need to be the same for the rest of the standards and samples that need the generated calibration curve.

7.4 The use of CFD model for tracer gas design

Tracer gas experiments are time consuming, especially if they are conducted on a trial and error basis. Careful planning will ensure meaningful data collected efficiently. CFD modeling is a powerful tool that can be used for experimental design. This tool can substantially reduce the effort that is expended in the field. In CFD modeling, tracers can be modeled in several ways. The two most common methods are the two species transport model or definition of a user defined scalar to model tracers. Parameters can be easily changed in the CFD model, such as the location and the release amount. This provides detailed information to achieve the desired results, which can help with the tracer gas experiment design. This section focuses on the discussion of the determination of some parameters using CFD modeling in the characterization of underground mine ventilation networks.

One important parameter is that the expected concentration in collected samples needs to be within the detection range of the GC. It is known that the concentration decreases as the distance between the sampling and release location increases. If these locations have been determined, the tracer gas release rate and duration can be used to determine the concentration level.

The release rate is the most sensitive parameter that influences the concentration. Figure 56 shows the SF_6 concentration profile results provided by one of the studies conducted by the authors. The scenario modeled was a belt entry connected with a crosscut entry shown in Figure 59. The release location is in the crosscut and is denoted as “Release Point 1.” The sampling location is 190 m away from the crosscut and is downstream from the velocity inlet in the belt entry. SF_6 was released under different rates for one minute in the CFD model. As can be seen in Figure 56, the basic shape of the concentration profile will not change by changing the release rate, but the profile is taller under larger release rate. The result can be used to find an optimized release rate that can produce a tracer concentration profile, which can be reasonably analyzed by GC or other instruments.

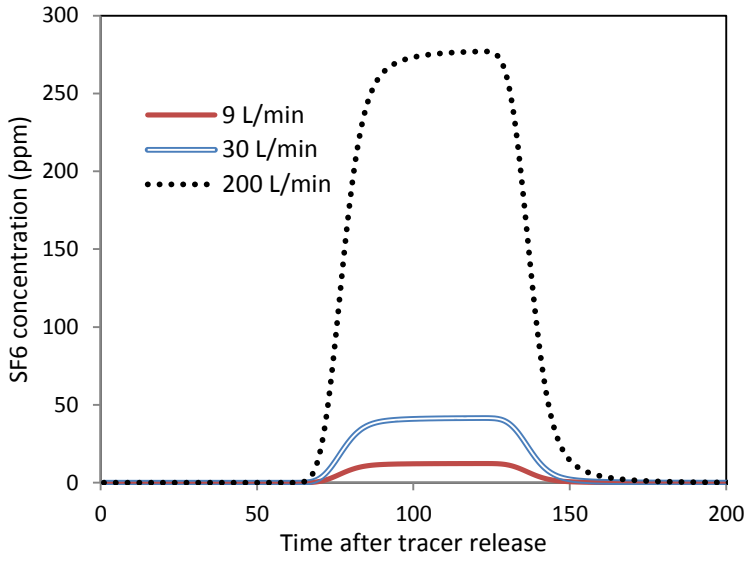

Figure 56. Tracer concentration profile under different release rate

The release duration also influences the concentration levels in collected samples but is not as sensitive as the release rate. Under certain circumstances, increasing the release duration will not necessarily increase the concentration level. In the same CFD model mentioned above, different tracer release durations were modeled under the same release rate (9 L/min). As can be seen in Figure 57, the 30 s release increased the concentration level when compared to the 10 s release. However, increasing the release duration further, to 1 min and 2 min, did not increase the concentration level. That is because the concentration reached its maximum under the fixed release rate and the maximum concentration leveled out. Although this is not always the case, the CFD results can provide the data that can be used to pre-determine the concentration level under certain release duration.

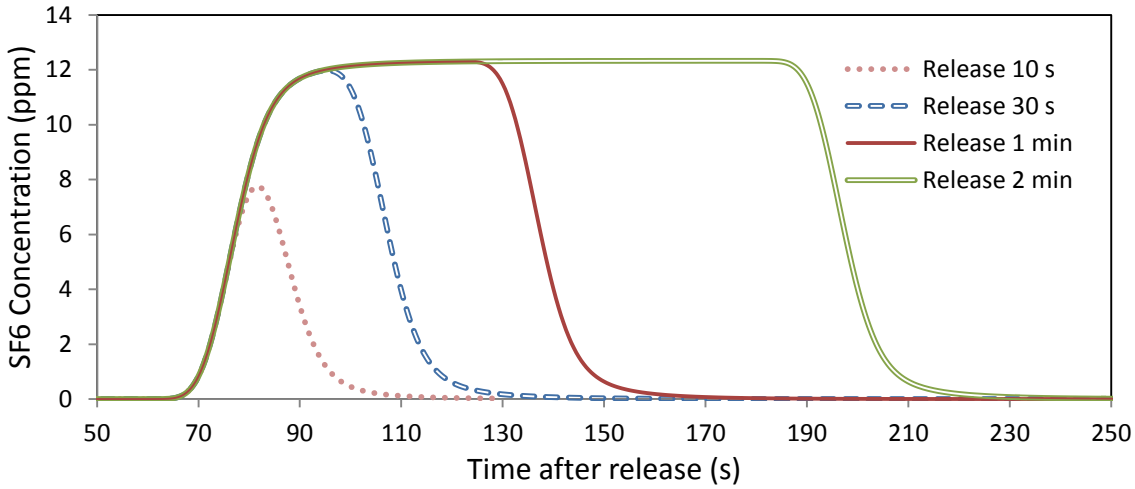

Figure 57. SF6 concentration profile under different release duration

Another important parameter that CFD can help to determine is the shape of the expected concentration profile. The farther the sampling location is from the release location, the broader and flatter the profile becomes. If the release and sampling locations are determined, longer release durations can produce broader profiles as well. Figure 57 shows that the concentration profile becomes broader as the release duration increased from 10 s to 2 min. Generally, a broader profile is better, especially when the sampling method is not continuous, such as syringe or Vacutainer sampling. A broader profile allows enough samples to be taken to accurately resolve the profile. If the profile is too narrow, for example it is only 10 s, but the sampling interval is 5 seconds, only 3 samples maximum can be taken within the 10 seconds time. This makes it very hard to accurately depict the concentration profile.

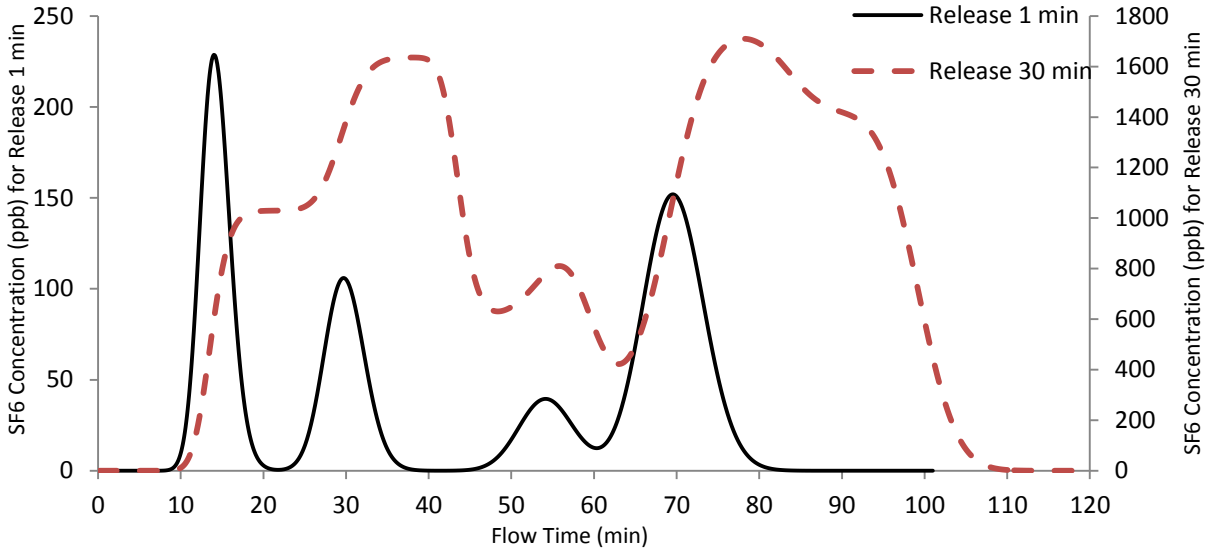

Figure 58. Tracer profile under different release duration

However, in some cases, too broad of a profile will not benefit the tracer experiment not only because it takes longer for sampling, but also because it weakens the profile characterization. As indicated from a CFD study presented in [140], under the normal ventilation scenario, there are four flow paths. If the tracer is released for 1 min, the profile is the solid line displayed in Figure 58, which has four peaks and each of them represent one flow path. However, if the release duration changes to 30 min, the profile is the dashed line shown in Figure 58. It not only requires 30 min more sampling time to capture the entire profile, but the characterization is also not as obvious as before. It is hard to tell that there are four flow paths from this kind of tracer profile. In summary, too short of a release duration may produce tracer profiles that are hard to capture with certain sampling intervals; too long of a release duration

may weaken the tracer profiles characterization. CFD modeling can be used to check if the release duration is good enough for certain sampling intervals and to characterize certain ventilation scenarios.

Changing the location of tracer release point will not only change the profile peak arrival time but also change the profile shape when the flow feature is complex. For example, in the 2D CFD model mentioned before and shown in Figure 59. Two tracer release points were examined in the model: point 1 is 38 m from the door, and point 2 is 2.5 m from the door. As can be seen in Figure 60, due to the recirculating flow featured in the zone at point 2, the downstream tracer profile not only appears later and broader compared to release at point 1, but the basic shape is also changed. The profile is much broader and has a longer tail. In this case, the basic tracer profile shape is different when released in the same entry but at different locations. The CFD model can identify these complex flow zones, which provides information that helps to decide where to release the tracer and get a profile that is suitable for certain purposes.

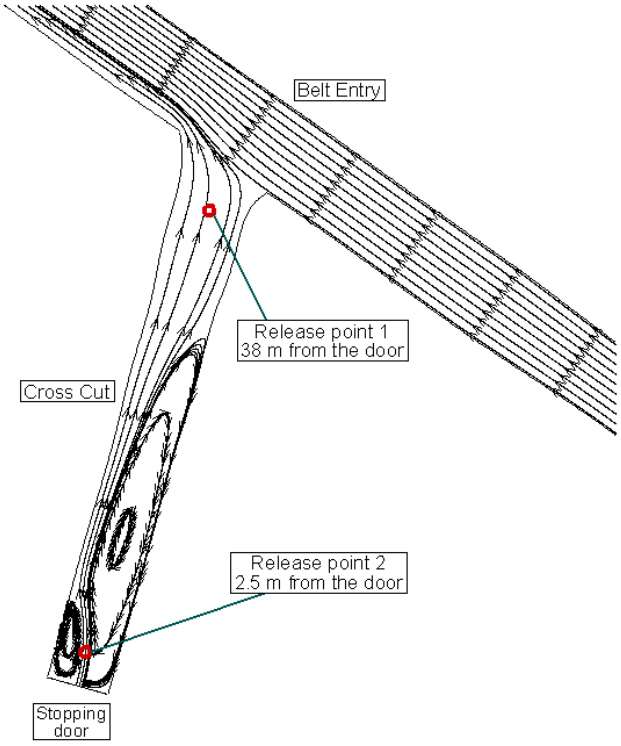

Figure 59. Tracer release at different locations

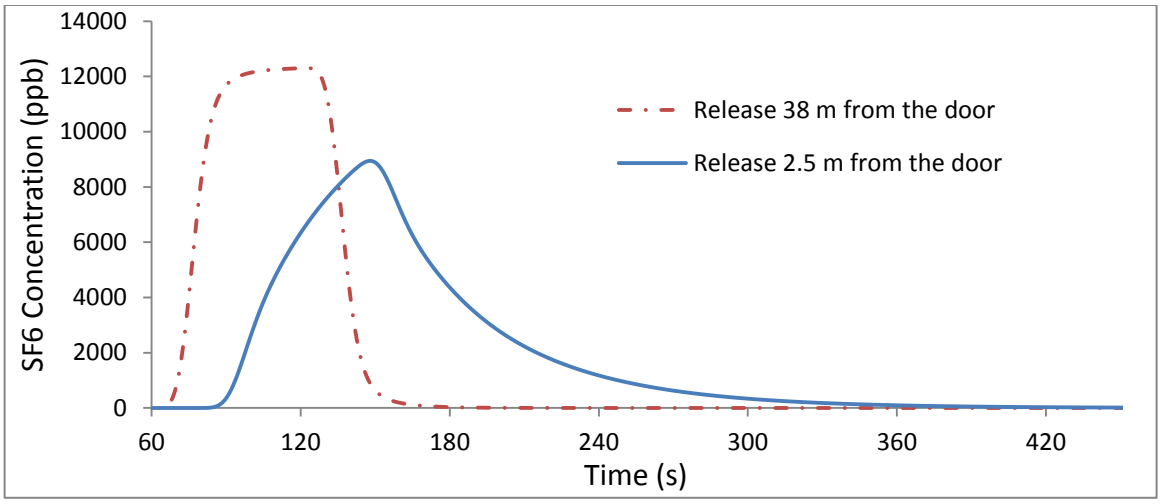

Figure 60. Tracer profile under different release location

The examples shown above demonstrate that CFD is a very powerful tool as an aid for tracer gas experimental design. The modeling results can provide information for determining some of the key experimental parameters mentioned above. Using these optimized parameters to perform the actual on-site experiment can help to avoid the trial and error process and obtain the desired results efficiently. However, the CFD model requires much more computational power compared to other modeling methods, such as network modeling. Using a high performance computer for the modeling is a solution to reduce computational time. In addition, starting from a 2D model can also save time tremendously. Although 2D flow is totally different from 3D flow, and the 2D model cannot provide as accurate a result as 3D, a 2D model can still provide enough information to determine most of the influencing factors. After those factors have been determined, using a 3D model to validate the 2D model can increase the confidence and the accuracy of the results. Finally, in cases where the flow regime is not complex, and the sampling and collection points relative to the entry cross-section are not considered critical to results, network modeling can even be used to understand expected results. The advantage of network modeling is much lower computational requirements along with less user skill.

7.5 Conclusions and discussion

The tracer gas technique is a precise and reliable methodology for characterizing underground mine ventilation networks. However, it is time consuming and resource heavy, especially when it is based on a trial and error basis. The guidelines and recommendations provided in this paper are based on the experiences and practices of the tracer gas research

conducted over the last few years. These recommendations can help other researchers and industries to reduce the effort in conducting tracer gas experiments.

Several common topics in the tracer gas techniques are discussed. As for the choice of tracers, $CBrF_3$ and CF_2Cl_2 are found to have been successfully used together with SF_6 using the same GC method. PMCH was also found to be a good tracer for use with SF_6. However, PMCH has not yet been proven in underground mines.

As for the tracer release techniques, commonly used flow meters are discussed and compared. Additionally, tracer release by permeation tube is introduced although has yet to be used in mines. It may prove to be a promising technique for tracer release in mines. These release methods control the flow rate differently and can be used to serve specific purposes.

There are several tracer gas sampling methods that have been used in mines. Both gas sampling bags and hypodermic syringes have a short storage time. Samples taken using these methods should be analyzed within 24 hours. The material of the sampling bags could affect its sampling capability for certain gas samples. It was reported in the literature that the sample loss in the hypodermic syringes are due to permeation through the walls, leaks in the seals, and adsorption of the tracer onto the syringes. Vacutainers have the longest storage time compared to other sampling methods. However, substantial loss of CO_2 in stored samples was reported due to permeation. CO concentration levels were found to be gradually increased over time in evacuated Vacutainers in one instance. Storage time and sample time for SF_6 have not been officially reported in the literature. An attempt to test its storage time for SF_6 was conducted during a month period and no obvious SF_6 concentration changes were found. However, the method used introduced significant amounts of systematic errors that are difficult to control and quantify. The minimum sample time of the Vacutainers is found to be 2 seconds, however, the minimum practical sampling interval for one person sampling manually is 5 seconds.

GC is a commonly used method for tracer analysis. The preparation of gas standards in the laboratory was described, which can be used to calibrate a GC when a certified gas mixture is not available. The correction method from one injection split ratio to another is discussed and found to be inaccurate, thus it should be avoided unless experiments show it is acceptably accurate. A procedure was proposed for generation of a calibration curve. These guidelines can be used to save time and guarantee an accurate GC result.

CFD modeling can help with the tracer experiment design. Examples are presented which illustrate how CFD modeling helps to determine the important factors in a tracer experiment, such as the release rate and duration, the expected concentration profile, and the release location. After these parameters are optimized in the CFD model, the trial and error process can be reduced and the desired results can be obtained more efficiently. However, for a large scale 3D CFD model, the computational time is considerable. Many of the parameters can be studied using a 2D model to save time. But the 2D model cannot provide as accurate result as the 3D model because 2D flow is totally different from 3D flow.

The aim of this work is to provide a practical guide for people with technical expertise who want to apply tracer gas techniques to mine ventilation. Although many impressive applications of tracer gas techniques are available in the literature, few, if any sources are available that provide a guide use of the method. This method can allow for characterization of the ventilation system from an assessment of leakage to the efficiency of designs for gas and dust dilution, and provide engineers with additional tools for improving health and safety.

8 Conclusions and Discussions

8.1 Conclusions

The objective of this research was to develop a new methodology that can characterize the underground mine ventilation systems remotely using tracer gas techniques and the CFD modeling method. This provides an alternate way to gather information that can be used for mine personnel and rescuers to take safe and effective actions after an unexpected event.

Ultimately, this work demonstrated that general determination of changes to a mine ventilation system is achievable through examination of tracer gas profiles, both at the lab and field scale, for transient and steady state release. Also, this work has informed the practical use of tracer gases in mines, and this body of knowledge is expected to contribute to more efficient and more common use of tracer gases by mine engineers, which will allow for better characterization of mine ventilation system and improved safety.

Experiments were conducted in the laboratory first before going to the field. A simplified conceptual mine model built with PVC pipes was used for tracer gas experiments. Different ventilation scenarios were simulated by opening or closing different valves. Instead of using pulse release, tracer gas was released constantly at designated location of the model mine. This is because the small size of the model mine caused that the tracer gas concentration profile lasts a short period of time, and could not be monitored frequently enough to be resolved. CFD models were built for assumed ventilation scenarios, and the results compared well with those were measured with reasonable errors. Ventilation scenarios can be predicted by comparing the experimental data and the CFD results. This laboratory study prepared for the on-site experiments, such as developing a proper GC method and sampling method for the field experiments. It also indicated that tracer gas parameters need to be optimized in order to obtain substantially different tracer gas profiles for different ventilation scenarios.

Based on the conceptual model mine laboratory experiments, a full scale model mine CFD simulation was conducted. This full scale mine CFD model allows for pulse release of tracer gas at the inlet and monitoring of tracer gas at the exhaust. Tracer gas concentration profiles are different because different ventilation scenarios have different air flow paths, which allows for analysis and prediction of the ventilation status. However, this work shows that tracer gas test parameters need to be optimized to successfully characterize each scenario. For example,

the amount of tracer gas released determines whether or not its concentration at the sampling location can be practically detected; the release duration determines whether or not the concentration profiles can be easily separated for different ventilation scenarios.

Following the previous studies, field experiments were conducted to examine the developed methodology in the field. A 2D CFD model was used to determine the optimal tracer gas test parameters, such as the tracer release locations, rate, and duration, and the sampling locations. After these parameters were determined, the 3D model was used to obtain more accurate results. The optimized parameters obtained from the models proved to be very useful as tracer data was successfully obtained after only one release. This is essential for rapid deployment of tracer in an emergency situation. However, detailed ventilation surveys and mine entry dimension parameters under normal conditions need to be available in order to establish and calibrate the CFD model. Computational resources required for this work illustrate that it is only practical to develop a model of a mine ahead of time and use it later, especially when applied to mine emergencies. Errors will occur as the result of the dynamic nature of a mine ventilation system, but this study demonstrated that the methodology is still valid even with these errors if the tracer gas test is carefully designed.

Finally, based on the laboratory and field scale work, a practical guide for people who want to apply tracer gas techniques to mine ventilation was provided. Some common topics of tracer gas techniques were discussed as well as new findings, such as the Vacutainer sample retention time and the inaccuracy of GC split ratio conversions. These recommendations can help other researchers and industries to reduce the effort in conducting tracer gas experiments and make them more attractive to operators. Examples are presented on the use of CFD modeling to determine the important factors in a tracer experiment, such as the release rate and duration, the expected concentration profile, and the release location. The trial and error process can be reduced and the desired results can be obtained more efficiently with the help of CFD modeling.

Although emergency situations need to be considered case by case, some rapid suggestions on the use of this methodology can always be provided based on available information. Most of the mines do not have an established CFD model, but network modeling can help estimate tracer gas arrival time, the number of expected peaks, and a reasonable sampling interval. The possible extent of the damage is also important to know to quickly determine the tracer gas release and sampling location, and the release amount. CFD modeling

may not be needed in some simple scenarios. However, CFD modeling can definitely assist in designing an effective tracer gas test and increasing the confidence of the results.

8.2 Highlights of the research

The methodology developed in this study proved to be successful in remotely characterizing underground mine ventilation systems both in the laboratory and in the field. It can be potentially used after unexpected event, such as explosion and roof fall, to collect information that will help decision makers to manage a mine emergency more effectively and increase safety for rescue personnel. The application can also be extended to circumstances other than unexpected events, such as to study the air flow in inaccessible and to understand complicated ventilation networks, although these are not the focus of this work.

A recommended general CFD modeling procedure was discussed which can be used as a guideline for a more reliable simulation. The mesh independence study is one of the most essential procedures that was emphasized. This is because the modeling results can be misleading if mesh independence is not achieved, especially when modeling multiple gas species.

Instead of using trial and error, this study used CFD modeling to design effective tracer tests. The optimized parameters obtained from the models proved to be very useful, and each field tracer test result was successfully obtained after only one tracer release. This is important because in emergency situations, underground information needs to be gathered quickly and the trial and error process is usually not allowed. Tremendous time and resources were saved by reducing such items as the number of trips to the mine and re-deployment of the tracer.

Finally, preliminary guidelines and recommendations for use of tracer gas were provided. Because tracer gas experiments are time and resource consuming in underground mines, the provided guidelines and recommendations can be used by other researchers and industries to design tracer gas experiments more efficiently.

8.3 Limitations and future work

The first step of the developed methodology is to estimate the level of damage and possible ventilation scenarios. This plays an important role in successfully identifying the actual ventilation scenario. This is because if ventilation damage occurs in a manner other than the assumed scenarios, the methodology may fail to identify it. Although this is one limitation of the

methodology and there could be many possible different scenarios after an unexpected event, it is usually possible to narrow down the possibilities that are of the most concern. For example, certain booster fan being on or off may be more important than others to rescue efforts than others; certain stopping door statuses may be more important than others to estimate the extent of an explosion. Therefore, it is still possible for this methodology to cover major possible ventilation scenarios with the help of experienced engineers.

The computational time for a large 3D CFD model is considerable. It is almost impossible to model a large portion or an entire mine. Sometimes 2D CFD models can be used, but their accuracy is limited compared to 3D models. Ventilation network modeling is more practical to simulate a full scale mine, but it cannot resolve the details of tracer gas behavior at the micro scale, such as how a tracer concentration is distributed over entry cross sections. Therefore, CFD is an important supplemental component of accurate tracer gas modeling and experimental design at the field scale. A hybrid scheme that combines the benefit of CFD and network modeling should be investigated in future work. This allows that CFD be used in critical areas, while most parts of a mine will be modeled using network modeling to save computational time with equally effective results.

Only one tracer (SF6) was used in this study, however, it has long been realized that multiple tracer gases can add flexibility to ventilation surveys in many ways. This not only allows the release of different tracers at different points without increasing the number of collected gas samples, but also provides more information because the source of each tracer in one sample can be identified and air flows in different zones can be investigated simultaneously. Although the advantages are apparent, the use of the multiple tracer technique is still less common in underground mines. Therefore, the application of multiple tracer gases in the field using the developed methodology is future application.

References

[1] E. D. Thimons and F. N. Kissell, "Tracer Gas as an Aid in Mine Ventilation Analysis," U.S. Bureau of Mines, Washington, DC (USA), 1974.

[2] W. G. Klinowski and D. J. Kennedy, "Tracer Gas Techniques Used in Mine Ventilation," in *5th US Mine Ventilation Symposium*, 1991, pp. 662–666.

[3] J. D. Anderson, *Computational fluid dynamics. The basics with applications*, 1 Edition. New York: McGraw-Hil, Inc., 1995.

[4] J. Blazek, *Computational fluid dynamics : principles and applications*, Second Edi. San Diego: Elsevier Science, 2005.

[5] T. Norton, D.-W. Sun, J. Grant, R. Fallon, and V. Dodd, "Applications of computational fluid dynamics (CFD) in the modelling and design of ventilation systems in the agricultural industry: A review.," *Bioresource technology*, vol. 98, no. 12, pp. 2386–414, Sep. 2007.

[6] B. S. Massey and J. Ward-Smith, *Mechanics of fluids*, 8th Editio. London and New York: Taylor & Francis, 2006.

[7] B. S. Massey and J. Ward-Smith, *Mechanics of fluids*. Taylor & Francis, 1998, p. 722.

[8] L. Yuan, A. C. Smith, and J. F. Brune, "Computational fluid dynamics study on ventilation flow paths in longwall gobs," in *11th U.S./North American Mine Ventilation Symposium*, 2006, pp. 591–598.

[9] T. X. Ren and R. Balusu, "CFD modelling of goaf gas migration to improve the control of spontaneous combustion in longwalls," in *Coal Operators' Conference*, 2005, pp. 259–264.

[10] H. K. Versteeg and W. Malalasekera, *An introduction to computational fluid dynamics, the finite volume method*. Prentice Hall, UK: Longman Scientific & Technical, 1995.

[11] S. A. Silvester, "The integration of CFD and VR methods to assist auxiliary ventilation practice," The University of Nottingham, 2002.

[12] H. L. Hartman, J. M. Mutmansky, R. V. Ramani, and Y. J. Wang, *Mine Ventilation and Air Conditioning*, 3. edition. New York, NY (United States): Wiley-Interscience, 1998.

[13] S. B. Pope, *Turbulent Flows*. New York, NY (United States): Cambridge University Press, 2000.

[14] S. Murakami, "Overview of turbulence models applied in CWE–1997," *Journal of Wind Engineering and Industrial Aerodynamics*, vol. 74–76, pp. 1–24, Apr. 1998.

[15] P. A. Durbin and G. Medic, *Fluid dynamics with a computational perspective*. New York, NY (United States): Cambridge University Press, 2007.

[16] J. Moureh and D. Flick, "Airflow characteristics within a slot-ventilated enclosure," *International Journal of Heat and Fluid Flow*, vol. 26, no. 1, pp. 12–24, Feb. 2005.

[17] A. Bakker, "The colorful fluid mixing gallery," 2008. [Online]. Available: http://www.bakker.org/cfm.

[18] L. Yuan and A. C. Smith, "Computational fluid dynamics modeling of spontaneous heating in longwall gob areas," in *SME Annual Meeting*, 2007, p. Preprint 07–101.

[19] L. Yuan and A. C. Smith, "Modeling the effect of barometric pressure changes on spontaneous heating in bleederless longwall panels," in *SME Annual Meeting*, 2007, p. Preprint 07–101.

[20] L. Yuan and A. C. Smith, "Numerical study on effects of coal properties on spontaneous heating in longwall gob areas," *Fuel*, vol. 87, no. 15–16, pp. 3409–3419, Nov. 2008.

[21] L. Yuan and A. C. Smith, "Effects of ventilation and gob characteristics on spontaneous heating in longwall gob areas," in *12th US/North American Mine Ventilation Symposium*, 2008, pp. 141–147.

[22] G. Collecutt, D. Humphreys, and D. Proud, "CFD simulation of underground coal dust explosions and active explosion barriers," in *7th International Conference on CFD in the Minerals and Process Industries*, 2009, pp. 1–6.

[23] J. Toraño, R. Rodriguez, I. Diego, J. Rivas, and A. Pelegry, "Influence of the pile shape on wind erosion CFD emission simulation," *Applied Mathematical Modelling*, vol. 31, no. 11, pp. 2487–2502, Nov. 2007.

[24] J. Toraño, S. Torno, M. Menéndez, and M. Gent, "Auxiliary ventilation in mining roadways driven with roadheaders: Validated CFD modelling of dust behaviour," *Tunnelling and Underground Space Technology*, vol. 26, no. 1, pp. 201–210, Jan. 2011.

[25] S. Torno, J. Toraño, M. Menéndez, and M. Gent, "CFD simulation of blasting dust for the design of physical barriers," *Environmental Earth Sciences*, vol. 64, no. 1, pp. 73–83, Nov. 2010.

[26] J. Aubin, D. F. Fletcher, and C. Xuereb, "Modeling turbulent flow in stirred tanks with CFD: the influence of the modeling approach, turbulence model and numerical scheme," *Experimental Thermal and Fluid Science*, vol. 28, no. 5, pp. 431–445, Apr. 2004.

[27] P. T. L. Koh, M. Manickam, and M. P. Schwarz, “CFD simulation of bubble-particle collisions in mineral flotation cells,” *Minerals Engineering*, vol. 13, no. 14, pp. 1455–1463, 2000.

[28] P. T. L. Koh and M. P. Schjwarz, “CFD modelling of bubble–particle attachments in flotation cells,” *Minerals Engineering*, vol. 19, no. 6–8, pp. 619–626, May 2006.

[29] G. L. Lane, M. P. Schwarz, and G. M. Evans, “Predicting gas-liquid flow in a mechanically stirred tank,” *Applied Mathematical Modelling*, vol. 26, pp. 223–235, 2002.

[30] M. G. Vegaa, K. M. A. Díaz, J. M. F. Oroa, R. B. Tajaduraa, and C. S. Morrosa, “Numerical 3D simulation of a longitudinal ventilation system: Memorial Tunnel case,” *Tunnelling and Underground Space Technology*, vol. 23, no. 5, pp. 539–551, Sep. 2008.

[31] T. Skjold, R. K. Eckhoff, B. J. Arntzen, K. Lebecki, Z. Dyduch, R. Klemens, and P. Zydak, “Simplified modelling of explosion propagation by dust lifting in coal mines,” in *Proceeding of the 5th International Seminar on Fire and Exoplosion Hazards*, 2007, pp. 23–27.

[32] D. D. Ndenguma, “Computational fluid dynamics model for controlling dust and methane in underground coalmine,” University of Pretoria, 2010.

[33] S. A. Silvester, I. S. Lowndes, and S. W. Kingman, “The ventilation of an underground crushing plant,” *Mining Technology: IMM Transactions section A*, vol. 113, no. 4, pp. 201–214, Dec. 2004.

[34] A. Mazzoldi, T. Hill, and J. J. Colls, “Assessing the risk for CO2 transportation within CCS projects, CFD modelling,” *International Journal of Greenhouse Gas Control*, vol. 5, no. 4, pp. 816–825, Jul. 2011.

[35] K. W. Moloney, I. S. Lowndes, M. R. Stokes, and G. Hargrave, “Studies on alternative methods of ventilation using Computational Fluid Dynamics (CFD), scale and full scale gallery tests,” in *Proceedings of the 6th International Mine Ventilation Congress*, 1997, p. 7.

[36] E. M. Marshall and A. Bakker, *Computational fluid mixing*. Fluent Incorporated, 2001.

[37] K. G. Gebremedhin and B. X. Wu, “Characterization of flow field in a ventilated space and simulation of heat exchange between cows and their environment,” *Journal of Thermal Biology*, vol. 28, no. 4, pp. 301–319, May 2003.

[38] P. a. Durbin, “A Reynolds stress model for near-wall turbulence,” *Journal of Fluid Mechanics*, vol. 249, no. 1, pp. 465–498, Apr. 2006.

[39] P. Spalart and S. Allmaras, “A one-equation turbulence model for aerodynamic flows,” *Recherche Aerospatiale*, no. 1, pp. 5–21, 1994.

[40] A. M. Wala, S. Vytla, C. D. Taylor, and G. Huang, “Mine face ventilation : a comparison of CFD results against benchmark experiments for the CFD code validation,” *Mining Engineering*, vol. 59, no. 10, pp. 49–55, 2007.

[41] M. Parra, J. Villafruela, F. Castro, and C. Mendez, “Numerical and experimental analysis of different ventilation systems in deep mines,” *Building and Environment*, vol. 41, no. 2, pp. 87–93, Feb. 2006.

[42] A. D. Gosman, “Developments in CFD for industrial and environmental applications in wind engineering,” *Journal of Wind Engineering and Industrial Aerodynamics*, vol. 81, no. 1–3, pp. 21–39, May 1999.

[43] D. N. Sørensen and P. V. Nielsen, “Quality control of computational fluid dynamics in indoor environments.,” *Indoor air*, vol. 13, no. 1, pp. 2–17, Mar. 2003.

[44] J. C. Edwards and C. C. Hwang, “CFD modeling of fire spread along combustibles in a mine entry,” in *SME Annual Meeting*, 2006, p. Preprint 06–027.

[45] H. Lomax, T. H. Pulliam, and David W. Zingg, *Fundamentals of computational fluid dynamics*. New York: Springer, 2001.

[46] J. M. Berkoe and D. M. Lane, “Putting computational fluid dynamics to work on mining and metals projects,” in *SME Annual Meeting*, 2000, p. Preprint 00–115.

[47] S. M. Salim and S. C. Cheah, “Wall y + strategy for dealing with wall-bounded turbulent flows,” in *Proceedins of International MultiConference of Engineers and Computer Scientists*, 2009, vol. II.

[48] T. T. Bui, “CFD analysis of nozzle jet plume effects on sonic boom signature,” in *47th AIAA Aerospace Sciences Meeting*, 2009, pp. 1–28.

[49] P. J. Roache, “Perspective: A method for uniform reporting of grid refinement studies,” *Journal of Fluid Engineering*, vol. 116, 1994.

[50] Fluent, “User’s guide.” 2006.

[51] M. Ariff, S. M. Salim, and S. C. Cheah, “Wall Y+ approach for dealing with turbulent flow over a surface mounted cube: Part 1-low reynolds number,” in *Seventh International Conference on CFD in the Minerals and Process Industries*, 2009, no. December, pp. 1–6.

[52] M. Ariff, S. M. Salim, and S. C. Cheah, “Wall Y+ approach for dealing with turbulent flow over a surface mounted cube: Part 2-high reynolds number,” in *Seventh International Conference on CFD in the Minerals and Process Industries*, 2009, no. December, pp. 1–6.

[53] R. Bhaskaran and L. Collins, “Introduction to CFD Basics,” *Direct*. pp. 1–17, 2005.

[54] P. Wesseling, *Principles of computational fluid dynamics*. New York: Apringer, 2001.

[55] W. L. Oberkampf and C. J. Roy, *Verification and Validation in Scientific Computing*. Cambridge University Press, 2010, p. 784.

[56] R. K. Jade and B. S. Sastry, "An experimental and numerical study of two-way splits and junctions in mine airways," in *12th U.S./North American Mine Ventilation Symposium*, 2008, pp. 293–298.

[57] F. F. Peng and Y. K. Xia, "Analysis of a dense-medium separator for course coal separation using computational fluid dynamics," *Minerals and Metallurgical Processing*, vol. 24, no. 1, pp. 1–12, 2007.

[58] F. F. Peng and Y. Xia, "Fluid dynamic modeling of fine particle separation in hindered-settling bed separators by CFD," in *SME Annual Meeting*, 2004, p. Preprint 04–033.

[59] J. Toraño, S. Torno, M. Menendez, M. Gent, and J. Velasco, "Models of methane behaviour in auxiliary ventilation of underground coal mining," *International Journal of Coal Geology*, vol. 80, no. 1, pp. 35–43, Oct. 2009.

[60] A. M. Wala, J. C. Yingling, J. Zhang, and R. Ray, "Validation study of computational fluid dynamics as a tool for mine ventilation design," in *Proceedings of the 6th International Mine Ventilation Congress*, 1997.

[61] J. B. Dick, "Measurement of ventilation using tracer gas," *Heating, Piping and Air Conditioning*, vol. 22, no. 5, pp. 131–137, 1950.

[62] R. J. Timko and E. D. Thimons, "Sulfur hexafluoride as a mine ventilation research tool-Recent field applications," U.S. Bureau of Mines, Washington, DC (USA), 1982.

[63] R. B. Krog, S. J. Schatzel, and H. N. Dougherty, "Airflow distribution patterns at a longwall mine depicted by CFD analysis and calibrated by a tracer gas field study," in *SME Annual Meeting*, 2011, p. Preprint 11–067.

[64] I. M. Konduri, M. J. McPherson, and E. Topuz, "Experimental and numerical modeling of jet fans for auxiliary ventilation in mines," in *Proceedings of the 6th International Mine Ventilation Symposium*, 1997, pp. 505–510.

[65] F. H. Post and T. van Walsum, "Fluid flow visualization," *Focus on Scientific Visualization*, vol. 40, pp. 1–37, 1993.

[66] A. Wala, D. Turner, and J. Jacob, "Experimental study of mine face ventilation system for validation of numerical models," in *Proceeding of the 9th North American U.S. Mine Ventilation Symposium*, 2002, pp. 191–196.

[67] D. M. Hargreaves and I. S. Lowndes, “The computational modeling of the ventilation flows within a rapid development drivage,” *Tunnelling and Underground Space Technology*, vol. 22, no. 2, pp. 150–160, Mar. 2007.

[68] C. D. Taylor, R. J. Timko, E. D. Thimons, and T. Mal, “Using ultrasonic anemometers to evaluate factors affecting face ventilation effectiveness,” in *SME Annual Meeting*, 2005, p. Preprint 05–080.

[69] H. Hartmann, J. J. Derksen, C. Montavon, J. Pearson, I. S. Hamill, and H. E. A. Van Den Akker, “Assessment of large eddy and RANS stirred tank simulations by means of LDA,” *Chemical Engineering Science*, vol. 59, no. 12, pp. 2419–2432, 2004.

[70] Z. Jaworski and J. Dudczak, “CFD modelling of turbulent macromixing in stirred tanks. Effect of the probe size and number on mixing indices,” *Computers & Chemical Engineering*, vol. 22, no. Supplement 1, pp. S293–S298, 1998.

[71] Z. Jaworski, K. N. Dyster, V. P. Mishra, A. W. Nienow, and M. L. Wyszynski, “A study of an up- and down-pumpling wide-blade hydrofoil impeller: Part II. CFD analysis,” *The Canadian Journal of Chemical Engineering*, vol. 76, no. 5, pp. 866–876, 1998.

[72] J. Sheng, H. Meng, and R. O. Fox, “Validation of CFD simulations of a stirred tank using particle image velocity data,” *The Canadian Journal of Chemical Engineering*, vol. 73, no. 3, pp. 611–625, 1998.

[73] A. M. Wala, J. C. Yingling, J. Zhang, and R. Ray, “Validation study of computational fluid dynamics as a tool for mine ventilation design,” in *Proceeding of the 6th International Mine Ventilation Congress*, 1997.

[74] A. M. Wala, S. Vytla, G. Huang, and C. D. Taylor, “Study on the effects of scrubber operation on the face ventilation,” in *12th U.S./North American Mine Ventilation Symposium*, 2008, pp. 281–286.

[75] A. M. Wala, J. C. Yingling, and J. Zhang, “Evaluation of the face ventilation systems for extended cuts with remotely operated mining machines using three-dimensional numerical simulations,” in *SME Annual Meeting*, 1998, vol. 5002, p. Preprint 98–209.

[76] Y. Zheng and J. C. Tien, “DPM dispersion study using cfd for underground metal/nonmetal mines,” in *12th U.S./North American Mine Ventilation Symposium*, 2008, pp. 487–494.

[77] X. Zhang, Y. Zhang, and J. C. Tien, “The efficiency study of the push-pull ventilation system in underground mine,” in *2011 Underground Coal Operators’ Conference*, 2011.

[78] S. M. Aminossadati, “Numerical simulation of ventilation air flow in underground mine workings,” in *12th U.S./North American Mine Ventilation Symposium*, 2008, pp. 253–260.

[79] R. E. Ray, M. J. Gilbey, and P. Kumar, “The application of vertically-mounted jet fans in ventilation shafts for a rail overbuild,” in *12th U.S./North American Mine Ventilation Symposium*, 2008, pp. 415–424.

[80] L. Yuan and A. C. Smith, “CFD modeling of spontaneous heating in a large-scale coal chamber,” *Journal of Loss Prevention in the Process Industries*, vol. 22, no. 4, pp. 426–433, Jul. 2009.

[81] A. C. Smith and L. Yuan, “Simulation of spontaneous heating in longwall gob area with a bleederless ventilation system,” in *SME Annual Meeting*, 2008, p. Preprint 08–043.

[82] J. C. Edwards, R. A. Franks, G. F. Friel, and L. Yuan, “Experimental and modeling investigation of the effect of ventilation on smoke rollback in a mine entry,” *Society for Mining Metallurgy and Exploration*, vol. 58, pp. 53–58, 2006.

[83] J. Huang, J. Bruining, and K.-H. A. A. Wolf, “Modeling of gas flow and temperature fields in underground coal fires,” *Fire Safety Journal*, vol. 36, no. 5, pp. 477–489, Jul. 2001.

[84] M. A. Trevits, L. Yuan, K. Teacoach, M. P. Valoski, and J. E. Urosek, “Understanding mine fires by determining the characteristics of deep-seated fires.” NIOSH Document, 2009.

[85] J. C. Edwards and C. C. Hwang, “CFD analysis of mine fire smoke spread and reverse flow conditions,” in *8th U.S. Mine Ventilation Symposium*, 1999, pp. 417–422.

[86] S. F. Luchian and A. G. Bendelius, “West Virginia memorial tunnel fire ventilation test program,” in *International Conference on Fires in Tunnels*, 1994.

[87] A. Kelsey, C. J. Lea, I. S. Lowndes, D. Whittles, and T. X. Ren, “CFD modelling of methane movement in mines,” in *30th International Conference of Safety in Mines Research Institutes*, 2003, pp. 475–486.

[88] T. X. Ren, J. S. Edwards, and R. R. Jozefowicz, “CFD modelling of methane flow around longwall coal faces,” in *Proceedings of the 6th International Mine Ventilation Congress*, 1997, pp. 247–251.

[89] K. Oraee and A. Goodarzi, “Mathematical modeling of coal seam methane drainage in longwall mining,” in *SME Annual Meeting*, 2010, p. Preprint 10–115.

[90] R. Balusu, N. Tuffs, D. White, and T. Harvey, “Surface goaf gas drainage strategies for highly gassy longwall,” *Journal of The Mine Ventilation Society of South Africa*, vol. 59, no. 3, pp. 78–84, 2006.

[91] C. Ö. Karacan, T. Ren, and R. Balusu, "Advances in grid-based numerical modeling techniques for improving gas management in coal mines," in *12th US/North American Mine Ventilation Symposium*, 2006.

[92] G. Esterhuizen and C. Karacan, "A methodology for determining gob permeability distributions and its application to reservoir modeling of coal mine longwalls," in *SME Annual Meeting*, 2007.

[93] T. X. Ren, R. Balusu, and P. Humphries, "Development of innovative goaf inertisation practices to improve coal mine safety," in *Coal Operators' Conference*, 2005, pp. 315–322.

[94] R. Mossad, A. Vella, and R. Balusu, "Inertisation of highwall mining to control methane concentrations at the Moura Mine," in *Seventh International Conference on CFD in the Minerals and Process Industries*, 2009, no. December, pp. 1–6.

[95] R. Balusu, P. Humpries, P. Harrington, M. Wendt, and S. Xue, "Optimum inertisation strategies," in *Queensland Mining Industry Health and Safety Conference*, 2002, pp. 133–144.

[96] M. A. Trevits, L. Yuan, M. Thibou, and G. Hatch, "Use of CFD modeling to study inert gas injection into a sealed mine area," in *SME Annual Meeting*, 2010, p. Preprint 10–207.

[97] A. Vella, "Ventilation of highwall mining to control methane concentration at the Moura Mine," The University of Southern Queensland, 2006.

[98] J. Van Heerden and P. Sullivan, "The application of CFD for evaluation of dust suppression and auxiliary ventilating systems used with continuous miners," in *Proceedings of the 6th US Mine Ventilation Symposium*, 1993, pp. 293–297.

[99] R. B. Srinivase, E. Y. Baafi, N. I. Aziz, and R. N. Singh, "Three dimensional numerical modelling of air velocities and dust control techniques in a longwall face," in *Proceeding of the 6th U.S. Mine Ventilation Symposium*, 1993.

[100] T. Ren and R. Balusu, "The use of CDF modelling as a tool for solving mining health and safety problems," in *Coal Operators' Conference*, 2010, pp. 339–349.

[101] D. M. Hargreaves and I. S. Lowndes, "The evaluation of the design and operation of alternative auxiliary ventilation layouts for use with continuous miner systems in rapid development drivages," *Final Report 7220-AC-857, Commission of the European Communities, Directorate-General Energy & Transport*, 2001.

[102] S. A. Silvester, I. S. Lowndes, and D. M. Hargreaves, "A computational study of particulate emissions from an open pit quarry under neutral atmospheric conditions," *Atmospheric Environment*, vol. 43, no. 40, pp. 6415–6424, Dec. 2009.

[103] J. Lichter, A. V Potapov, and R. Peaker, “The use of computational fluid dynamics and discrete element modeling to understand the effect of cell size and inflow rate on flotation bank retention time distribution and mechanism performance,” in *Proceedings 39th AGM of Can. Min. Proc.*, 2009, pp. 473–496.

[104] F. D. Ardejani, E. Baafi, K. S. Panahi, R. N. Singh, and B. J. Shokri, “Application of Computational Fluid Dynamics (CFD) for simulation of acid mine drainage generation and subsequent pollutants transportation through groundwater flow systems and rivers,” in *Computational Fluid Dynamics Technologies and Applications*, 2011, pp. 123–160.

[105] A. Mazzoldi, T. Hill, and J. Colls, “A Consideration of the jet-mixing effect when modelling CO2 emissions from high pressure CO2 transportation facilities,” *Energy Procedia*, vol. 1, no. 1, pp. 1571–1578, Feb. 2009.

[106] C. Dixon, O. Heynes, and M. Hasson, “Assessing the hazards associated with release and dispersion of liquid carbon dioxide on offshore platforms.” MMI Engineering Ltd., Warrington, UK, 2008.

[107] G. Arpa, A. Widiatmojo, N. P. Widodo, and K. Sasaki, “Tracer gas measurement and simulation of turbulent diffusion in mine ventilation airways,” *Journal of Coal Science and Engineering (China)*, vol. 14, no. 4, pp. 523–529, Nov. 2008.

[108] R. Suglo and S. Frimpong, “Accuracy of tracer gas surveys in auxiliary ventilation systems in mines,” in *The 9th U.S./North American Mine Ventilation Symposium*, 2002.

[109] E. D. Thimons and F. N. Kissell, “Tracer gas as an aid in mine ventilation analysis,” *Bureau of Mines Report of Investigations*, 1974.

[110] M. G. Grenier, S. G. Hardcastle, G. Kunchur, and K. Butler, “The use of tracer gases to determine dust dispersion patterns and ventilation parameters in a mineral processing plant,” *American Industrial Hygiene Association Journal*, vol. 53, no. 6, pp. 387–394, 1992.

[111] D. a Kirchgessner, S. D. Piccot, and S. S. Masemore, “An improved inventory of methane emissions from coal mining in the United States.,” *Journal of the Air & Waste Management Association (1995)*, vol. 50, no. 11, pp. 1904–19, Nov. 2000.

[112] Z. Zhang, X. Chen, S. Mazumdar, T. Zhang, and Q. Chen, “Experimental and numerical investigation of airflow and contaminant transport in an airliner cabin mockup,” *Building and Environment*, vol. 44, no. 1, pp. 85–94, Jan. 2009.

[113] Z. Zhang and Q. Chen, “Experimental measurements and numerical simulations of particle transport and distribution in ventilated rooms,” *Atmospheric Environment*, vol. 40, no. 18, pp. 3396–3408, Jun. 2006.

[114] X. Yang, “Performance of three air distribution systems in VOC removal from an area source,” *Building and Environment*, vol. 39, no. 11, pp. 1289–1299, Nov. 2004.

[115] J. L. Santiago, A. Martilli, and F. Martin, “Passive Tracer Dispersion over A Regular Array of Cubes Using CFD Simulations,” in *14th Joint Conference on the Applications of Air Pollution Meteorology with the Air and Waste Management Assoc*, 2005, no. Tracer 8, pp. 2–6.

[116] R. Klopfenstein Jr., “Air velocity and flow measurement using a Pitot tube,” *ISA Transactions*, vol. 37, no. 4, pp. 257–263, Sep. 1998.

[117] R. G. Gurtunca, “Possible impact of new safety technology developments on the future of the United States mining industry,” in *1st International Future Mining Conference*, 2008.

[118] D. J. Kennedy, A. W. Stokes, and W. G. Klinowski, “Resolving Complex Mine Ventilation Problems with Multiple Tracer Gases,” in *3rd Mine Ventilation Symposium*, 1987.

[119] E. D. Thimons and F. N. Kissell, “Tracer Gas as an Aid in Mine Ventilation Analysis,” U.S. Bureau of Mines, Washington, DC (USA), Pittsburgh, PA, BM-RI-7917, 1974.

[120] G. Arpa, A. Widiatmojo, N. P. Widodo, and K. Sasaki, “Tracer gas measurement and simulation of turbulent diffusion in mine ventilation airways,” *Journal of Coal Science and Engineering (China)*, vol. 14, no. 4, pp. 523–529, Nov. 2008.

[121] T. P. Mucho, W. P. Diamond, F. Garcia, J. D. Byars, and S. L. Cario, “Implications of recent NIOSH tracer gas studies on bleeder and gob gas ventilation design,” in *SME Annual Meeting*, 2000.

[122] E. D. Thimons, R. J. Bielicki, and F. N. Kissell, “Using sulfur hexafluoride as a gaseous tracer to study ventilation systems in mines,” Pittsburgh, PA, 1974.

[123] K. W. D. Cheong, E. Djunaedy, and T. K. Plh, “Measurements and computations of contaminant’s distribution in an office environment,” *Building and Environment*, vol. 38, no. 1, pp. 135–145, Jan. 2003.

[124] G. Y. Hua, W. Wang, Y. H. Zhao, and L. Li, “A study of an optimal smoke control strategy for an Urban Traffic Link Tunnel fire,” *Tunnelling and Underground Space Technology*, vol. 26, no. 2, pp. 336–344, Mar. 2011.

[125] C. M. K. Se, E. W. M. Lee, and A. C. K. Lai, “Impact of location of jet fan on airflow structure in tunnel fire,” *Tunnelling and Underground Space Technology*, vol. 27, no. 1, pp. 30–40, Jan. 2012.

[126] R. Gao, A. Li, X. Hao, W. Lei, and B. Deng, “Prediction of the spread of smoke in a huge transit terminal subway station under six different fire scenarios,” *Tunnelling and Underground Space Technology*, vol. 31, pp. 128–138, Sep. 2012.

[127] H. Copur, M. Cinar, G. Okten, and N. Bilgin, “A case study on the methane explosion in the excavation chamber of an EPB-TBM and lessons learnt including some recent accidents,” *Tunnelling and Underground Space Technology*, vol. 27, no. 1, pp. 159–167, Jul. 2011.

[128] G. Xu, J. R. Bowling, K. D. Luxbacher, and S. Ragab, “Computational fluid dynamics simulations and experimental validation of tracer gas distribution in an experimental underground mine,” in *2011 SME Annual Meeting*, 2011, p. Preprint 11–121.

[129] R. Klopfenstein Jr., “Air velocity and flow measurement using a Pitot tube,” *ISA Transactions*, vol. 37, no. 4, pp. 257–263, Sep. 1998.

[130] W. J. Fisk, J. Binenboym, H. Kaboli, D. T. Grimsrud, A. W. Robb, and B. J. Weber, “A multi-tracer system for measuring ventilation rates and ventilation efficiencies in large mechanically-ventilated buildings,” in *AIC 6th Conference Ventilation Strategies and Measurement Techniques*, 1985, pp. 69–92.

[131] R. W. Freedman, W. G. Humphrey, and R. L. Craft, “Use of vacutainers for collection of mine atmosphere samples,” *Bureau of Mines Report of Investigations*, 1975.

[132] R. W. Freedman and B. I. Ferber, “Sampling capability of vacutainers for fixed gases and low-molecular-weight hydrocarbons,” *Bureau of Mines Report of Investigations*, 1976.

[133] EPA, “Characteristics of gases-concentration,” *EPA*, 2010. [Online]. Available: http://www.epa.gov/apti/bces/module2/concentrate/concentrate.htm.

[134] I. Ansys, *Ansys fluent 12.0 theory guide*, no. April. 2009.

[135] W. A. Tucker and L. H. Nelken, “Diffusion coefficients in air and water,” in *Handbook of Chemical Property Estimation Methods*, Washington, DC: American Chemical Society, 1990, pp. 17.1–17.25.

[136] J. S. Bai, L. Y. Zou, T. Wang, K. Liu, W. B. Huang, J. H. Liu, P. Li, D. W. Tan, and L. Liu, “Experimental and numerical study of the shock-accelerated elliptic heavy gas cylinders,” *World Academy of Science, Engineering and Technology*, pp. 324–328, 2011.

[137] D. B. Ward and C. V. William, “Verification of the integrity of barriers using gas diffusion,” 1997.

[138] ANSYS, “ANSYS ICEM CFD 11.0 Tutorial Manual,” no. January. p. 286, 2007.

[139] ANSYS, “Ansys fluent 12.0 tutorial guide,” *Computer Communications*, vol. 10, no. 1. ANSYS, Inc., Feb-2009.

[140] G. Xu, E. Jong, K. Luxbacher, and S. Ragab, “Computational fluid dynamics study of tracer gas dispersion in a mine after different ventilation damage scenarios,” in *SME Annual Meeting*, 2012, p. Preprint 12–051.

[141] M. E. Adam, C. E. Brechtel, J. F. T. Agapito, and E. D. Thimons, “Leakage testing of large ventilation control structures for room and pillar oil shale mining,” in *3th Mine Ventilation Symposium*, 1987, pp. 365–370.

[142] J.-J. A. A. Akoua, F. Allard, C. Beghein, and B. Collignan, “Experimental and numerical studies on indoor air quality in a real environment,” in *2nd Mediterranean Congress of Climatization*, 2005, no. Ddd.

[143] G. Xu, K. D. Luxbacher, S. Ragab, and S. Schafrik, “Development of a remote analysis method for underground ventilation systems using tracer gas and CFD in a simplified laboratory apparatus,” *Tunnelling and Underground Space Technology*, vol. 33, pp. 1–11, 2012.

[144] R. J. Timko and E. D. Thimons, “Sulfur Hexafluoride as a mine ventilation research tool - recent field applications,” *Bureau of Mines Report of Investigations*, 1982.

[145] M. G. Grenier, S. G. Hardcastle, G. Kunchur, and K. Butler, “The use of tracer gases to determine dust dispersion patterns and ventilation parameters in a mineral processing plant.,” *American Industrial Hygiene Association journal*, vol. 53, no. 6, pp. 387–394, Jun. 1992.

[146] R. R. Patterson, J. R. Bowling, and G. Xu, “Design of an Experimental Apparatus for the Testing of Novel Tracer Gases in Underground Mines,” in *13th United States/North American Mine Ventilation Symposium*, 2010.

[147] E. Jong, S. Underwood, G. Xu, K. Luxbacher, and H. McNair, “A technique for creating perfluorocarbon tracer (PFT) calibration curves for tracer gas studies,” in *14th U.S./North American Mine Ventilation Symposium*, 2012.

[148] D. Lester and L. A. Greenberg, “The toxicity of sulfur pentafluoride,” *Arch. Ind. Hyg. Occup. Med.*, vol. 2, no. 3, pp. 348–9, 1950.

[149] OSHA, “Chemical Sampling Information,” *United States Department of Labor*, 1993. [Online]. Available: http://www.osha.gov/dts/chemicalsampling/data/CH_268600.html.

[150] D. J. Kennedy, A. W. Stokes, and W. G. Klinowski, “Resolving complex mine ventilation problems with multiple tracer gases,” in *3rd Mine Ventilation Symposium*, 1987, pp. 213–218.

[151] S. Batterman, C. Jia, G. Hatzivasilis, and C. Godwin, “Simultaneous measurement of ventilation using tracer gas techniques and VOC concentrations in homes, garages and vehicles,” *Journal of Environmental Monitoring*, vol. 8, no. 2, pp. 249–56, Feb. 2006.

[152] R. R. Patterson, “Determination of a novel mine tracer gas and development of a methodology for sampling and analysis of multiple mine tracer gases for characterization of ventilation systems,” Virginia Tech, 2011.

[153] W. Mailahn, B. Seifert, D. Ullrich, and H. Moriske, “The use of a passive sampler for the simultaneous determination of long-term ventilation rates and VOC concentrations,” *Environment International*, vol. 15, pp. 537–544, 1989.

[154] R. N. Dietz and E. A. Cote, “Air infiltration measurements in a home using a convenient perfluorocarbon tracer technique,” *Environment International*, vol. 8, pp. 419–433, Jan. 1982.

[155] K. A. Johnson, H. H. Westberg, J. J. Michal, and M. W. Cossalman, “The SF6 tracer technique: methane measurement from ruminants,” in *Measuring Methane Production From Ruminants*, H. P. S. Makkar and P. E. Vercoe, Eds. Springer, 2007, pp. 33–67.

[156] M. J. Peach and W. G. Carr, “Air sampling and analysis for gases and vapors,” 1986.

[157] F. J. Schuette, “Plastic bags for collection of gas samples,” *Atmospheric Environment*, vol. 1, no. 4, 1967.

[158] V. Bush, “The Evolution of Evacuated Blood Collection Tubes,” 2009. [Online]. Available: http://www.bd.com/vacutainer/labnotes/Volume19Number1/. [Accessed: 17-Jan-2011].

[159] J. J. Leonard, J. J. R. Feddes, and J. B. McQuitty, “Measurement of ventilation rates using a tracer gas,” *Canadian Agricultural Engineering*, vol. 26, no. 1, pp. 49–51, 1984.

[160] H. M. McNair and J. M. Miller, *Basic gas chromatography*. John Wiley & Sons, 1998.

Appendix A

Appendix for Citations of Copyrighted Works

Chapter 3 [copyright belongs to the authors]
Xu, G., Bowling, J. R., Luxbacher, K. D., & Ragab, S. (2011). Computational fluid dynamics simulations and experimental validation of tracer gas distribution in an experimental underground mine. 2011 SME Annual Meeting (Preprint 11–121). Denver, CO (USA).
Although this paper was published at SME annual meeting, SME does not have copyright of this paper and all copyrights belong to the authors. Call SME at 303-948-4200 for more information.

Chapter 4 [author have the right to include the paper in the dissertation]
Xu, G., Luxbacher, K. D., Ragab, S., & Schafrik, S. (2012). Development of a remote analysis method for underground ventilation systems using tracer gas and CFD in a simplified laboratory apparatus. Tunnelling and Underground Space Technology, 33, 1–11. This paper can be found at the link: http://www.sciencedirect.com/science/article/pii/S0886779812001551.For papers published at Elsevier, the authors have the right to include the published paper in a thesis or dissertation without needing to seek permission.Authors' rights can be found here: http://www.elsevier.com/authors/author-rights-and-responsibilities.

Chapter 5 [copyright belongs to the authors]
Xu, G., Jong, E., Luxbacher, K., & Ragab, S. (2012). Computational fluid dynamics study of tracer gas dispersion in a mine after different ventilation damage scenarios. SME Annual Meeting (p. Preprint 12–051). Seattle, Washington (USA).
Although this paper was published at SME annual meeting, SME does not have copyright of this paper and all copyrights belong to the authors. Call SME at 303-948-4200 for more information.